PB-214 184

THERMASONDE DATA PROCESSING TECHNIQUES

W. D. Mount, et al

Sperry Rand Research Center

Prepared for:

Environmental Protection Agency

October 1972

DISTRIBUTED BY:

NTIS

National Technical Information Service
U. S. DEPARTMENT OF COMMERCE
5285 Port Royal Road, Springfield Va. 22151

EPA-R3-72-022

PB 214 184

Reproduced by
NATIONAL TECHNICAL
INFORMATION SERVICE
U S Department of Commerce
Springfield VA 22151

SPERRY RAND

RESEARCH CENTER SUDBURY, MASSACHUSETTS

BIBLIOGRAPHIC DATA SHEET	1. Report No. EPA-R3-72-022	2.	3. Recipient's Accession No. PB 214 154
4. Title and Subtitle THERMASONDE DATA PROCESSING TECHNIQUES			5. Report Date October 1972 6.
7. Author(s) W.D. Mount, A. C. Anway, B. R. Fow, et al			8. Performing Organization Rept. No. SRRC-CR-72-5
9. Performing Organization Name and Address Sperry Rand Research Center Atmospheric Sciences Laboratory 100 North Road Sudbury, Massachusetts 01776			10. Project/Task/Work Unit No. 11. Contract/Grant No. EHSD 71-26
12. Sponsoring Organization Name and Address ENVIRONMENTAL PROTECTION AGENCY Air Pollution Control Office Raleigh, North Carolina 27605			13. Type of Report & Period Covered Final 14.

15. Supplementary Notes

16. Abstracts A study was conducted in which three data processing techniques developed under the previous contract were refined and tested on a small sample of simulated and observed radiometric data. The results were compared and the input data and computer and manpower requirements for operational use of each technique were assessed. The report is organized as follows: Section 2 is devoted to the simulation discrepancy. Participation in the various field experiments is described, and the significant results leading to establishment of the discrepancy are presented. The present state of the art for simulating the observed antenna temperatures and the impact of this capability upon system performance is discussed. Section 3 describes the data processing techniques. Specific work performed in developing each technique is discussed, results are presented, and hardware and software requirements to implement each technique are indicated. Section 4 discusses the effects of a non-ideal antenna pattern, with a detailed description of a method of formulating the analysis of these effects. Section 5 contains the conclusions derived from this work and their implications.

17. Key Words and Document Analysis. 17a. Descriptors

Air pollution
Data analysis
Data processing
Radiometers
Simulation
Computerized simulation
Antenna radiation patterns

17b. Identifiers/Open-Ended Terms

Thermasonde

17c. COSATI Field/Group 13B, 9B

18. Availability Statement	19. Security Class (This Report)	21. No. of Pages
Unlimited	UNCLASSIFIED	114
	20. Security Class (This Page) UNCLASSIFIED	22. Price $3.00

FORM NTIS-35 (REV. 3-72) THIS FORM MAY BE REPRODUCED USCOMM-DC 14952-P72

EPA-R3-72-022

SPERRY RAND CORPORATION

THERMASONDE™ DATA PROCESSING TECHNIQUES

Contract No. EHSD 71-26

Final Report

Covering Period 1970 October 9 to 1972 February 9

Submitted by: Sperry Rand Research Center
Atmospheric Sciences Laboratory
100 North Road
Sudbury, Massachusetts 01776

Prepared by: W. D. Mount, Principal Investigator
A. C. Anway
B. R. Fow
C. M. Maloy
C. V. Wick

October 1972
SRRC-CR-72-5

Prepared for: Air Pollution Control Office
Raleigh, North Carolina 27701

SPERRY RAND RESEARCH CENTER
SUDBURY, MASSACHUSETTS 01776

TABLE OF CONTENTS

Section		Page
1	INTRODUCTION AND GENERAL SUMMARY	1
	1.1 Introduction	1
	1.2 Summary	1
	1.3 Organization of Report	4
2	SIMULATION DISCREPANCY	6
	2.1 Introduction	6
	2.2 Establishment of the Simulation Discrepancy	7
	2.3 Significance of the Discrepancy	14
	2.4 Possible Causes of the Discrepancy	14
	2.5 Elimination of Causes	18
	2.6 Verification of Simulation Capability	22
	2.7 Summary	29
3	DEVELOPMENT OF DATA PROCESSING TECHNIQUES	30
	3.1 Historical Perspective	30
	3.2 Analog Technique	30
	3.3 Gradient Altitude Model	40
	3.4 Limited Range Relaxation Technique	53
	3.5 Comparison of Techniques	67
	3.6 Summary	80
4	ANALYSIS OF ANTENNA PATTERN EFFECTS	82
	4.1 Introduction	82
	4.2 The Problem	82
	4.3 Calculation of Antenna Temperature	85
	4.4 Operational Significance of the Antenna Pattern Response	90
	4.5 Antenna Optimization Study	95
	4.6 Summary	101
5	CONCLUSIONS AND RECOMMENDATIONS	103
	5.1 Conclusions	103
	5.2 Recommendations	106
	REFERENCES	107

LIST OF ILLUSTRATIONS

Figure	Description	Page
1	Comparison of simulated scans and MK I scan for Raleigh, N.C., 0618 EST, 1970 December 9.	11
2	Comparison of simulated scans and MK I scan for Raleigh, N.C., 1417 EST, 1970 December 9.	12
3	Revised correction curve for MK I frequency meter.	19
4	Comparison of MK I scan and scans simulated with and without antenna pattern correction.	21
5	MK I and simulated scan without ground temperature data.	23
6	Correlation between radiosonde-measured and MK I-measured inversion heights.	34
7	Boulder overlay format.	36
8	Model temperature profile.	38
9	Brightness temperature scans for different surface pressures.	39
10	GAM temperature profile model.	42
11	Comparison of actual profile with GAM profiles determined from errorless data (lapse condition).	47
12	Comparison of actual profile with GAM profiles determined from errorless data (low elevated inversion).	48
13	Comparison of actual profile with GAM profiles determined from errorless data (ground-based inversion).	49
14	Comparison of actual profile with GAM profiles determined from errorless data (high elevated inversion).	50
15	Relaxation technique applied to the brightness temperatures computed from a model profile having a 5 C elevated inversion from 0.5 to 0.75 km.	61
16	Relaxation technique applied to the brightness temperatures computed from a model profile having a 5 C elevated inversion from 1.0 to 1.25 km.	63
17	Relaxation technique applied to the brightness temperatures computed from the observed radiosonde data taken at St. Louis, Mo., 0529 CST, 1970 October 6.	64
18	Relaxation technique applied to the brightness temperatures computed from the observed radiosonde data taken at St. Louis, Mo., 0547 CST, 1970 October 16.	66

LIST OF ILLUSTRATIONS - Cont'd

Figure	Description	Page
19	GAM, relaxation and analog results for simulated data for Raleigh, N.C., 1323 EST, 1970 December 2.	70
20	GAM, relaxation and analog results for simulated data for Raleigh, N.C., 0624 EST, 1970 December 9.	71
21	GAM, relaxation and analog results for simulated data for Raleigh, N.C., 0933 EST, 1970 December 5.	72
22	GAM, relaxation and analog results for simulated data for St. Louis, Mo., 1154 CST, 1970 October 16.	73
23	GAM and analog results for MK I data obtained at Raleigh, N.C., 1322 EST, 1970 December 2.	74
24	GAM and analog results for MK I data obtained at Raleigh, N.C., 0618 EST, 1970 December 9.	75
25	GAM and analog results for MK I data obtained at Raleigh, N.C., 0932 EST, 1970 December 5.	76
26	GAM and analog results for MK I data obtained at St. Louis, Mo., 1143 CST, 1970 October 16.	77
27	Contributions to source brightness distribution.	83
28	Angular relationships for antenna temperature calculations.	86
29	Results using antenna temperature computation (ANTEMP).	89
30	Antenna response to a step brightness change.	91
31	Ground contribution variation.	93
32	Distortion of sky brightness distribution.	94

LIST OF TABLES

Table	Discription	Page
I	IMPACT OF OBSERVED VERSUS SIMULATED BRIGHTNESS TEMPERATURE DISCREPANCY	15, 16, 17
II	ABSOLUTE TEMPERATURE SIMULATION ERROR FOR MK 0 THERMASONDE™	26
III	ABSOLUTE TEMPERATURE SIMULATION ERROR FOR MK I THERMASONDE™	26
IV	VERIFICATION OF MEASURED ANTENNA TEMPERATURE	27
V	SUMMARY OF PARAMETER VALUE CONSTRAINTS BUILT INTO THE GAM COMPUTER PROGRAM	44
VI	ANGLE-HEIGHT GRID	55
VII	ERROR CONSTANTS AND FINAL TRANSMISSIVITIES	57
VIII	AVERAGE TEMPERATURE ERRORS FOR THE INVERSION TECHNIQUE	79
IX	SUMMARY OF ANTENNA PERFORMANCE CHARACTERISTICS	98
X	MAXIMUM ANTENNA ERRORS FOR DIFFERENT PROFILES	100
XI	ERRORS FOR DIFFERENT SCAN PARAMETERS	101

SECTION 1

INTRODUCTION AND GENERAL SUMMARY

1.1 INTRODUCTION

This final report describes work performed by the Sperry Rand Research Center in accordance with requirements of Contract No. EHSD 71-26, "THERMASONDE™ Data Processing Techniques." The work was performed between 1970 October 9 and 1972 February 9, principally at the Sperry Rand Research Center (SRRC), Sudbury, Massachusetts, with certain field experiments performed at various Government facilities. Work performed under this contract was a natural extension and logical outgrowth of that previously completed under Contract CPA 22-69-116, "Three Data Analysis Techniques for Measuring Air Temperature Profiles," 1970 November.

A significant redirection of effort was implemented to search for the source of a somewhat consistent difference between computer-simulated and actually observed radiometric data. This situation developed as a result of two events. First, the radiometer's performance was greatly improved and noise suppressed. Second, a large set of observations was taken with simultaneous RAOBs which, when averaged together, made this discrepancy more apparent. The absolute difference found was about 3° K. The significance of this is that each data reduction technique currently considered for operational usage requires a good agreement between measurement and computer simulation either in its development or real time use. Therefore it was mandatory to isolate and minimize this discrepancy if the full capability of the data reduction techniques is to be realized.

1.2 SUMMARY

The three data processing techniques developed under the previous contract were refined and tested on a small sample of simulated and observed radiometric data. The results were compared and the input data and computer and manpower requirements for operational use of each technique were assessed.

At the request of the Government, we participated in Government-sponsored field experiments at Clearwater, Florida; St. Louis, Missouri; and at Boulder, Colorado. Analysis of data from these experiments revealed a discrepancy between our simulation model and measurement implementation. A

list of conceivable sources was compiled. Each item was ranked according to its likelihood of being the source, the approach needed to resolve it, and the level of effort and assignments required. Arrangements were made with Dr. E. Westwater, NOAA Research Laboratories in Boulder, Colorado, to use his program to simulate radiometric data from selected RAOBs. His results and ours were in close agreement. Neither of the computer simulations included the integrating effect of the antenna pattern. While work on this antenna pattern problem was being performed, other likely candidates were investigated. Using our computer simulation model, it was possible to work backward to determine which error in frequency or absorption coefficient would yield best confirmation of the observed data. It was found that the small differences in frequency or absorption coefficient required for confirmation were within the existing level of measurement uncertainty. In cooperation with personnel from Sperry Microwave Electronics Division (SMED), the MK I radiometer was tested with a highly accurate frequency standard. It was on frequency, and that was eliminated from the list. Radiometric data gathered at various locations and pressure altitudes were used to show that altering the absorption coefficients did not properly correct the simulated profiles under a variety of meteorological regimes. A computer program was formulated which combined the effects of antenna pattern, ground emissivity and reflectivity, radiation transfer, and antenna scanning. Antenna temperatures were simulated with this program using the on-site RAOB air temperature profiles as ground truth, and the results were compared with observed antenna temperatures. Agreement was excellent, and held up for the variety of meteorological regimes. A study of different antenna configurations was performed, a cost-effective improved design was determined, and the performance of this configuration was evaluated.

This work has produced the following salient results:

1. Excessive response of conventional antennas to off-axis radiation from the ground and sky results in distortion of the source brightness distribution, which, in turn, leads to erroneous indication of the air temperature profile. High main-beam efficiency (as opposed to aperature efficiency) and narrow beam width minimize this distortion, with optimum values for the proposed MK II system being about 95% and 2 degrees, respectively.

2. Calculations indicate that the sky brightness distortion for a typical profile will be reduced from a maximum deviation of 1.5 C for the MK I antenna to 0.35 C for the MK II antenna (a reduction of 76%). For the worst case condition (superadiabatic lapse at the ground), maximum deviation is less than 0.5 C for the optimum antenna.

3. Reduction of the brightness distortion to this low level (cp dynamic fluctuations of the atmosphere) makes it unnecessary to introduce the additional data processing complexity needed to reduce it further.

4. Refinements in formulation of the three data processing techniques have achieved improved performance and operational simplifications. It has been demonstrated, on a small sample of representative observed profiles, that the analog and gradient altitude model specify the temperature profile over 1.5 km to less than 2 C average (or average absolute) error. This performance was achieved with incomplete (or no) correction for the brightness distortion discrepancy. It is estimated, on the basis of simulated data, that the resolution limit of all three techniques, as presently formulated, is approximately 1 C.

5. Field experience with the MK I THERMASONDE using an analog library with only seven discrete mixing heights has demonstrated a capability of indicating mixing layer height to within an average of about 15% of the true height in the first 1500 m above the surface. This figure will be reduced with the MK II system because: (a) improved antenna design will significantly reduce the error from extraneous ground and sky radiation, (b) automatic production of the analog library will increase the profile resolution available, and (c) introducing the surface pressure parameter will aid profile selection.

6. The two computerized techniques suffer somewhat from an

inadequate error criterion; nevertheless, both have clearly demonstrated their inherently greater profile resolution capability.

7. The analog technique is essentially operationally ready and has had some field testing. The GAM technique should be further refined to accommodate direct data read-in from the THERMASONDE, reduce running time, and incorporate any improved error criterion. Only limited field experience was obtained with this technique. The limited-range relaxation technique has had no field use and does require additional development in the error criterion and to accommodate surface pressure variations. It is clear that in operational usage only moderate computer core storage capability is required for either of these techniques and that the data processing can accommodate a 30-minute scan cycle time.

8. Finally, it is recommended that final selection of a single technique for operational usage be deferred until a statistically sound comparative field evaluation of all available techniques can be performed.

1.3 ORGANIZATION AND CONTENT OF THIS REPORT

Each of the remaining four sections of this report is devoted to a particular topic.

Section 2 is devoted to the simulation discrepancy. Participation in the various field experiments is described, and the significant results leading to establishment of the discrepancy are presented. Efforts to identify and account for the simulation discrepancy are described. Finally, this section discusses the present state of the art for simulating the observed antenna temperatures and the impact of this capability upon system performance.

Section 3 describes the data processing techniques. Specific work performed in developing each technique is discussed, results are presented, and hardware and software requirements to implement each technique

are indicated. The present status of development and areas of possible future improvements are indicated. Finally, results of a comparative evaluation of the techniques are given for five typical meteorological conditions.

Section 4 is a discussion of the effects of a non-ideal antenna pattern, with a detailed description of our method of formulating the analysis of these effects. Results and implications of our analysis of the MK I system are given. Evaluation of several antenna types is given, including that of the fan-beam antenna originally proposed for MK II. Performance estimates are shown for a prototype antenna optimized for use in the MK II system.

Section 5 contains the conclusions derived from this work and their implications. Recommendations for future action are suggested.

SECTION 2

SIMULATION DISCREPANCY

2.1 INTRODUCTION

This section describes the work performed to arrive at an adequate experimental verification of our simulation and, conversely, a proper simulation of our measurements. This absolute agreement between simulation and measurement is necessary because each data processing technique employs the basic principle of comparing measurements from the real world with predictions (simulations) from various assumed hypothetical models of the real world. Each simulation is compared with the real measurement until the model is found (from the ensemble of available models) which produces the smallest resultant error. It is then assumed that that particular model is representative of the real world. It is obvious that such an approach necessarily requires that measurement and simulation give the same result when both are derived from the same model or real atmosphere. Furthermore, to be certain of the "universal" applicability of the simulation and the measurements, the real and model atmospheres used should represent a wide range of climatological conditions and/or locations.

The field experiments, to be described later in this section, were designed to accomplish a double purpose. In the first place, radiometric measurements were "inverted" by the various techniques and the resultant air temperature profiles were verified using the directly measured profile. This aspect is discussed in Section 3. The second application is just the reverse, where the directly measured profile was used as a model from which to simulate or predict the measured quantity. Verification of the simulation was accomplished by comparing the predictions with the actual radiometric measurements. This aspect is the subject of this section.

Before proceeding to discussion of the experimental verification, it will be helpful to the reader to introduce the concept of antenna temperature. Antenna temperature is a fictitious, or effective (integrated), radiative temperature at the "input" (feed point) of an antenna system; it should not be confused with the kinetic temperature of the antenna structure.

In the context of this report, antenna temperature differs from source brightness, or simple brightness temperature, in that the former is the integrated, weighted resultant of energy from many directions impinging upon the collecting area of the antenna, whereas the latter term is a property of the source (atmosphere) in one ray direction. (This distinction is more clearly defined in Section 4.) Furthermore, antenna temperature differs from the effective radiative temperature seen at the physical output terminal(s) of the antenna structure. This difference is due to resistive power losses in the antenna's metal conductors and associated feed lines and to the noise power emitted by that resistance at the physical temperature of the metal structure. Thus, antenna temperature is not a directly measurable quantity but can only be estimated by correcting the radiative temperature seen at the output terminals (we have called this quantity the "calibration temperature") for the contribution due to losses.

2.2 ESTABLISHMENT OF THE SIMULATION DISCREPANCY

The text of this section briefly describes the highlights of our participation in a series of field experiments, conducted by the Government, which led to a definitive establishment of the simulation discrepancy. The subsequent search for the specific cause, among the likely possible causes, is discussed. Finally, an assessment of the present simulation capability is given.

2.2.1 Clearwater Acceptance Test

Under separate contract with the Government, Sperry Microwave Electronics Division provided electrical and mechanical maintenance, sensitivity improvement, and additional calibration for the MK I THERMASONDE. In 1970 September, APCO personnel, along with representatives of SMED and SRRC, conducted a field evaluation and acceptance test at Clearwater, Florida. This occasion was also used to operationally test the analog model technique for processing THERMASONDE data and to inform and indoctrinate Environmental Meteorological Support Unit (EMSU) personnel from St. Louis in operation of the THERMASONDE. For this field experiment SRRC prepared and provided a limited library of model scan overlays (see Sec. 3.2.2) which were visually compared with the strip chart record from the MK I scans. SRRC also loaned to the Government a strip chart recorder and auxiliary equipment needed to produce a permanent record of the MK I scans in a format compatible with the model scan overlays. This brief experiment showed that the MK I was opera-

tionally satisfactory and that the reduction in system noise achieved allowed more significant comparisons between measured scans and simulated ones.

Systematic differences between the observed scan records and the analog model scans were noted for the majority of scans. The consistency of these differences raised suspicions about the performance of the MK I and the simulation model that was used to obtain the analog model scans. Since the analog model scans (not scans simulated from air temperature profiles existing during the observation) were compared with the observed scans, positive proof of a discrepancy between simulation and observation could not be established at that time.

This experiment did establish the real-time applicability of the analog model technique and the results were sufficiently encouraging to warrant refinement for use at St. Louis.

2.2.2 St. Louis EMSU Field Evaluation

In 1970 October, SRRC provided technical services to APCO during a field evaluation test of the MK I THERMASONDE conducted at St. Louis, Mo., by an Environmental Meteorological Support Unit of the Weather Bureau. Our participation in the experiment was limited to providing instruction on the physical setup of equipment, the procedures for calibration and operation, and the process of translating the radiometric data into temperature-height profiles. We provided a library of model scans, applicable to the fall season at St. Louis, for use with the analog model technique. After two days' indoctrination, EMSU personnel were sufficiently skilled to proceed on their own.

Later, copies of the MK I records and the corresponding radiosonde sounding data were independently analyzed by SRRC personnel. The data were analyzed both from the standpoint of testing the performance of the analog model technique in inverting the radiometric data and also in testing the correspondence between radiometric measurements and their corresponding simulation. Our selection of the "best fit" models corresponded with those of EMSU in most cases, with only minor differences in selected profiles for the remaining cases. In a few instances, precipitation and/or very low clouds precluded the possibility of any good selection by either EMSU or SRRC. Such

conditions have little importance from an air pollution trapping point of view; therefore they do not represent a serious operational deficiency of the THERMASONDE system.

Some of the St. Louis radiosonde sounding data were used to simulate the observed brightness distributions. This was accomplished in the usual manner by extrapolating the on-site RAOB data with time-related, upper-level data obtained from routine synoptic soundings made at a nearby U. S. National Weather Service Station. Source brightness temperatures were calculated for a set of discrete elevation angles using our formulation of the radiative transfer equation. The calculated brightness temperatures were plotted as a function of elevation angle on a coordinate system corresponding with that on the MK I strip chart record. Transparent overlays of observed antenna temperature versus elevation angle distribution were made from the scan recordings. Visual comparison of the two graphs for each scan showed a gross similarity of form, but observed records showed less temperature change with elevation angle than did the simulation. The main features of this discrepancy were relatively consistent for the scans in this sample, except for the one case of ground-based inversion conditions. Unfortunately, the high incidence of thick, low clouds and the fact that many of the radiosonde observations were made in downtown St. Louis (12 miles from the MK I site) made only a few of the cases suitable for accurate analysis. There were not enough cases to establish with confidence whether the discrepancy was a fluke, due to human error in the MK I operation, or caused by some unknown factor peculiar to the St. Louis site.

The St. Louis experiment was significant in at least three respects. First, it revealed a heretofore unobserved difference between measurement and simulation. Secondly, it showed the practical utility and value of the THERMASONDE system in the context of an operational air pollution monitoring environment. Finally, it gave user-operators first-hand experience in its use and an opportunity to reflect their reactions and desires into the system design.

2.2.3 Raleigh Experiments

During 1970 December, the MK I THERMASONDE was operated by APCO personnel at Raleigh, N. C., for the purpose of operationally evaluating the analog model technique. Following the experiment, copies of the observed data were sent to SRRC for independent analysis. The data were processed in the

manner described above to show the comparison between simulated and measured brightness temperatures. The discrepancy observed earlier in the St. Louis data was also seen in the Raleigh data. This was a sample of about 70 scans, most of which were obtained during clear-sky conditions with excellent space and time correlation between the MK I and radiosonde observations.

In Figs. 1 and 2 are shown MK I antenna temperature and computer-simulated brightness temperature scans for Raleigh, N. C. On-site radiosonde data taken during the MK I scans were used to compute simulated scan data. The air temperature profiles existing during the MK I scans were, respectively, a ground-based inversion and an elevated inversion for the times 0618 and 1417 EST. The curves were translated to correspond at zero degrees; therefore, the smallest brightness temperature discrepancies are seen in the lowest elevation angles, whereas above 30 degrees the differences begin to increase more rapidly--reaching their largest difference at 90 degrees. The data in these figures typify the discrepancy between simulation and observation that has been noted for all cases that have been employed in the discrepancy study.

The Raleigh experiment data confirmed that a discrepancy existed between the measured and calculated variation of brightness temperature with elevation angle. Further, it was established that the magnitude of this brightness distribution distortion was on the order of 3 C. This temperature error was too large to be explained by any reasonably anticipated malfunction in THERMASONDE operation. The most significant result of the Raleigh experiment was that the MK I THERMASONDE system was capable of meeting the user requirements for indicating mixing layer depth despite the existence of this simulation discrepancy.

2.2.4 Boulder Experiment

The Sperry Rand Research Center was requested by APCO to participate in a multi-faceted cooperative field experiment sponsored by the Wave Propagation Laboratory of the NOAA Environmental Research Laboratory. This experiment brought together thermal and acoustical indirect sensors and balloons and aircraft-borne direct sensors. This array of atmospheric sensors was to provide a comprehensive and, hopefully, definitive picture of the dynamic state of the atmosphere.

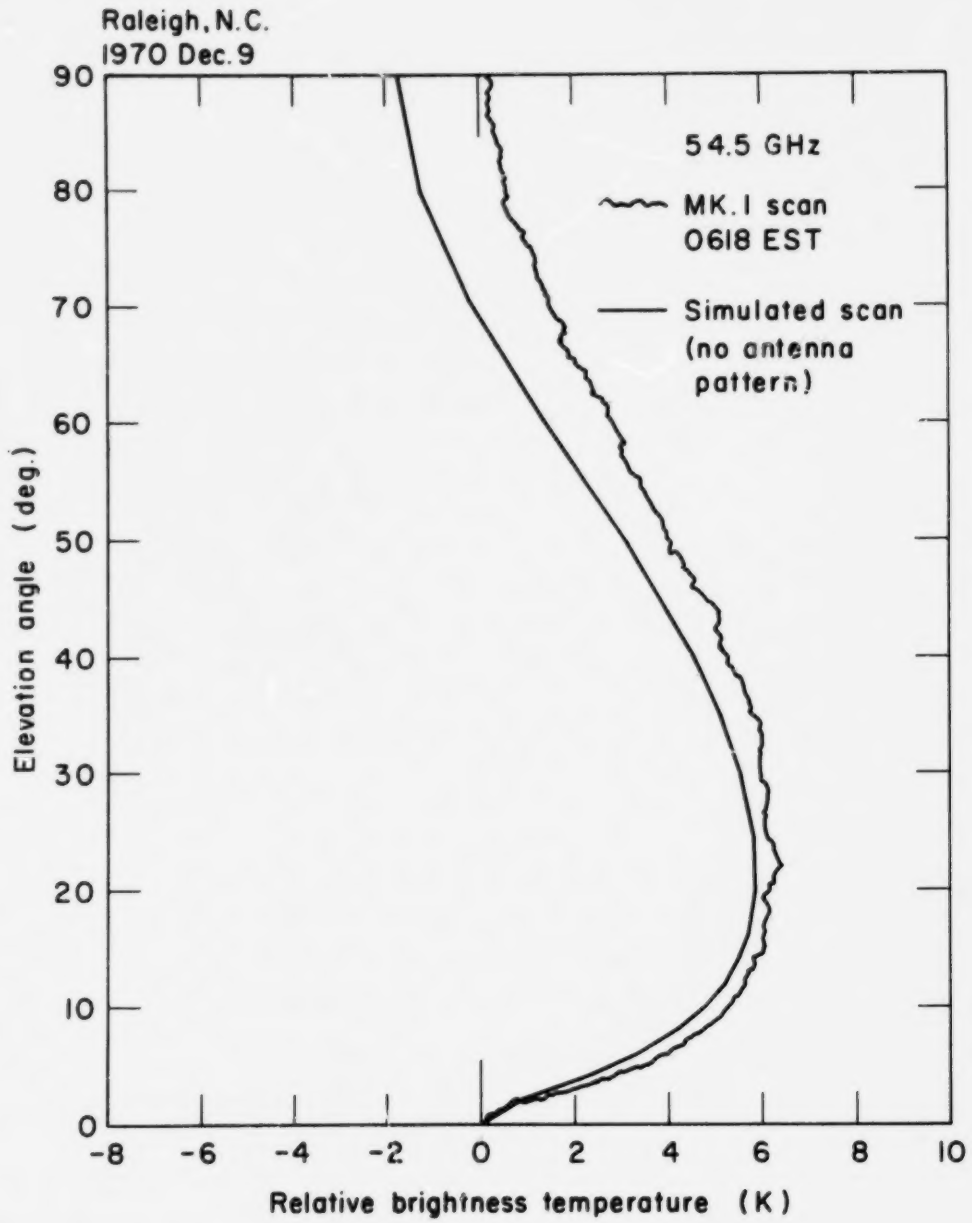

FIG. 1 Comparison of simulated scans and MK I scan for Raleigh, N.C., 0618 EST, 1970 December 9.

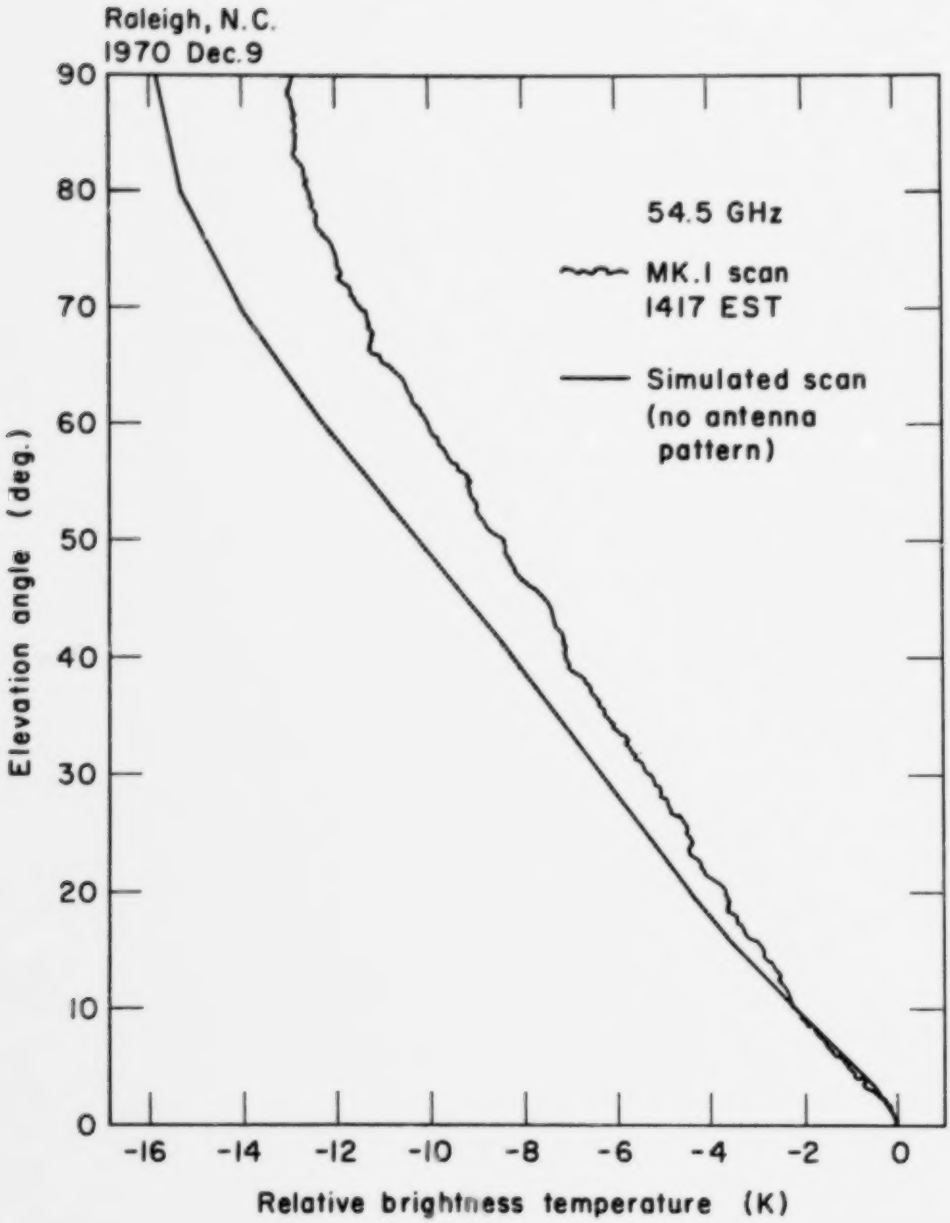

FIG. 2 Comparison of simulated scans and MK I scan for Raleigh, N.C., 1417 EST, 1970 December 9.

Our participation in this experiment required considerable preparatory effort. To use the analog technique, a library of model scans applicable to the site and season was prepared. Model temperature profiles were defined, brightness temperature calculations were made, and transparent overlays were produced. Calculations for this library were performed for an operating frequency of 54.5 GHz and an upward scan rate of 4 degrees per minute. In order that the known discrepancy between observed and measured brightness distributions would not unfavorably bias the analog technique, the artifice of arbitrarily increasing all calculated absorption coefficients by 10% was employed. This had the effect of reducing the overall change in calculated brightness without seriously altering the relative shape of the brightness distribution.

Since it was desired to also perform on-site processing of the observed data using the gradient altitude model technique, a special deck of program cards was prepared in a form compatible with the WPL CDC 6600/3600 computer. A test case was prepared and run for verification, by WPL personnel, that the program was indeed compatible and performed properly.

The temperature control system in the MK 0 equipment was modified to minimize a problem with frequency stability of the local oscillator and long-term stability of the electronics. The frequency meter was recalibrated to correct for its operating at an elevated temperature. Finally, the temperature calibration was re-established at the desired operating frequencies. All modification and calibration work on MK 0 was performed at no cost to the Government.

The Boulder experiment was initially scheduled for 1970 November and was rescheduled several times at the convenience of the Government. It was finally performed in 1971 April.

Subsequent analysis of the Boulder data also revealed the same type discrepancy observed at the other locations. These data, obtained at 5400 feet above sea level, along with the data for St. Louis and Raleigh (which are much lower in elevation), substantiate the discrepancy's existence and persistence and establish that it is not a location-related phenomenon.

2.3 SIGNIFICANCE OF THE DISCREPANCY

Existence of this discrepancy has important implications regarding the accuracy with which any data processing techniques can invert radiometric data into indicated air temperature profile information. It means that the inverting process compensates for the discrepancy by altering the indicated profile from what would have been produced had no discrepancy existed. In other words, the processing technique is biased by the discrepancy to produce a poorer indication of the true air temperature profile. Therefore, in order to realize the full potential of any data processing technique it is imperative that the discrepancy be eliminated, or at least reduced as much as possible.

Thus it was empirically indicated that: (a) the discrepancy was real and not a fluky occurrence, (b) it was apparently related to inadequate or improper simulation of the measuring process, and (c) it was of sufficient magnitude to be significant for low-level temperature profile monitoring purposes. On this basis, a search for the cause(s) of the discrepancy was warranted and indeed required.

2.4 POSSIBLE CAUSES OF THE DISCREPANCY

At the outset of the search for the discrepancy it was not known whether the differences were due to simulation inadequacies or to deficiencies in the equipment, or to both of these. Because of the large number of possible causes, it was necessary to plan the attack on the problem instead of proceeding haphazardly. Thus a list of possible sources of the discrepancy was created, including a method of attack for each possibility. These are shown in Table I. Those possibilities which were pertinent to design of the MK II THERMASONDE were given priority in order to allow for modifications in its design within the necessary timetable should modifications become necessary.

Studies indicated that a number of these possible sources could be readily tested as causes of sizeable simulation-observation differences, whereas others were difficult to prove or disprove as being the cause. For example, the frequency meter of MK I could easily be checked to see if a slight error in its indication could cause an error in the desired operating frequency large enough to produce the differences between simulation and observation that had been noted. On the other hand, to establish oxygen absorption coefficients as

TABLE I

IMPACT OF OBSERVED VERSUS SIMULATED BRIGHTNESS TEMPERATURE DISCREPANCY

Possible Source	Degree of Difficulty and Suggested Method of Identifying the Cause	Relevance to Equipment Design	Status of Work on the Problem
1. Frequency uncertainty or offset	Moderately easy. Accurately calibrate working frequency meter and carefully adjust operating frequency at time of observation.	Very relevant to MK II design specifications concerning frequency stability and precision and accuracy.	Determined that the use of 54.6 GHz gave calculated T_B records that correspond better to measured records than did 54.5 GHz. This apparent 0.1 GHz difference between intended operating frequency and the actual operating frequency has not been borne out by frequency measurements on the MK I.
2. Bandpass characteristics of radiometer	Very time-consuming to do in detail. Calculate T_B records at many frequencies spanning the bandpass and then perform a weighted average with the bandpass function being the weighting function. Compare weighted average T_B record with actual.	Very relevant to MK II design specifications. Single side band radiometer would be very desirable, but prohibitively expensive.	Made cursory investigation of this cause. Concluded that the magnitude of the effect was considerably less than magnitude of discrepancy.
3. Antenna gain pattern	Requires modeling and computer programming of the assumed axially symmetric 3-dimensional antenna pattern in a three-dimensional field of incident radiation. Radiation field assumed axially symmetric about a vertical axis in the earth reference frame.	Very relevant to MK II antenna design.	This model has been computer-programmed and tested on several profiles for which existence of the discrepancy has been verified. Inclusion of the antenna pattern eliminates most of the discrepancy. More work required to properly include ground contributions to T_B.
4. Finite differencing in the numerical integrations of our models	Moderately easy, provided there is an error in the logic and it can be found. Repeat simulation calculations with different step sizes in the T_B integral equation and in the filter function used to obtain the scanning effect.	None.	Preliminary investigations showed that the magnitude of the effect due to this cause should be less than the discrepancy.

Impact of Observed Versus Simulated Brightness Temperature Discrepancy - Cont'd

Possible Source	Degree of Difficulty and Suggested Method of Identifying the Cause	Relevance to Equipment Design	Status of Work on the Problem
5. Oxygen absorption coefficient	A direct detailed investigation difficult. Would involve analysis and measurement of the spectroscopic constants in the microwave spectrum of oxygen. Alternative indirect approach is to intuitively change the constants in such a manner as would improve the agreement between measured and calculated THERMASONDE records, then test the new empirically determined constants on independent data.	None	Preliminary investigation showed that the effects of this cause were almost equal to that of Cause 1. Modifications to the calculated absorption coefficient of about +7 or 8% seem to result in the best correspondence between measured and calculated T_B records. The accuracy of the physical mathematical models for O_2 absorption results in differences greater than 5% between measured and calculated values.
6. Absorption coefficient dependence on pressure and temperature	Same type of problem as No. 5. Would choose the indirect approach.	None	Preliminary look at temperature dependence. Does not seem to be a likely cause thus far.
7. Index of refraction	A moderate complication to our models and programs. Not yet incorporated. Would introduce considerable complexity if incorporated with a three-dimensional antenna gain pattern as well.	None	Discussions with E. Westwater at NOAA, Boulder, indicate that the magnitude of the difference between low-angle T_B's calculated when refraction is taken into account and not taken into account is on the order of .2° K. Considerably less at higher elevation angles.
8. Incorrect water vapor profile	Moderate. Requires more reliable water vapor profiles than those obtained with our RAOB's.	None	Cursory investigations show that even grossly erroneous water vapor profile data could not account for more than a fraction of the discrepancy.
9. Incorrect water vapor absorption	Same type of problem as No. 5. Would choose the indirect approach.	None	Still using published water vapor absorption. Results of work on Problem No. 8 indicate that this cause alone could not account for more than a fraction of the discrepancy.

Impact of Observed Versus Simulated Brightness Temperature Discrepancy - Cont'd

Possible Source	Degree of Difficulty and Suggested Method of Identifying the Cause	Relevance to Equipment Design	Status of Work on the Problem
10. RAOB profile not measuring same T, P, and R.H. profile that is being observed by THERMASONDE	Very difficult, if not impossible. RAOB's only practical method for getting the profile at the higher altitudes even if helicoptors used for low altitudes.	None	None
11. Factory calibration inaccuracies (after assembly of THERMASONDE)	Moderate. Check calibration by two independent methods: 1) Anechoic chamber (direct), 2) calibration temperature input (indirect).	Pertinent to design of MK II. Design influences the technique, implementation, and accuracy of calibration process.	Confirmed that both methods give comparable results.

the cause would be a much more difficult problem. Present models of the coefficients are based upon assumptions that are questionable due to gaps in the fundamental knowledge of absorption and, for this reason, could not be readily shown to be or not to be the discrepancy cause.

2.5 ELIMINATION OF CAUSES

Consideration of the information in Table I suggested that sources 1, 3, and 5 were the most likely possibilitities and, therefore, the ones to address first. On the basis of the preliminary and cursory work indicated in the "Status..." column, all other sources were provisionally eliminated from more detailed investigation.

Since the observed discrepancy looked like that which would be obtained from a frequency error, and since this question could be easily resolved experimentally, a check of the frequency meter calibration was performed. In 1971 January, the frequency meter from the MK I THERMASONDE was received at the Research Center for calibration verification. This meter, Microlab/FXR Model M410-X, Serial No. 384, was compared with a working standard instrument TRG Model V551, Serial No. 30. Calibration of the working standard was established at SMED using an accurately set low-frequency oscillator and a harmonic multiplier to produce a known standard frequency. Initial calibration of the working standard was performed on 1970 December 12 and a correction curve for the MK I meter was given to APCO on 1971 January 13. Since then, a more accurate determination of the working standard calibration was obtained, and MK I frequency meter calibration was repeated on 1971 February 14. This calibration was established to an accuracy of better than 0.005 GHz (approx. 0.01%). The original correction curve was corrected accordingly and a revised correction curve for the MK I instrument is shown in Fig. 3. The results of this frequency meter calibration show that the meter was not significantly in error under the laboratory conditions existing at the time of calibration. Thus, it was quite difficult to attribute the discrepancy in observed brightness distribution solely to an error in the frequency meter.

Oxygen absorption coefficients used in brightness temperature simulations were suspect due to the methods that have been employed to estimate the line-broadening parameter. Elaboration on this subject is given by Carter, et al[1]. The accepted expression for the line-broadening parameter was given

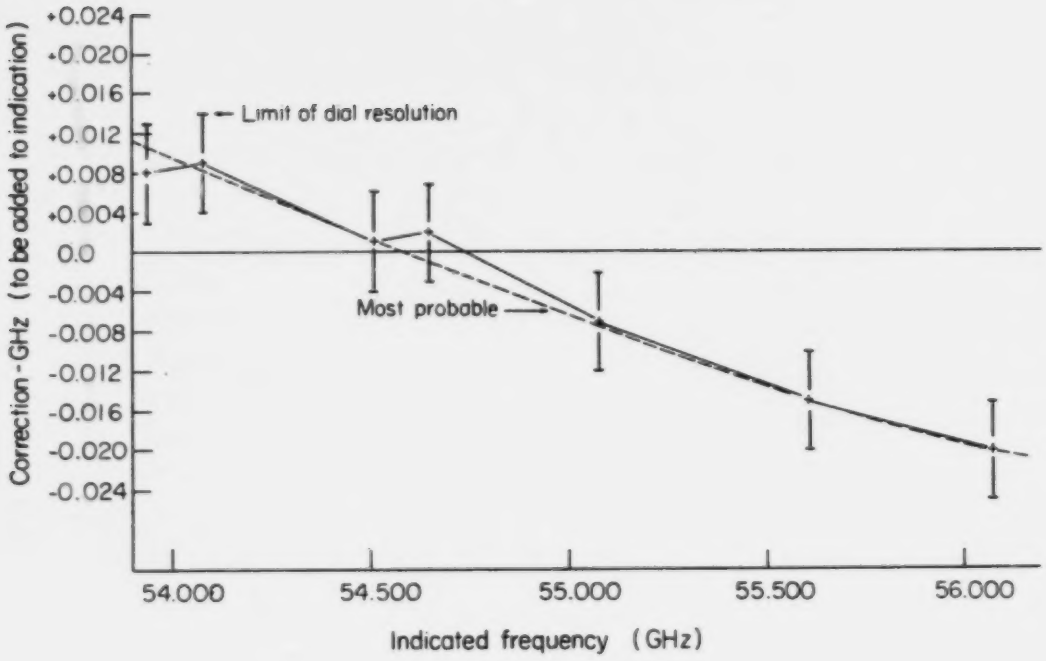

FIG. 3 Revised correction curve for MK I frequency meter.

by Meeks and Lilley[2] in 1963 and contains a collision efficiency parameter whose value and variation has only been inferred from limited laboratory simulation or modeling. There is no known direct corroboration for the atmospheric environment.

In order to test the sensitivity of the simulation model to absorption coefficient changes, brightness temperatures were calculated for observed temperature profiles from several locations with the oxygen absorption coefficient equation modified to introduce a 10% increase for these simulations. In general, this increase in absorption yielded somewhat better fit between the simulated and the observed MK I scans than did the simulations without the absorption increase. For the Raleigh cases the fits were good; but the Boulder cases did not fit as well, although they were better with the 10% increase than without it. Thus, it was found that for near sea level stations, small changes (10%) in absorption coefficient values produced an alteration in the simulated brightness distribution on the order of the observed discrepancy. However, since there is no justifiable physical basis for altering the existing absorption coefficient model and since using an arbitrary increase was not efficacious for all locations, investigation of this possible cause for the discrepancy was not pursued further.

Until 1971 July, our computer simulation did not include effects of the antenna power response pattern. In July, a computer program incorporating the MK I antenna pattern was tested in order to more accurately synthesize the observations. (For a detailed discussion of this program, see Sec. 4.) Simulations with the antenna pattern included showed a reduction in the discrepancy. Additional tests were made on a variety of temperature profiles for which MK I scans were available. These cases were taken from the sample used to establish the discrepancy. In all these tests the discrepancy was reduced by including the effect of the antenna response pattern. Figure 4 presents one of these cases, showing the simulation with the antenna pattern falling much closer to the MK I observed scan than does the simulation without the antenna pattern.

One consequence of a finite beam is that incident energy from the ground (soil and vegetation) is sensed through the main, side, and back lobes. As the antenna elevation angle changes during a scan, the ground contribution changes. Thus, computer simulations must be performed with the correct antenna

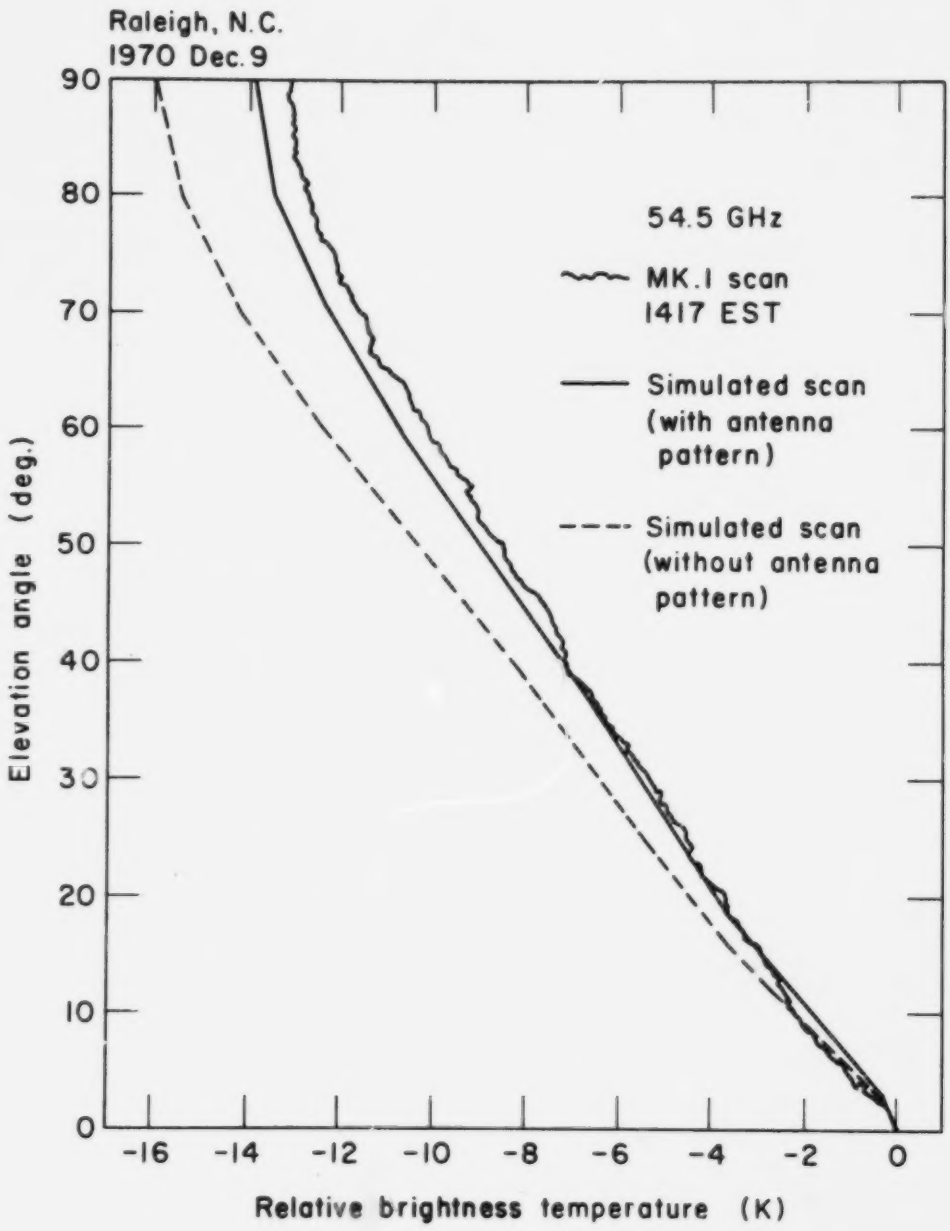

FIG. 4 Comparison of MK I scan and scans simulated with and without antenna pattern correction.

gain pattern and with a knowledge of the radiative characteristics of the ground. If the ground conditions are not known, radiometric simulation cannot be performed properly. This fact is depicted in Fig. 5, which displays a MK I scan observation and a simulated scan with the MK I antenna pattern for a case in which the ground conditions were not known. Since the ground temperature was not known at observation time for this simulation, ground temperature was taken to be the air temperature a few feet above the ground. Lack of agreement between the MK I and the simulated scans shown in this figure is attributed to this factor. This scan was made during ground-based inversion conditions in the early morning when it was likely that ground temperature was actually colder than that assumed for the simulation. Consequently, the zero degree simulated temperature is overestimated and the curve appears offset in the colder direction from the measured MK I scan. During the hottest times of the day, ground temperatures may be warmer than air temperatures, but whatever the time of day, it is necessary to have a measure of the ground temperature in order to provide accurate simulation.

2.6 VERIFICATION OF SIMULATION CAPABILITY

The previous four sections of this chapter describe efforts to improve our ability to simulate observed brightness distributions on a digital computer. This section is a brief summary of our present simulation state of the art and an operational assessment of that capability. Here it is desired to establish quantitatively the degree of correlation between measurement and simulation. Data from the Boulder experiment were used for this study. A brief description of the experiment and its results follows:

The primary objective of our participation in the experiment was to assist in evaluation of the accuracy and precision of the WPL four-frequency radiometer system and the Sperry Rand angle-scanning THERMASONDE system. In addition, it was desired to compare the capability of various techniques for deriving mixing layer depth from brightness temperature data. There were also secondary and tertiary objectives of interest to other associated experimenters, but these are not discussed here. Participants and their activities which have a pertinent association with this contract included:

1. Sperry Rand Research Center
   - Operation of the MK 0 THERMASONDE system in the null-

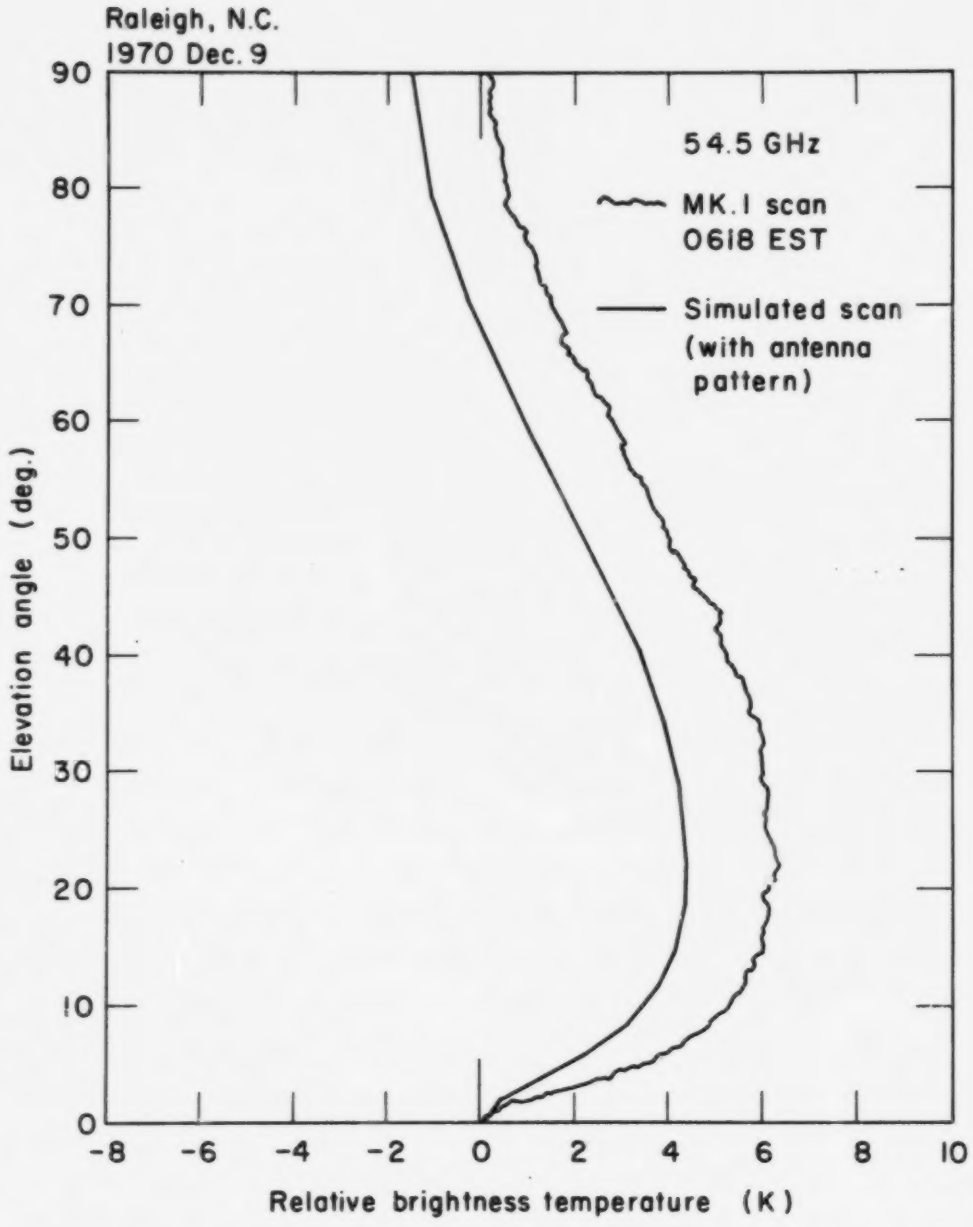

FIG. 5 MK I and simulated scan without ground temperature data.

balance, discrete angle scan mode at 54.5 GHz.

2. Air Pollution Control Office
   - Operation of the MK I THERMASONDE system in the non null-balance continuous angle scan mode at 54.5 GHz.
3. Wave Propagation Laboratory
   - Operation of the WPL radiometer in the non null-balance multi-frequency, discrete angle scan mode. (Frequencies were 52.5, 53.5, 54.5, and 55.5 GHz.) Operation of the surface meteorological sensor system, the radiosonde system, and the instrumented aircraft system.

The experiments were conducted at Building T-22 of the WPL Table Mountain Field Site near Boulder, Colorado. Each participant performed his own observations and measurements during two-hour observation time intervals, commencing daily at 0400, 0900, and 1500 hours MDT.

Data were obtained by SRRC personnel throughout the following time intervals:

Date	Observing Time Interval MDT (nominal)
27 April	1000 - 1130 1500 - 1632
28 April	0400 - 0545 0900 - 1045 1500 - 1621
29 April	0400 - 0544 0900 - 1049 1500 - 1655
30 April	0400 - 0536 0900 - 1037 1500 - 1617

Observations of the following parameters were made aperiodically throughout the observing intervals and data were manually recorded along with the observation time.

1. Measurements of 54.5 GHz calibration temperature (K) at elevation angles of 0, 5, 10, 15, 20, 30, 45, 60, 75 and 90 degrees. (These data are correctable to antenna temperature.)
2. Observations of present local weather.

3. Estimates of sky cover (%), visibility (mi.), cloud type, cloud amount (%), and cloud height (ft.).
4. Measurements of surface pressure (mb), surface dry-bulb temperature (C), surface wet-bulb temperature (C), soil temperature (C), and air temperature at 35 feet (C).

APCO and WPL personnel obtained companion data during these same observing time intervals. Each participant was responsible for reducing and processing his own data, and there was to be free interchange of data among each of the principals.

Delay in starting the experiment and in reducing the RAOB data to usable temperature, humidity, pressure, and height information precluded complete analysis of all the available data. In particular, it was not possible to perform all the inter-comparisons of results from the different sensors.

Ten of the eleven RAOB temperature profiles were used to calculate source brightness temperature distributions, integrated antenna temperature distributions, and scanned antenna temperature distributions. The first two distributions are for an infinitely slow scan, i.e., null-balance, and the third distribution is for a 4-degree-per-minute upward scan. The null-balance calibration temperatures observed with MK 0 were corrected for antenna line loss contribution and produced 10 sets of null-balance antenna temperatures at each of the 10 discrete elevation angles. Seven of the eleven continuous angle scans made with MK I had the balance attenuator setting recorded. This made it possible to sample the scan record at each of the elevation angles and obtain 7 sets of scanned antenna temperatures at 10 elevation angles. The antenna temperature values, calculated from the appropriate RAOB sounding, were subtracted from the corresponding measured values to give the error or simulation discrepancy. The results are tabulated in Tables II and III. Only six runs are shown for the MK 0 data because the other four clearly showed excessive error due to frequency drift throughout the run. Table IV is a statistical summary of these data. The overall average errors for both MK 0 and MK I are not significantly different from zero. This suggests that, on the average, there is agreement between the measurements and the simulation when proper account is taken for antenna pattern effects. At least there is no offset or bias which is greater than the experimental variability. The greatest average error occurs at zero degrees elevation angle for both instruments. This reflects the fact our knowledge of the air

TABLE II

ABSOLUTE TEMPERATURE SIMULATION ERROR

FOR MK 0 THERMASONDE

Elev. Angle (deg.) / Error (C)	0	5	10	15	20	30	45	60	75	90
	+0.3	+0.1	-0.2	-0.1	-0.3	+0.4	+0.3	0.0	-0.2	-0.4
	-2.0	-0.3	0.0	-0.3	-0.4	0.0	-0.5	-0.5	+0.1	+0.3
	+2.6	+1.9	+1.6	+2.1	+1.5	+0.9	-0.6	+0.3	+0.6	+1.1
	-2.0	-0.6	-0.5	0.0	-0.4	-0.1	-0.1	-1.1	-0.9	-0.7
	-0.1	+0.7	+0.4	+0.5	+0.4	+0.7	+0.2	+0.8		+0.7
	-1.9	-0.4	-0.3	-0.2	+0.4	0.0	+0.1	+0.1	-0.1	+0.6

TABLE III

ABSOLUTE TEMPERATURE SIMULATION ERROR

FOR MK I THERMASONDE

Elev. Angle (deg.) / Error (C)	0	5	10	15	20	30	45	60	75
	+0.2	-0.2	-0.8	-0.9	-1.3	-1.2	-1.1	-0.8	-1.0
	-1.7	-0.9	-0.3	-0.2	-0.1	-0.4	0.0	+0.2	+0.3
	+0.5	+0.7	+0.7	+0.4	+0.3	+0.4	+0.3	+0.6	+0.4
	-2.5	-2.3	-2.0	-1.6	-1.2	-0.9	-0.5	-0.1	0.0
	-0.3	-0.1	-0.2	-0.1	0.0	-0.1	+0.3	+0.7	+1.0
	-1.1	-1.0	-0.8	-0.8	-1.1	-0.9	-0.8	-0.4	-0.1
	-1.5	-1.0	-0.6	-0.5	-0.6	-0.5	-0.3	-0.1	+0.3

temperature profile over the valley at and below the height of the THERMASONDE is the least well-known portion of the profile. The consistency of average errors with elevation angle (i.e., less than the standard deviation) indicates that the simulation model accurately predicts the shape, or variation with elevation angle, of the observed antenna temperature distributions. This feature is the most necessary requirement as far as use with data processing techniques is concerned. MK I data suggests a trend of average error, with increasing elevation angle, of about 1 C maximum variation. A residual variation of this magnitude could result from the operating frequency being high by only 20 MHz. This order of frequency error is quite possible considering that frequency was not measured (or adjusted) at the time of observation and that this is about the practical resolution limit of the frequency meter.

TABLE IV

VERIFICATION* OF MEASURED ANTENNA TEMPERATURE

	Elevation Angle (deg.)										
Instrument	0	5	10	15	20	30	45	60	75	90	over-all
MK 0 Average Error (C)	-0.52	+0.23	+0.17	+0.33	+0.20	+0.32	-0.10	-0.07	-0.10	+0.27	+0.08
MK 0 Standard Deviation (C)	1.68	0.85	0.70	0.83	0.68	0.38	0.34	0.60	0.49	0.63	0.85
MK I Average Error (C)	-0.91	-0.69	-0.57	-0.53	-0.57	-0.51	-0.30	+0.01	+0.13		-0.44
MK I Standard Deviation (C)	1.02	0.86	0.76	0.59	0.60	0.53	0.50	0.47	0.57		0.74

* Computed from on-site RAOB and corrected for MK I antenna pattern integration. Ground plane assumed 3 feet below THERMASONDE and emission temperature equal to surface layer air temperature.

On the basis of this small sample of only 7 runs, the data show that measurement techniques (direct and indirect) employed at Boulder are capable of establishing measured and simulated values of antenna temperature to within 0.75 C rms absolute error of each other (approx. 0.3%). This is remarkably excellent agreement considering the wide variety of possible error sources. In particular, it should be recalled that the radiosonde accuracy is on the order of ±0.5 C. Since radiosonde error will not be present in any operational data processing system, the rather more fundamental limitation will be to properly represent a complex and dynamic real atmosphere by a relatively simplistic static model. Given that such a static model does, in fact, truly represent the atmosphere's state over a sampled time and space, it appears that we should be able to predict (simulate) the antenna temperatures measured with the MK 0 and MK I THERMASONDEs to within somewhat less than 3/4 C rms. Such accuracy is usable with existing data processing systems, but further improvement is needed and achievable if their maximum capability is to be realized for determining mixing layer depth and/or estimating inversion intensity and depth.

It is important to remember that the Boulder data were obtained in a setting where ground radiation contribution was minimal. In any real operational situation the ground contribution will be more or less significant, depending upon the setting situation and the antenna beam pattern. It is believed that if ground temperature observations were made and incorporated into the data processing technique a somewhat greater accuracy of inversion could be achieved.

In actual practice, the THERMASONDE measures antenna temperatures, but the data processing techniques predict brightness temperature from an assumed model atmosphere (and ground temperature). We have seen that predicting antenna temperatures can be accomplished in a research context, but that the present formulation is too slow for the iterative processing techniques proposed for operational use. A fast antenna integration algorithm or a predictor of brightness temperature from antenna temperature would be very beneficial.

2.7 SUMMARY

Sperry Rand participation in Government field experiments has produced several significant benefits. Principally, it led to identification of an important limitation of our earlier simulation model. This limitation has been corrected by accounting for off-axis radiation from the ground and sky. It has been shown that our present capability of corroborating measurement and theory is at least 0.75 C rms. This figure includes radiosonde system errors, which can be an important fraction of the total.

In addition, we have seen that careful attention must be given to THERMASONDE operating frequency. It must be maintained within 20 MHz (0.020 GHz) of the desired frequency for accurate measurements. It should be standard operating procedure for both MK O and MK I THERMASONDEs to check and adjust, as needed, the local oscillator frequency prior to each observation interval.

Finally, it has been observed that better simulation can be obtained if ground temperature information is included. An improved antenna system and a good setting situation will materially reduce effects of ground radiation. This is not believed to represent a serious operational limitation for the MK II THERMASONDE.

SECTION 3

DEVELOPMENT OF DATA PROCESSING TECHNIQUES

3.1 HISTORICAL PERSPECTIVE

Work performed under previous contracts has shown that the radiometric brightness temperature of the atmosphere is a complex function of observing frequency and elevation angle and the particular variation of meteorological parameters (temperature, pressure, and humidity) with vertical height. More importantly, it was demonstrated that for a given frequency, it is possible to extract usable information about the air temperature variation with height contained in the brightness temperature variation with elevation angle. Direct analytical inversion techniques have proved very difficult and often unstable, primarily because of measurement error. At the end of the last contract, SRRC had advanced concepts for three fundamentally iterative techniques for inverting observed brightness distributions into air temperature profiles over a limited height range. These techniques are varied in their manner of comparing the observed data with the trial solution, in the number of possible solutions available for trial, and in the criterion for selection of the best fitting solution. It was the goal of this present contract to advance and refine each technique and to indicate the computer hardware requirements to implement each. Since the three techniques are broadly diverse in sophistication, it is likely they will each be most useful or applicable to various operational requirements.

The next three sections discuss each technique in terms of approach, implementation, performance and operational requirements. The final section gives a comparative analysis of the three techniques.

3.2 ANALOG TECHNIQUE

3.2.1 Introduction

The analog technique was developed for deriving air temperature profiles of the lower atmospheric levels for air pollution purposes from radiometric observations. The technique has been applied to MK I THERMASONDE observations taken at several U. S. locations. It has successfully indicated the heights of bases of atmospheric temperature inversions up to the opera-

tional limit of 1.5 km. Less success was noted in the technique's ability to specify temperature versus height gradients, which is partially due to the simulation-observation discrepancy discussed in Section 2 of this report and to the limited number of analog models available for comparison with the observations.

3.2.2 Theory of the Analog Technique

To derive temperature profiles with the analog technique, antenna temperature records are compared to a library of simulated brightness temperature records computed from a large number of air temperature profiles. The library is searched until the best fit between the observed record and a simulated record is found. Having found the best fit, one concludes that the air temperature profile existing during observation is the same as, or similar to, the air temperature profile model used to obtain the simulated record that yields the best fit. Thus one has a specification of the air temperature profile.

The best fit is obtained by visually matching simulated brightness temperature records with the observed record, although in theory the matching can be done by computer, with the library being contained in appropriate form in the computer storage. To facilitate visual matching, the simulated records are contained on transparent overlays which are superposed on the observed record. The overlays are ordered in the library to rapidly locate any desired simulated record. Through experience, one acquires knowledge of brightness temperature patterns for different temperature profile shapes. This fact, in conjunction with the ordering of the library, makes possible selection of the best fit simulated record within a short time after completion of the observation.

3.2.3 The Initial Analog Library

During the previous contract a study of simulated brightness temperature versus elevation angle curves was made for 163 temperature profile models. The analog technique was developed and showed from this study promise of being able to specify air temperature profiles. The 163 profile models and their corresponding simulated angle scans were adopted for use as an analog library. The scans were simulated at 54.5 GHz for a scan rate of 4 deg/min in the upward direction from 0 through 90 degrees elevation angle, and for an integration time of 60 seconds. These parameters were employed during MK I observations; thus the initial analog library was compatible with them.

The initial analog library was tested on real radiometric data obtained by the MK I at Cincinnati, Ohio in 1969 February; at Raleigh, North Carolina in 1969 October; and at Vandenberg Air Force Base, California in 1969 December. The tests were not performed on a real-time basis, but were performed at the Research Center upon advent of the first analog library during mid-1970. The inverted profile results of these tests were shown in the previous final report[3]. The first real-time test of the library occurred during the MK I acceptance test in 1970 September at Clearwater, Florida. The test was sufficiently encouraging to warrant expansion of the analog library to increase its capability for deriving temperature profiles.

3.2.4 Expanded Analog Library

The initial library consisted of lapse, ground-based inversion, and elevated inversion temperature profiles and corresponding brightness temperature models for a surface pressure of 1013.25 mb. All the temperature profile models containing an elevated inversion consisted of the U. S. Standard Atmosphere vertical temperature gradient of -6.5 C/km below the inversion layer and the U. S. Standard Atmosphere (1962) profile above the inversion layer. The Standard Atmosphere temperature profile was also used above inversion layers in the ground-based inversion profile models. The largest inversion intensity was 10 C for both the ground-based and elevated inversion profiles.

Additions to the library included inversion profiles and simulated scans for inversion intensities of 15 C and 20 C for elevated and ground-based inversion profiles, with a temperature gradient of -6.5 C/km below the inversion base for the elevated inversion profiles. Elevated inversions based at 0.75 km were also added to fill in the gap between the elevated inversion models based at 0.5 km and 1.0 km. Further additions to the library were made to increase the analog technique's capability during times when the temperature lapse rate in the lower atmosphere is near the dry adiabatic rate (9.8 C/km). Elevated inversion profile models having a temperature gradient of -6.5 C/km below the inversion bases were modified to change this gradient to -9.8 C/km. Simulated scans were obtained for these profile models and model scan overlays were generated for all of the analog library additions at the same surface pressure, radiometric operating frequency, integration time and scan mode used for the initial library. Thus, the expanded analog library, calculated for a surface pressure of 1013.25 mb, consists of the initial library and the additions

thereto, and contains simulated scans for temperature profile models having inversion base heights, intensities and thicknesses as follows:

Height of Base (km)	Intensity (C)	Thickness (km)
0	0 (isothermal)	0.1
0.1	1	0.3
0.3	2.5	0.5
0.5	5	1.0
0.75	10	1.5
1.0	15	
1.5	20	

Simulated scans for the profile models containing inversions having combinations of the above heights, intensities, and thicknesses that were not considered compatible with atmospheric dynamic characteristics are not included in the library. The additions were completed in time for the expanded library to be used in the MK I operational assessment by EMSU at St. Louis during 1970 October.

The entire library was also assessed by APCO during the MK I observational program in Raleigh in 1970 December, during which time a number of elevated temperature inversions were observed. Figure 6 displays inversion base heights measured by radiosonde and by MK I in conjunction with the analog technique. Although there is some scatter in the points, there is a good correlation between the remote and the in situ measured height.

3.2.5 Boulder Analog Library

In early 1971 a new analog library was required for the upcoming Boulder, Colorado field experiment. Since the simulation discrepancy had been observed for near sea level locations, we could only conjecture whether it would also occur for the Boulder location (5400 feet above sea level). Accordingly, the computer simulation routine was modified (for the Boulder Library run only) to effect a reduction of this discrepancy. The modification increased the oxygen absorption coefficients by 10 per cent over the values used previously.

Simulations of brightness temperature versus elevation angle for

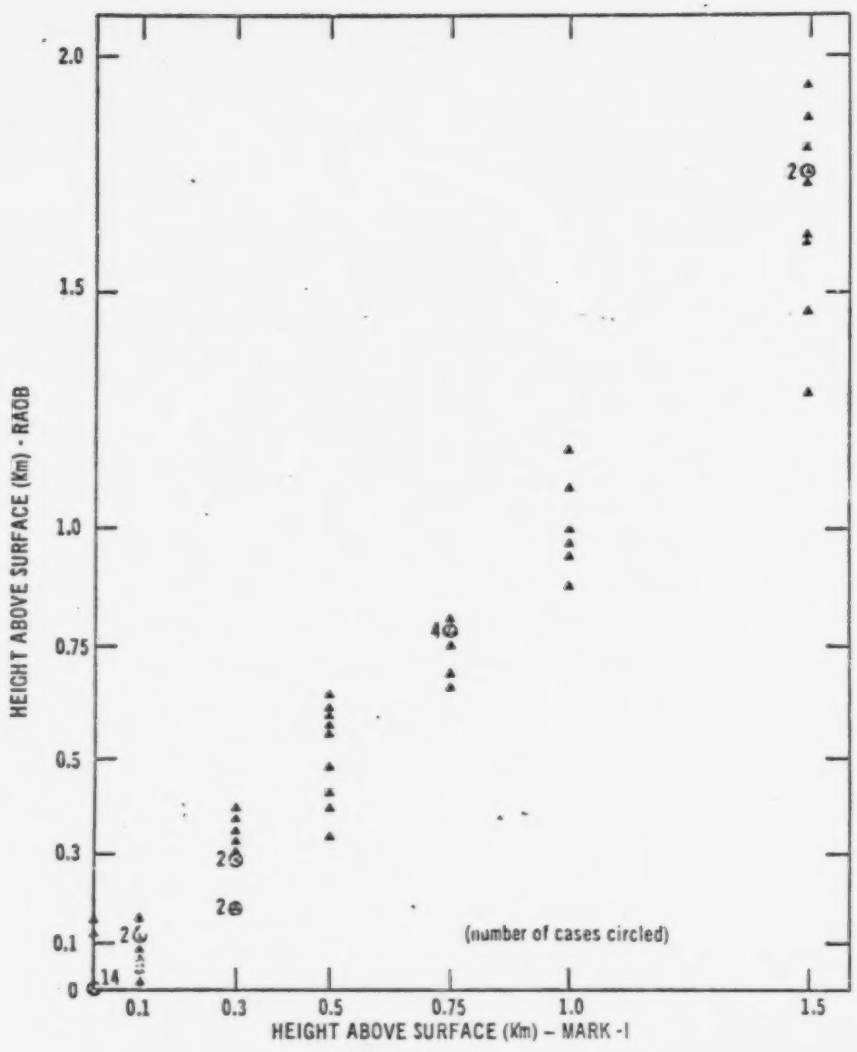

FIG. 6 Correlation between radiosonde-measured and MK I-measured inversion heights. (Courtesy Mr. T. Lemmons, Air Pollution Control Office, Raleigh, N. C.)

the Boulder analog library were performed for a frequency of 54.5 GHz, a 60-second integration time and a scan rate of 4 deg/min. Surface pressure was 830 mb throughout. Lapse, ground-based inversion, and elevated-inversion temperature profile models were used to simulate the analog model scans. Inversion base heights, intensities, and thicknesses are shown below.

Height of Base (km)	Intensity (C)	Thickness (km)
0	0 (isothermal) through 20 in steps of 2 C	0.1
0.1		0.2
0.3		0.3
0.5		0.4
0.75		0.5
1.0		0.75
1.5		1.0
		1.5

Thicknesses of 0.2 and 0.4 km shown in the table were included for only the ground-based inversions and the elevated inversions based at 0.1 km. This yielded 0.1 km increments in thickness up to 0.5 km for these inversion cases.

The Boulder analog library was originally intended to be applied to data obtained at this location during the month of February. In anticipation of this date, available average temperature profiles at Boulder for 1967 December and 1968 March were used to derive an upper level temperature profile which was employed in the computer simulation for generating the analog model scans. An average low-level temperature gradient (-6.4 C/km) was also derived on the basis of the average profiles. This gradient was used below elevated inversions and also in many of the lapse profile models.

A total of 112 multiple-scan overlays constitute the Boulder analog library. One of the overlays, corresponding to several elevated-inversion profile models, is depicted in Fig. 7. The number at the top of each curve is the inversion intensity, whereas the height of the inversion base is denoted by Z and the inversion thickness is given by ΔZ. The temperature gradient below the inversion base is indicated by the indexed section of the library in which the overlay is contained. Since all the overlays have the same scale

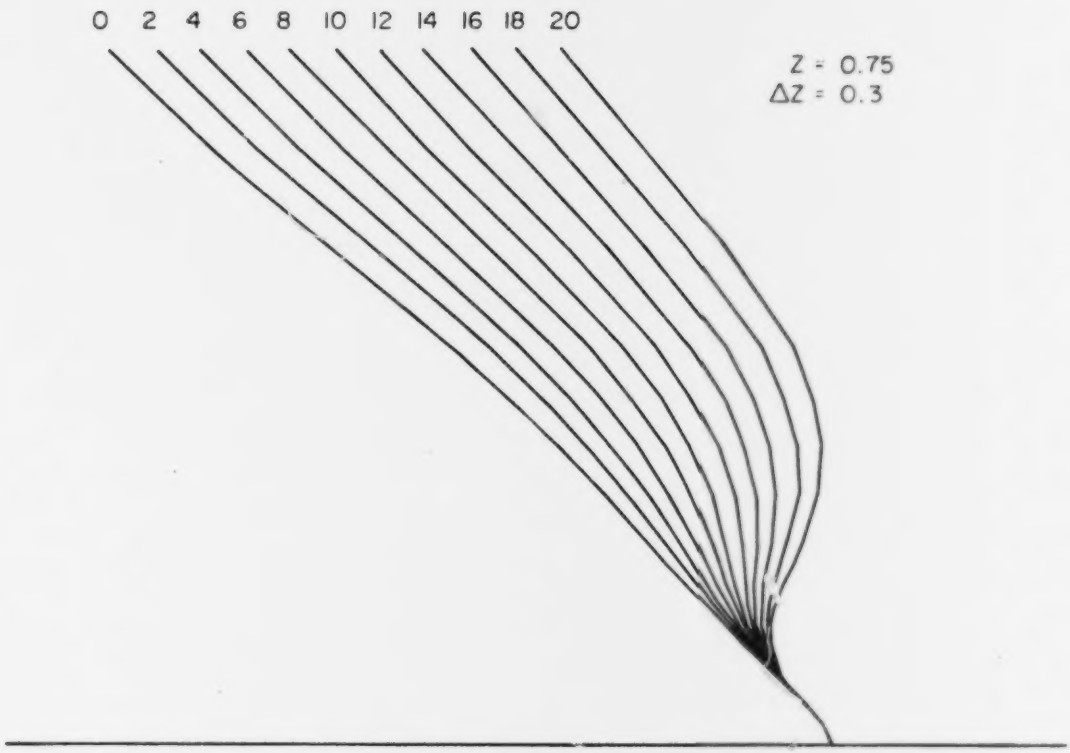

FIG. 7 Boulder overlay format.

factor as the MK I recorder, no numbers are needed on the overlay axes to identify the scale.

3.2.6 Surface Pressure Effects on the Analog Technique

Atmospheric pressure variations are encountered at each observing location. Accuracy of the analog technique depends, to some extent, upon the ability to account for these variations. Figures 8 and 9 show a temperature profile model and the corresponding brightness temperature scans simulated for different surface pressures. The air temperature versus height distribution was fixed, while the surface pressure (and pressure versus height distribution) was changed to obtain the effects of different surface pressures. As shown in the figure, the largest differences in brightness temperature occur at 90 degrees, amounting to about 1 C per 30 mb. Simulations performed in the vicinity of 840 mb surface pressure also show the largest differences at 90 degrees. These differences are of the order of 1 C per 20 mb. Figure 9 suggests a potential difficulty. Suppose THERMASONDE observations were being made at 1031.4 mb, but the only library available was for 1001.3 mb. The discrepancy in surface pressure might be compensated for by erroneously selecting a best-fit model whose corresponding temperature profile was considerably different than the profile existing during observation. This problem is overcome by making available analog model scans at several surface pressures over the pressure range occurring at the station. As the technique's discrimination is increased through inclusion of more library models, its full capability is realized when surface pressure is accounted for.

3.2.7 A Computer Program for Generating Temperature Profile Models and Corresponding Brightness Temperatures.

In the past, construction of analog libraries was slow because temperature profile models used to compute model scan data were derived manually. In addition, a large amount of time was required to keypunch the profile data onto cards. A computer program to automatically generate temperature profile models and their corresponding brightness temperatures was created.

The program uses a four-layer grid within which the temperature and humidity versus height distributions are varied. There are two regimes: the upper, fixed portion and the lower, variable portion. In the fixed profile portion, upper level profiles of humidity and temperature are read in by the user

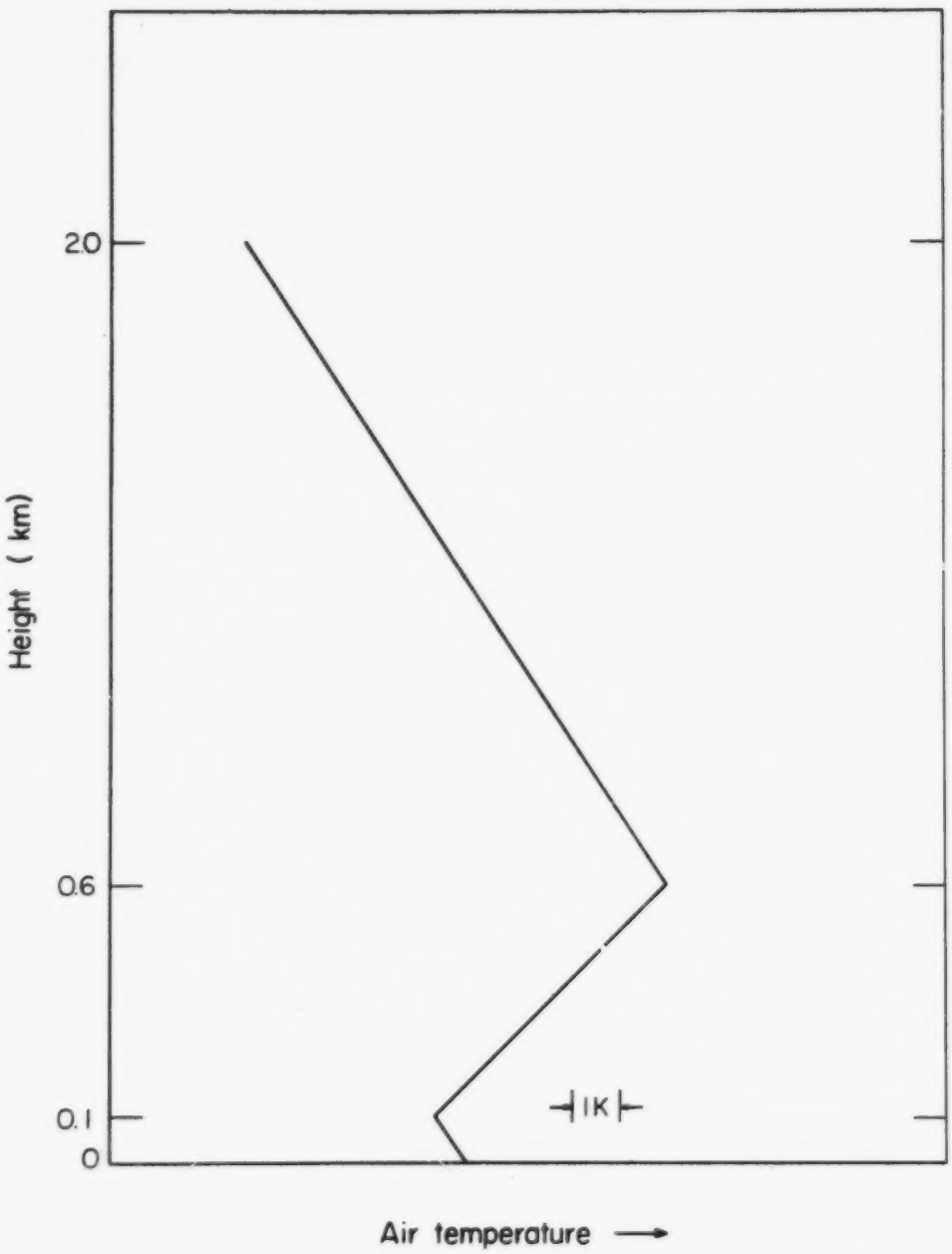

FIG. 8 Model temperature profile.

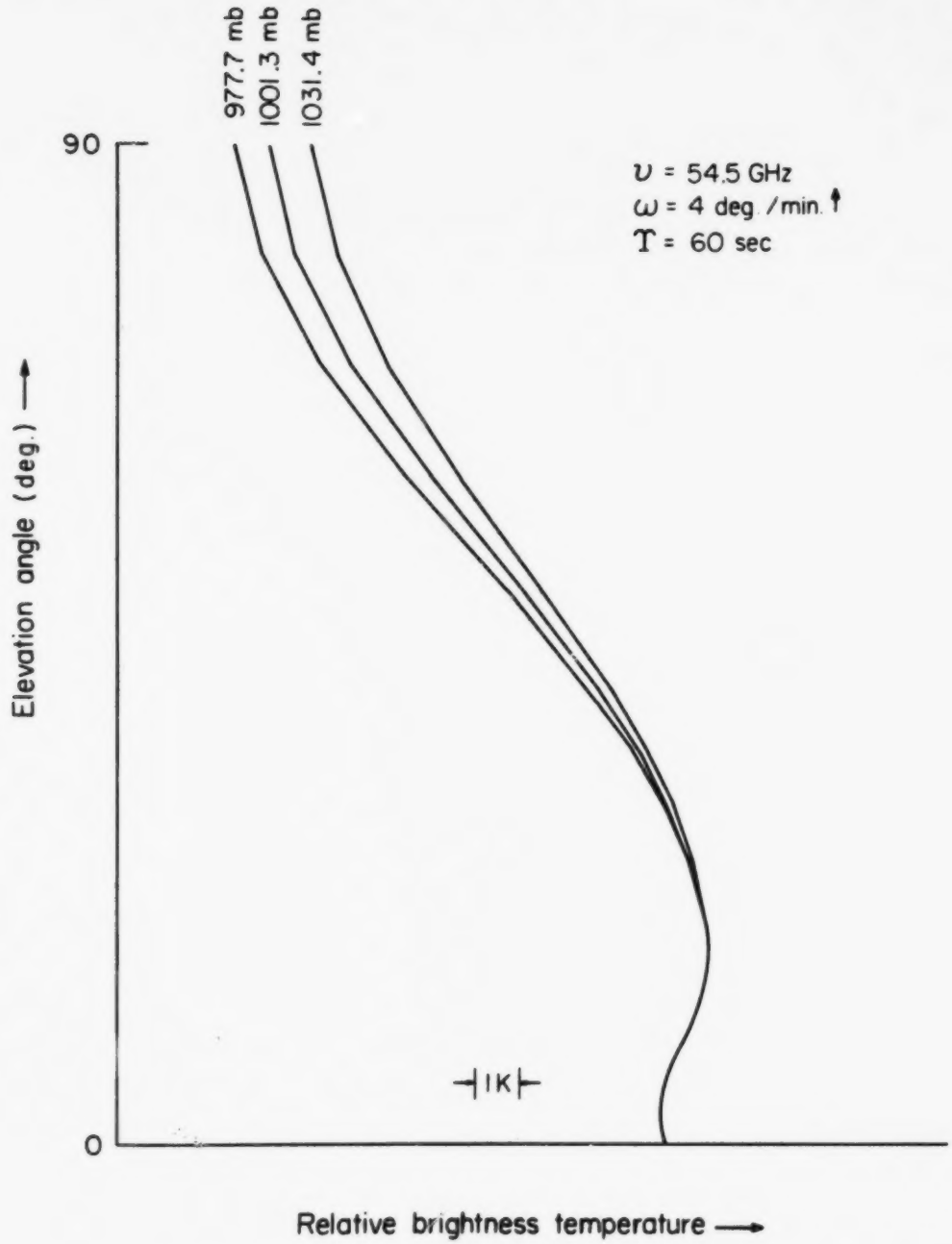

FIG. 9 Brightness temperature scans for different surface pressures.

and remain fixed during execution of all profile variations allowed by the variable profile portion.

The principal input data consists of thicknesses and vertical temperature gradients for each of the four grid layers. The program generates profiles from all of the thickness-gradient combinations. The user specifies maximum allowable temperature inversion intensities and thicknesses for single-inversion and for double-inversion profiles, as well as the greatest height above ground to which superadiabatic gradients are to be allowed. All profiles which exceed these limits are automatically eliminated from entering the brightness temperature computation section of the program.

An additional feature of the program is that several surface pressures can be specified by the user. The program calculates the different pressure versus height distributions for the same temperature and humidity versus height profiles for the several surface pressures. Brightness temperature distributions are calculated at all the specified surface pressures.

The program provides a rapid and easy means for creating temperature profile models and model brightness temperature scans for analog libraries. The only meteorological knowledge required is the aforementioned maxima criteria for temperature inversions and superadiabatic gradients. Input data requirements are minimal because a small number of thicknesses and gradients for each layer yields a large number of thickness-gradient combinations (profiles).

3.2.7 Results of Inverting MK I Data by the Analog Technique

Several simulated and MK I THERMASONDE scans were inverted into temperature profiles using the analog technique. These results are shown in subsection 3.5, where similar results for the GAM and LRRT and analog techniques are compared.

3.3 GRADIENT ALTITUDE MODEL (GAM) RADIOMETRIC DATA ANALYSIS TECHNIQUE

3.3.1 Introduction

The GAM technique, initially developed during the previous contract, is a radiometric data analysis technique specifically geared to the needs of the air pollution meteorologist. The temperature profile model form determined by the GAM, illustrated in Fig. 10, is the same as that of the analog technique. The GAM technique determines particular parameter values of the model tempera-

ture profile shown in Fig. 10. Specifically, they are the heights of first and second break points (Z_1 and Z_2) and the first, second, and third temperature gradients (Γ_1, Γ_2 and Γ_3).

Input data to the GAM is measured antenna temperatures and elevation angles. Observations can be taken in either the angle scan or discrete angle mode. Surface temperature and pressure at the THERMASONDE site are also required. The user must supply: (1) a termination height (pressure) which specifies the maximum (or cut-off) height of the temperature profile to be determined from the measured radiometric data, (2) a residual temperature-pressure profile for the atmosphere above the termination height, and (3) a number of guess-values for each of the GAM parameters*. The user may elect to provide the GAM computer program with an estimated relative humidity profile. If this is not done, the program inserts a fixed relative humidity profile of 0.0% at all levels.

The user may also elect not to supply a residual profile. In this case, the program supplies the U. S. Standard Atmosphere (1962) for use above the termination height.

The procedure for selecting particular parameter values producing a GAM temperature profile best representing the actual profile is described in the next sub-section. The overall nature of this procedure is such that generally better results are obtained when a residual profile and a relative humidity profile are supplied which more closely approximate the actual conditions than do the built-in fixed profiles. Although it has not been conclusively demonstrated, there are strong indications that a residual profile derived from the regularly scheduled U. S. Weather Service RAOB profile closest in time prior to the radiometric observations and closest in distance to the THERMASONDE site specified the upper air conditions at the time of the radiometric observations more accurately than the fixed profile.

---

* The user provides guess-values for the parameters Z_1, Z_2, Γ_1, and Γ_2. The program determines the value of Γ_3 for a given combination of the values of Z_1, Z_2, Γ_1, and Γ_2 and the values of the surface temperature, termination height, and temperature at the termination height which is contained in the residual profile.

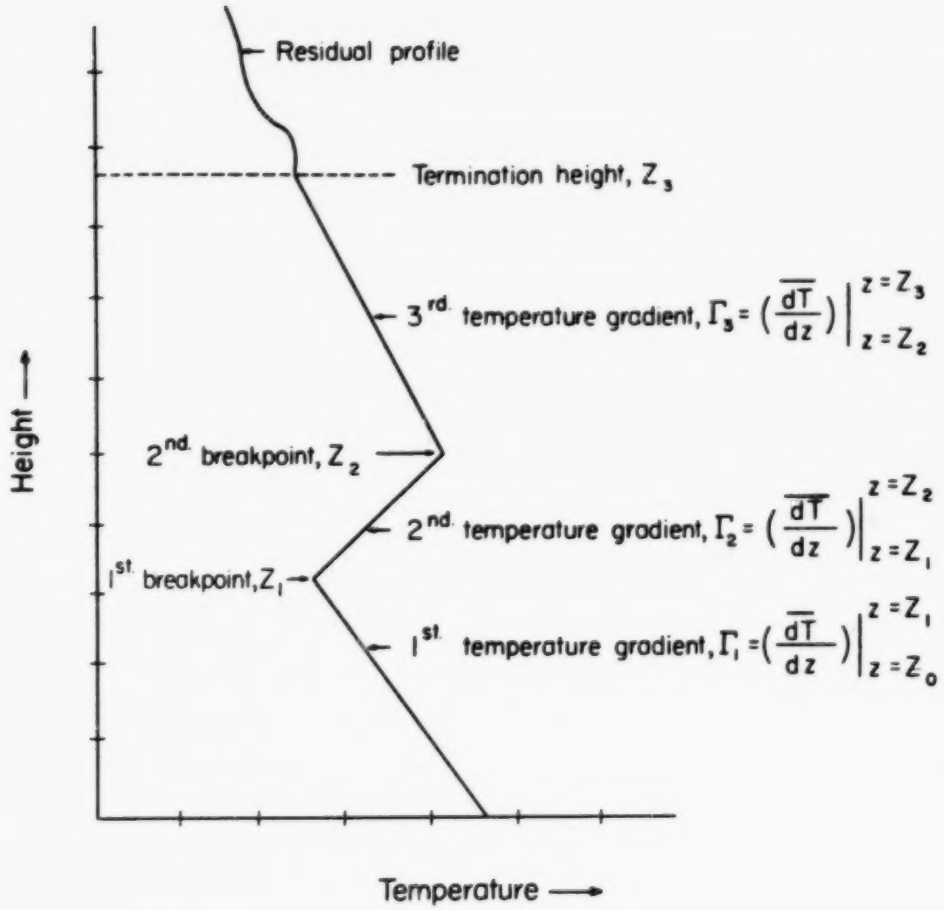

FIG. 10 GAM temperature profile model.

3.2.2 The GAM Analysis Procedure

In the GAM technique, the observed antenna temperature distribution (in digital form) is compared with an ensemble of brightness temperature distributions. The ensemble is derived from the various GAM temperature profiles corresponding to all physically realizable combinations of input guess-values of the GAM parameters. The GAM computer program contains certain constraints on the values for parameters taken individually and in combination with one another. A listing of these constraints is given in Table V. GAM temperature profiles containing combinations of parameter values which violate these constraints are deemed physically unrealizable and are eliminated from further consideration.

In addition to the explicit constraints on particular combinations of parameter values built into the program, the user imposes a set of implied constraints by his process of selecting parameter value-guesses. For example, a THERMASONDE antenna temperature distribution which shows an increase in antenna temperature in the lowest elevation angles starting at zero degrees corresponds to only a ground-based inversion or a very low elevated inversion. Consequently, the set of guessed-parameter values should be confined to those corresponding to these types of inversions. This results in more efficient use of computer time, since brightness temperature distributions corresponding to lapse and higher elevated inversion profiles are not calculated. In addition, a better correspondence between the GAM temperature profile and the actual profile will probably result, since a greater variety of appropriate low inversion type GAM temperature profiles can be tried in a given amount of computation time.

The criterion for selecting the best model temperature profile is a good fit of the calculated brightness temperature distribution with the measured distribution. For evaluation by visual means, "good fit" implies a close matching of the shapes of the two distributions. Accurate matching of the shapes of two curves, in the mathematical sense, implies considerably more than the usual meaning of best fit, i.e., a minimum in the sum of squares of differences between observed and calculated distributions.

Originally, the GAM technique used the minimum of squares of the differences between observed antenna and calculated birghtness temperatures as a best-fit criterion. Another criterion based on a minimum sum of the absolute

TABLE V

SUMMARY OF PARAMETER VALUE CONSTRAINTS
BUILT INTO THE GAM COMPUTER PROGRAM

Parameter or Combination of Parameters	Constraint	Rationale for Constraint
Γ_1 when $Z_1 \geq .2$	$\Gamma_1 > -15.0$	Superadiabatic lapse rates can exist only in a relatively thin layer near the surface. This constraint expresses the heights to which superadiabatic lapse rates equal to or less than specified intensities can exist.
Γ_1 when $Z_1 \geq .3$	$\Gamma_1 > -14.0$	
Γ_1 when $Z_1 \geq .4$	$\Gamma_1 > -13.0$	
Γ_1 when $Z_1 \geq .6$	$\Gamma_1 > -12.0$	
Γ_1 when $Z_1 \geq 1.0$	$\Gamma_1 > -11.0$	
Γ_1 and Z_1	$\Gamma_1 Z_1 \leq 25.0$	Restricts the temperature increases due to inversions to within what is held to be a reasonable range on the basis of historical precedent.
Γ_2, Z_1 and Z_2	$\Gamma_2(Z_2-Z_1) \leq 25.0$	
Γ_1, Γ_2, Z_1 and Z_2	$\Gamma_1 Z_1 + \Gamma_2(Z_2-Z_1) \leq 25.0$	
Z_1 and Z_2	$Z_2 \geq Z_1$	The upper boundary of an elevated inversion must be higher than its base.
Γ_2	$\Gamma_2 \geq -10.0$	Slightly superadiabatic lapse rates may exist in elevated layers above but close to the surface, but not over great depths (i.e, greater than about 1.0 km).
Γ_3	$\Gamma_3 \geq -9.8$	

Note: Γ units are C/km, Z units are km, ΓZ units are C.

value of the difference between observed antenna and calculated brightness temperatures was also investigated during the previous work. These two criteria generally give the same results, although at times they did differ significantly. However, neither criterion was substantially better than the other. Both yielded satisfactory results in the sense that they distinguished lapse and elevated inversions and determined the elevated inversion bases in most cases with good accuracy. There was, nevertheless, considerable opportunity for improvement on these results and it was felt that investigations of other criteria might be particularly rewarding. This followed from the fact that both the minimum sum square and minimum sum of absolute value criteria are intended for application when the differences between the observed and calculated values are random. However, in the GAM, these differences are not entirely random except when the GAM temperature profile is identical to the true temperature profile. Furthermore, these criteria may not sufficiently emphasize similarities in the shapes of the observed and calculated radiometric distributions.

3.3.3 Comparison of Criteria

Calculation of the correlation coefficient of the observed antenna and calculated brightness temperature distributions was incorporated into the GAM program. The criterion for selecting the best parameter values was a maximum value of the correlation coefficient. It was felt that the maximum correlation coefficient criterion (MCCC) would give somewhat more emphasis to shape similarities than either the minimum sum of squares criterion (MSSC) or the minimum sum of absolute differences criterion (MSADC).

The GAM computer program lists (in order) the top twenty-five choices of parameter values using each of the aforementioned criteria. In practically all cases, the top three or four parameter value combinations selected are the same using the MSSC and the MSADC. However, at least with the initial set of the user's guess-values, the top few parameter value combinations selected by the MCCC generally were not the same as those obtained by the other criteria. With the second and subsequent sets of user guesses, where the spread in the parameter values was much smaller, the best set of values obtained by the MCCC was sometimes the same as that obtained by the MSSC and MSADC.

3.3.4 Results

The GAM technique was tried on errorless brightness temperature data

calculated from four basic types of temperature structure. Both simulated scans and simulated discrete angle errorless brightness temperature data were generated. Two sets of parameter guess-values were used on the errorless discrete angle brightness temperatures and three sets of parameter guess-values were used on the simulated angle scan brightness temperatures. The first set of parameter guess-values was the same for both the scan and discrete angle cases. It was composed without knowledge of the air temperature profiles from which the brightness temperatures were calculated. Only the presently accumulated general body of knowledge on the relationship between specific types of temperature structures and the characters of the radiometric records they produce was used to construct these initial sets of parameter guess-values.

For both the discrete angle and scan data, the second set of parameter guess-values selected was based upon the best values obtained from the first set using the MSSC. The third set of parameters used on the scan data was based upon the best results obtained from the first set using the MCCC.

To determine effects of scanned data on the GAM technique, top ranking temperature profiles for the discrete angle and scanned data were selected from the second guess-value parameter sets. The two temperature profile models selected for each of the four basic types of air temperature structure were compared. In two cases, the top ranking temperature profiles obtained from the discrete angle data and the scanned angle data were identical. In the other two cases, they were very nearly identical. Thus it appears that discrete angle and scanned angle data are equally suitable for use in the GAM technique.

The top-ranking parameter values selected by the MSSC and MCCC from the second and third sets of parameter guess-values used on the errorless scan data are shown in Figs. 11 through 14. In all cases, the MCCC gave an equal or superior indication of the air temperature profile model. The improvement was particularly evident in the low-elevated and ground-based inversion cases (Figs. 12 and 13, respectively). Section 3.5.4 shows results using MK I observed data for these same cases.

3.3.5 Computer Requirements

The computer time required for the analysis of THERMASONDE data depends upon the number of allowable temperature profiles that can be generated from the set of guess-values of the GAM parameters. We have found from experi-

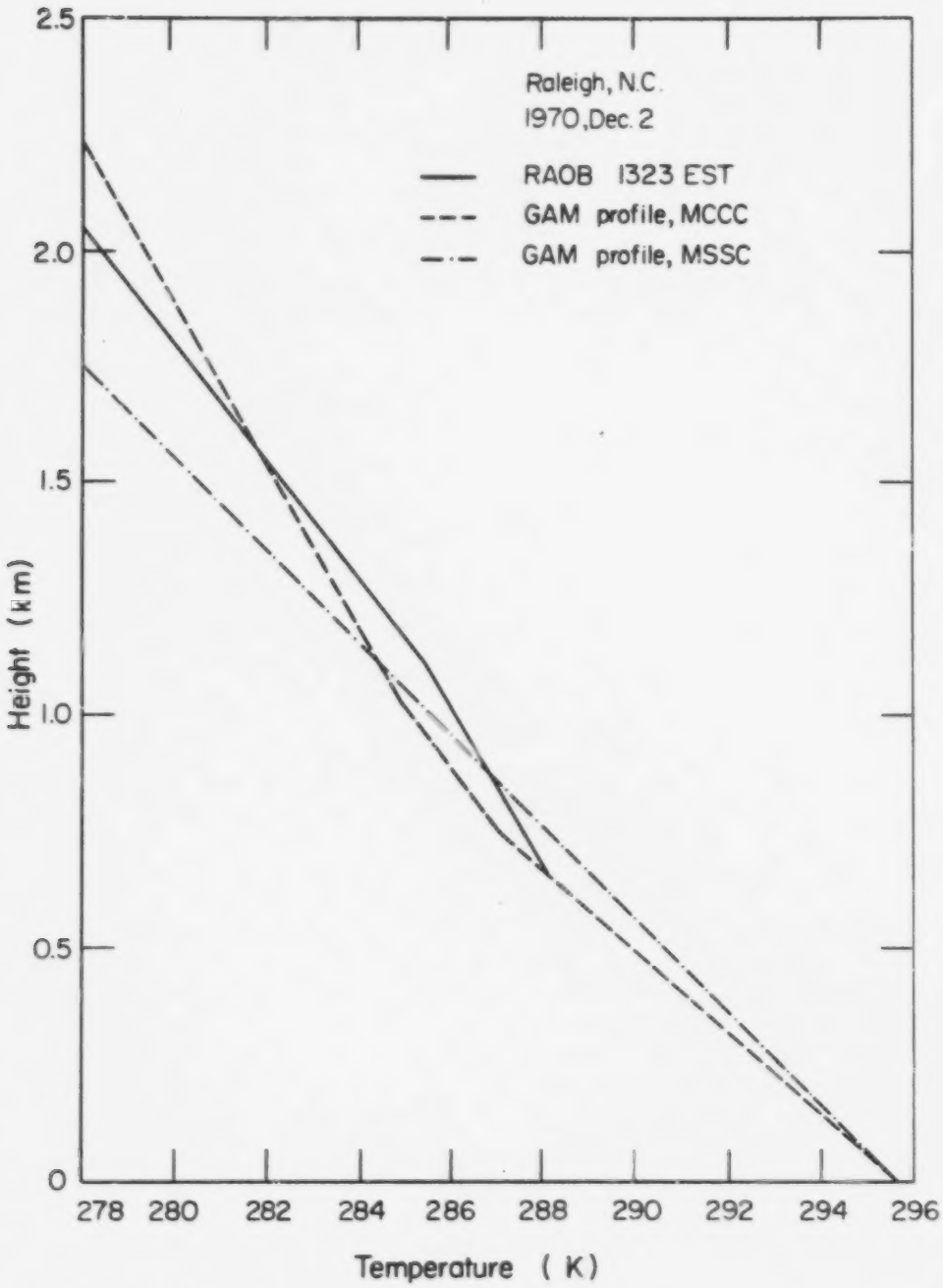

FIG. 11 Comparison of actual profile with GAM profiles determined from errorless data (lapse condition).

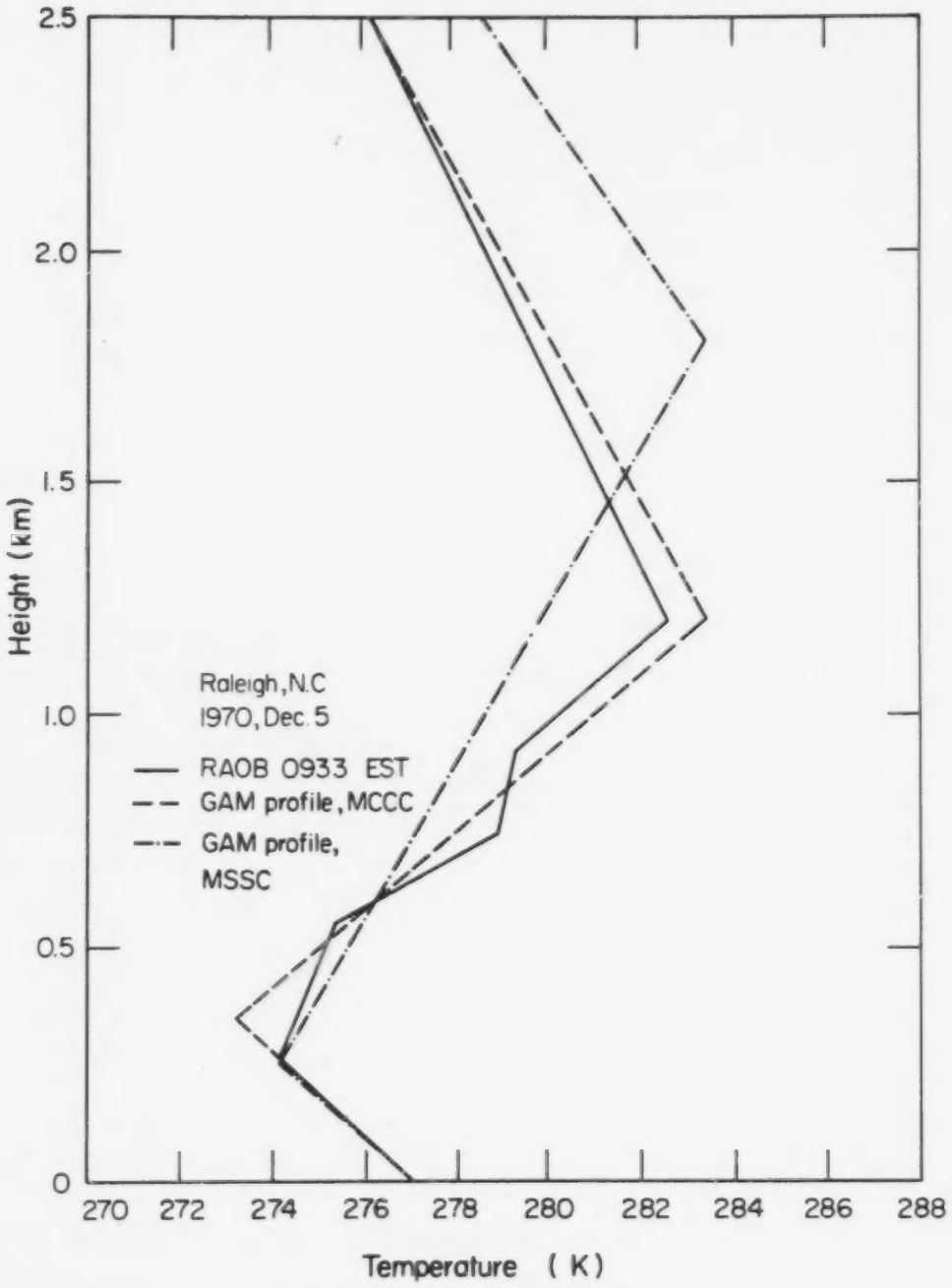

FIG. 12 Comparison of actual profile with GAM profiles determined from errorless data (low elevated inversion).

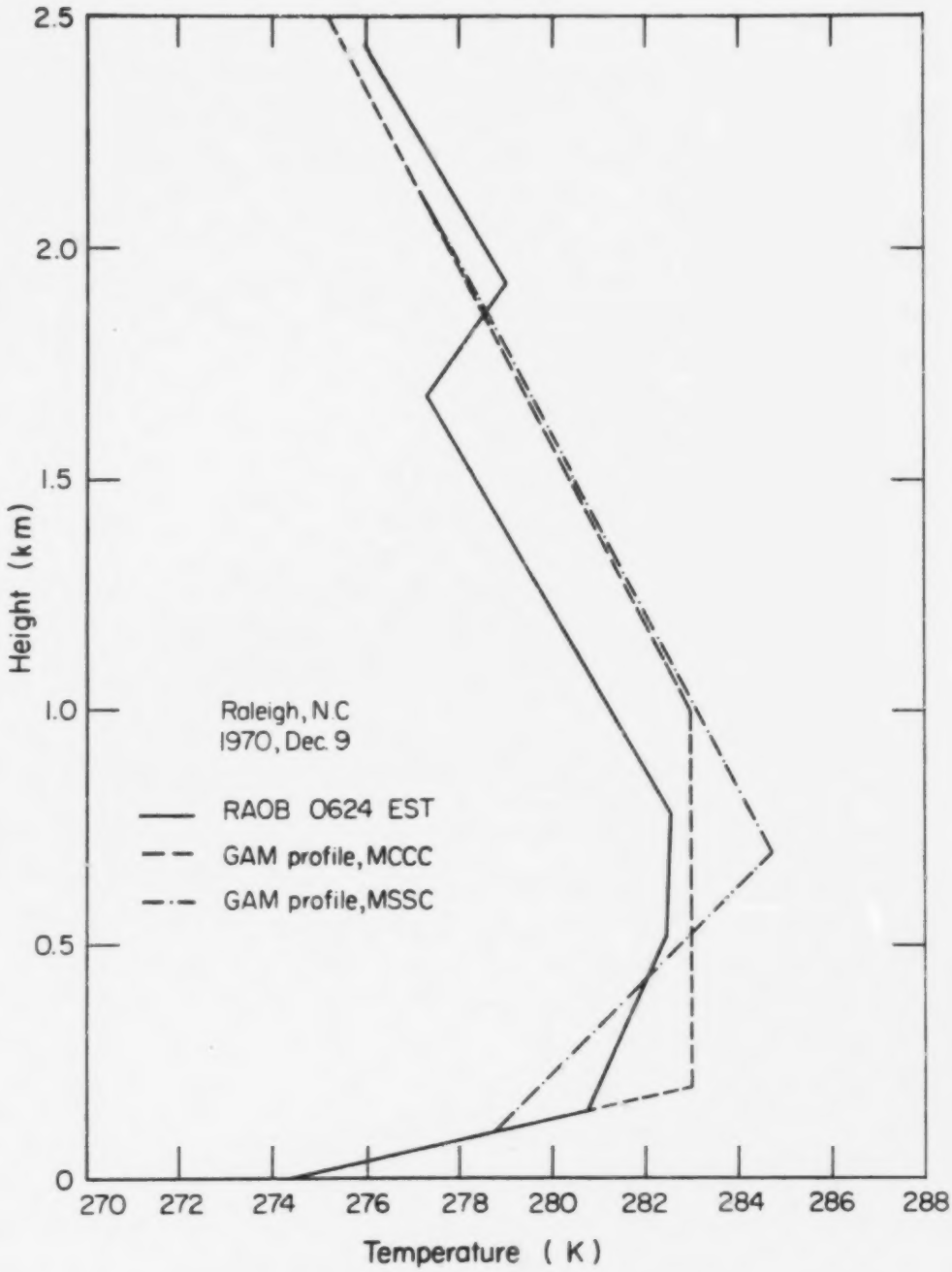

FIG. 13 Comparison of actual profile with GAM profiles determined from errorless data (ground based inversion).

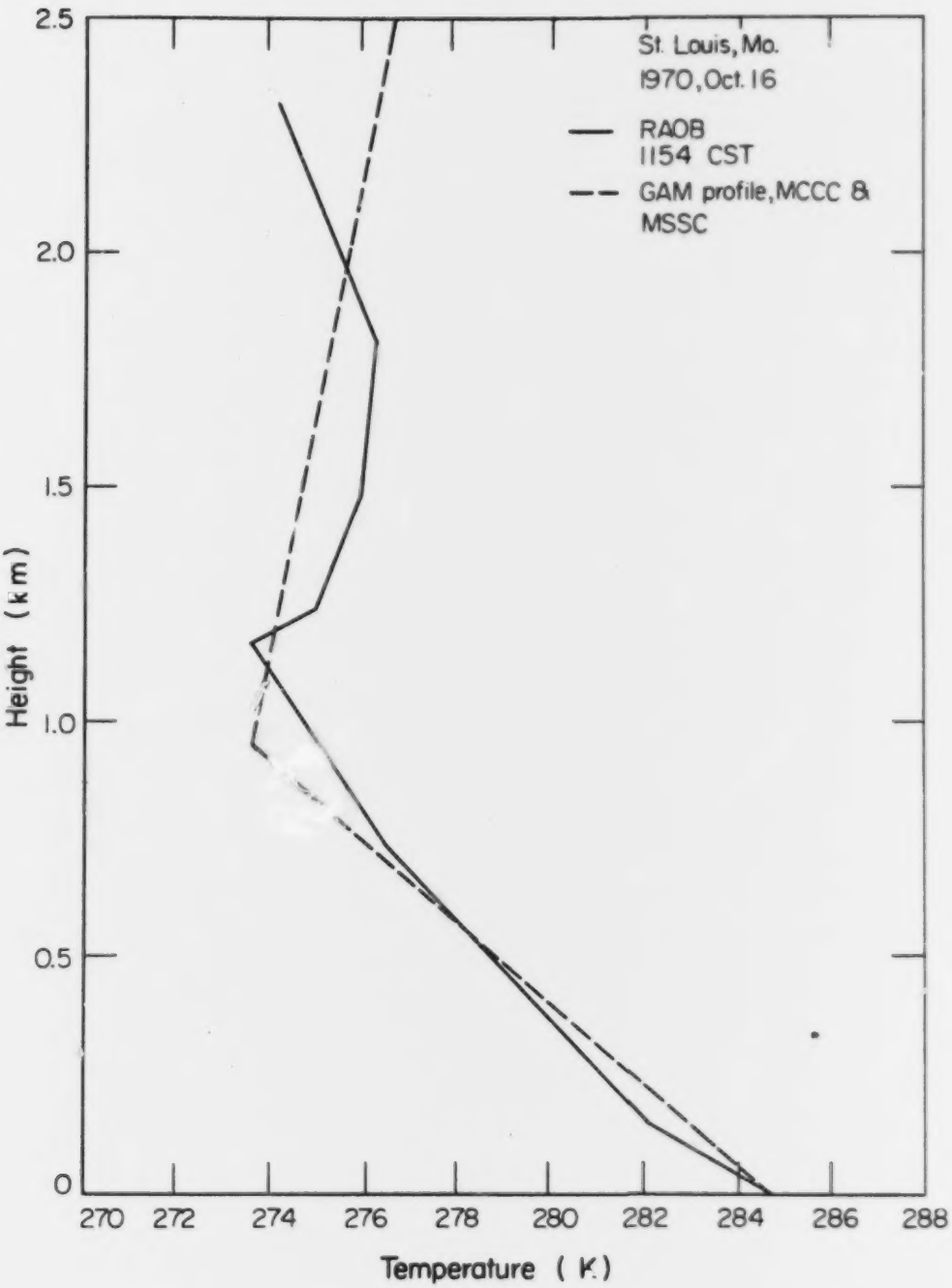

FIG. 14 Comparison of actual profile with GAM profiles determined from errorless data (high elevated inversion).

ence that about 1500 allowable GAM temperature profiles are formed from the user's first set of guess-values. A run this size takes about 30 minutes on a machine the size and speed of a UNIVAC 418-III or 3 to 4 minutes on the larger and faster UNIVAC 1108.

The rather large computer time requirement of the GAM is due to the many thousands of brightness temperature calculations it must perform. The time requirement would be even greater had we not developed (in the preceeding contract) a routine for making an approximation of the brightness temperatures from the GAM parameters for each elevation angle of observation. This routine, known as the fast-running brightness temperature model, is described in detail in Ref. 3. The brightness temperatures obtained using it generally agree to within an average of about 0.15° K of the brightness temperatures calculated from the exact equations. We have never observed a deviation greater than 0.3 K. The fast-running brightness temperature model is about two-to-three times faster in calculating brightness temperatures than the exact expression.

The core requirement for the GAM computer program is about 40,000 eighteen-bit words. This storage requirement could be reduced considerably, principally because the program in its present form contains numerous arrays of variable names which are only occasionally used for checking purposes. These arrays would be deleted from an operational model of the GAM computer program. Additional storage (and quite likely time) could be saved by recoding the program from the standpoint of operational use rather than research and development usage.

3.3.6 Suggested Future Work on the GAM Technique

The GAM technique as presently constituted is a suitable operational method for analyzing radiometric data . The present program could stand some recoding to decrease its core requirements and running time.

Should field tests and operational evaluations indicate more fundamental changes are needed, there are three areas in which additional work would likely be beneficial in improving the actual temperature profile representativeness of the GAM profiles.

The first is investigation of other criteria or combinations of criteria for selecting the best values of the GAM parameters. In our opinion, the best way to implement this would be to select as the best parameter values

those which minimize the differences between the measured and calculated radiometric scan records and their respective derivatives. The function F(P) to be minimized would be of the form

$$F(\underline{P}) = \left\{ T_B(\underline{P},\theta) - \hat{T}_B(\theta) \right\}^2 + \sum_{i=1}^{N} \left\{ \frac{\partial^i (T_B(\underline{P},\theta))}{\partial \theta^i} - \frac{\partial^i (\hat{T}(\theta))}{\partial \theta^i} \right\}^2 \qquad (1)$$

where

$T_B(\underline{P},\theta)$ = calculated brightness temperatures

$\underline{P}$ = GAM parameters

θ = elevation angle

$\hat{T}_B(\theta)$ = observed brightness temperatures

N = maximum order of derivatives considered

$\frac{\partial^i ( )}{\partial \theta^i}$ = i^{th} order derivative with respect to θ

The most significant drawback of a criterion based on the minimization of such a function lies in the problem of calculating the derivatives of the observed scan distributions. Noise in the observations would result in significant errors in calculation of the derivatives. The effect becomes more severe for higher-order derivatives. So, although in theory the minimization of F(P) is an excellent criterion for establishing the closest match in shape between the observed and calculated records, inclusion of pre-processing, or smoothing, of the raw THERMASONDE data would probably be needed for its successful implementation. The second area is investigation of the effect of allowing the temperature gradient in the third layer to be determined more directly by the radiometric data. Presently it is severely constrained by the requirement that the GAM temperature profile be contiguous with the residual profile at the termination pressure. Finally, some thought and investigation could profitably be directed toward automating the selection of parameter value-guesses in the second and subsequent passes. This would simplify the meteorologist's task and allow a more rapid determination of the final results.

3.4 LIMITED RANGE RELAXATION TECHNIQUE

3.4.1 Introduction

The limited range relaxation technique (LRRT) is an iterative numerical method which was developed for deriving the ambient temperature profile from the surface to a height of 2.54 km from radiometric data collected at 54.5 GHz. This section presents the basic relaxation technique, describes the importance of proper implementation of the relaxation equation, shows sample results, and suggests the areas of work necessary to complete the development of the relaxation technique.

3.4.2 Theoretical Basis

Before proceeding to a discussion of results obtained by the LRRT, the equations which are the basis of this technique are presented. The source brightness temperature at any angle is given from the theoretical equation as the sum of two integrals, as follows:

$$T_{B_\nu}(\theta) = \int_0^{2.54} T(z) \left(- \frac{\partial \tau_\nu(\theta,z)}{\partial z} \right) dz + \int_{2.54}^{z_f} T(z) \left(- \frac{\partial \tau_\nu(\theta,z)}{\partial z} \right) dz \qquad (2)$$

where

$T(z)$ = ambient air temperature profile

$\tau_\nu(\theta,z)$ = transmissivity at height z and angle θ for the frequency ν

z_f = height beyond which no significant contribution is received by the radiometer. There is no direct power term in the equation, since the frequency under consideration is 54.5 GHz, which produces a negligible direct power term.

The LRRT endeavors to determine the ambient temperature profile from $z = 0.0$ to $z_{16} = 2.54$ km and to specify only the <u>value</u> of the second integral in Eq. (2).

The predicted brightness temperature at any angle is based upon an estimated temperature profile from $z_1 = 0.0$ to $z_{16} = 2.54$ km and a prediction of the contribution [the value of the second integral in Eq. (2)] which is due to radiation coming from beyond 2.54 km. The predicted contribution on the n^{th} iteration for the radiation beyond 2.54 km is given by

$$\hat{T}B2(\theta)_n = \hat{\bar{T}}_{90}\left[z_{16}\ z_f\right]_n \frac{T_{B_\nu}(\theta)}{T_{B_\nu}(90)} \cdot \frac{1-\tau_\nu(90,z_f)}{1-\tau_\nu(\theta,z_f)}\left[\tau_\nu(\theta,z_{16}) - \tau_\nu(\theta,z_f)\right] + \beta(\theta) \quad (3)$$

where

$\hat{\bar{T}}_{90}[z_{16},z_f]_n$ = n^{th} predicted mean value temperature over the height range $[z_{16},z_f]$ associated with the source brightness temperature at $\theta = 90$ degrees.

$T_{B_\nu}(\theta)$ = source brightness temperature at angle θ

$\tau_\nu(\theta,z)$ = transmissivity at angle θ and height z

$\beta(\theta)$ = error term, treated as an empirical constant.

The n^{th} predicted mean value temperature over the height range $[z_{16},z_f]$ associated with the source brightness temperature at $\theta = 90$ degrees is based upon the source brightness temperature at $\theta = 90$ degrees and the n^{th} predicted temperature profile from $z_1 = 0.0$ to $z_{16} = 2.54$ km. It is given by

$$\hat{\bar{T}}\left[z_{16},z_f\right]_n = \frac{T_{B_\nu}(90) - \int_{z_1}^{z_{16}} \hat{T}(z)_n \left(\frac{\partial\tau_\nu(\theta,z)}{\partial z}\right) dz}{\tau_\nu(90,z_{16}) - \tau_\nu(90,z_f)} \quad (4)$$

where $\hat{T}(z)_n$ is the temperature at height z for the n^{th} prediction.

The nth predicted brightness of any angle is then given by

$$\hat{T}_{B_\nu}(\theta)_n = \int_0^{2.54} \hat{T}(z)_n \left(-\frac{\partial \tau_\nu(\theta,z)}{\partial z}\right) dz + \hat{T}B2(\theta)_n \qquad (5)$$

It has been shown in a previous report[3] that transmissivity is only a weak functional of temperature and that its value is nearly constant for a given angle beyond a height of 30 km. For this reason it is assumed that the transmissivity function in Eq. (5) is identical to the corresponding transmissivity function in Eq. (2) and that the final transmissivity values $\tau_\nu(\theta,z_f)$ in Eq. (3) are known.

By providing an initially guessed temperature profile $\hat{T}(z)_0$, a set of predicted brightness temperatures $\hat{T}_{B_\nu}(\theta)_0$ can be computed from Eq. (5) for any elevation angle. The applicable height concept[3] has been shown to provide some measure of the true temperature profile. For this reason, the applicable height profile is always used as the initially guessed temperature profile. A set of sixteen angles has been selected to define the height grid. It is assumed that brightness temperatures are available at each of these angles. The set of angles and the height grid to which they correspond (via the applicable height concept) are presented in Table VI. The angle θ_j is the elevation angle in degrees corresponding to the applicable height z_j in km.

TABLE VI

ANGLE-HEIGHT GRID

j	θ_j	z_j	j	θ_j	z_j	j	θ_j	z_j	j	θ_j	z_j
1	0.0	.0	5	10.0	.26	9	30.0	.84	13	60.0	1.96
2	2.5	.07	6	15.0	.40	10	35.0	1.01	14	70.0	2.27
3	5.0	.13	7	20.0	.54	11	40.0	1.19	15	80.0	2.47
4	7.5	.20	8	25.0	.69	12	50.0	1.59	16	90.0	2.54

Using the applicable height concept, the initially guessed profile is given by $T(z_j)_0 = T_{B_\nu}(\theta_j)$. Substituting $T(z_j)_0$ into Eq. 5, a set of predicted brightness temperatures can be computed at each angle corresponding to a brightness temperature measurement. For each angle, the difference between the predicted brightness temperature and the true source brightness temperature is a "residual" representing that portion of brightness temperature not explained by the guessed temperature profile.

Letting

$$C(\theta_j) = \frac{T_{B_\nu}(\theta_j)}{T_{B_\nu}(90)} \cdot \frac{1-\tau_\nu(90,z_f)}{1-\tau_\nu(\theta_j,z_f)} \cdot \frac{\tau_\nu(\theta_j,z_{16})-\tau_\nu(\theta_j,z_f)}{\tau_\nu(90,z_{16})-\tau_\nu(90,z_f)} \tag{6}$$

the residuals between the n^{th} predicted and source brightness temperatures can be shown to be given by

$$\varepsilon(\theta_j)_n = \int_{z_1}^{z_{16}} \left\{\hat{T}(z)_n - T(z)\right\} \left(-\frac{d\tau_\nu(\theta_j,z)}{dz} + C(\theta_j)\frac{d\tau_\nu(\theta_j,z)}{dz} \right) dz + \beta(\theta_j) \tag{7}$$

It is clear from Eq. (7) that the formulation of the equations has been such that the residuals are dependent upon the predicted temperature profile only from the surface $z_1 = 0.0$ to a height of $z_{16} = 2.54$ km . $\beta(\theta)$ is the error term in predicting the contribution to brightness temperature coming from beyond 2.54 km. Its value does depend upon the predicted temperature profile, but to date it has been treated as a constant independent of the predicted temperature profile. Table VII contains the values of $\beta(\theta)$ that are currently used, as well as the final transmissivity values $\tau_\nu(\theta,z_f)$ that are used in the computation of $C(\theta)$.

The relaxation equation for correcting the temperature profile at each of the 16 levels in Table VI is based upon the residuals as defined in Eq. (7) The exact motivation and development of the relaxation equation was presented in the previous final report[3], where the following notation was used in the relaxation equation:

$$D_i \equiv \Delta\tau_\nu\left(\theta_j, [z_i, z_{i+1}]\right) - C(\theta_j)\Delta\tau_\nu\left(90, [z_i, z_{i+1}]\right)$$

TABLE VII

ERROR CONSTANTS AND FINAL TRANSMISSIVITIES

θ	$\beta(\theta)$	$\tau_\nu(\theta, z_f)$
0.0	.0	.0
2.5	.002	.0
5.0	.004	.0
7.5	.006	.0
10.0	.010	.0
15.0	.031	.0
20.0	.073	.0
25.0	.122	.00006
30.0	.152	.00026
35.0	.161	.00075
40.0	.149	.00161
50.0	.102	.00451
60.0	.056	.00840
70.0	.023	.01220
80.0	.006	.01492
90.0	.0	.01590

and

$$\bar{\epsilon}_i \equiv \frac{\epsilon(\theta_i) + \epsilon(\theta_{i+1})}{2}$$

The relaxation equations are as follows:

$$\hat{T}(z_1)_n = \hat{T}(z_1)_{n-1} - \epsilon(\theta_1)_{n-1} \tag{8a}$$

$$\hat{T}(z_j)_n = \hat{T}(z_j)_{n-1} - \frac{1}{\Delta\tau_\nu\left(\theta_j, [z_{j-1}, z_{j+1}]\right)} \times \left\{\epsilon(\theta_j) - \left(\sum_{i=1}^{j-2} + \sum_{i=j=1}^{15}\right)\bar{\epsilon}_i D_i\right\}_{n-1} \tag{8b}$$

$$\hat{T}(z_{16})_n = \hat{T}(z_{16})_{n-1} - \left[\hat{T}(z_{15})_n - \hat{T}(z_{15})_{n-1}\right] \tag{8c}$$

where Eq. (8a) provides the temperature correction at height z_1 ; Eq. (8b) is the principal relaxation equation and is valid for all heights z_j such that $2 \le j \le 15$; and Eq. (8c) is used for the height level $z_{16} = 2.54$ and states that temperature correction determined for height z_{15} is also applied to height z_{16} .

3.4.3 Implementation

Considerable improvement has been achieved during this contract in the results obtained with the relaxation technique. The improvement is not due to any change in the relaxation equation, but rather to a change in implementation of the equation. Previously, two methods of implementation were used. The first was to apply the relaxation equation to all sixteen grid heights z_j on each iteration. The second was to apply the relaxation equation on each iteration to those grid heights corresponding to and above the angle having the maximum residual in absolute value. Both methods assumed independence among the residuals to the extent that the indicated temperature corrections (due to the residuals) were in the right direction and of appropriate size for each grid height. Both methods provided good results for temperature profiles having ground-based inversions and strong elevated inversions below 0.5 km. For

profiles having temperature inversions at higher heights, very little success was obtained. For both methods of implementation, the sign of $\epsilon(\theta_j)$ caused a correction to be made away from the true temperature profile in the region of a temperature discontinuity, even though the majority of temperature corrections were toward the true profile. Since the residuals are weighted averages of the temperature errors at all grid points, the subsequent set of residuals were smaller at all angles, including the angle θ_j corresponding to the height where an incorrect temperature correction had been made. The residuals being smaller implies that the corrections in the next predicted temperature profile cannot be as significant as those in the previous profile. It was, therefore, virtually impossible for the technique to overcome the bad temperature corrections made on previous iterations. The result was that the technique was locked in or biased toward an incorrect profile due to the first or second iteration.

An important observation which affects all inversion schemes follows from the above analysis of the results previously obtained via the relaxation technique. Convergence of the residuals to a small value does not imply convergence of the predicted temperature profile to the true temperature profile. As along as the residuals are not identically zero, significant differences can exist between the predicted temperature profile and the true temperature profile. Further, it has been shown that typical error criteria--namely, $\Sigma\epsilon(\theta_j)$, $\Sigma|\epsilon(\theta_j)|$, and $\Sigma\epsilon(\theta_j)^2$ --actually have increased when an improvement to the predicted temperature profile has been made. For this reason, none of these error criteria are acceptable. The derivation of an optimum error criterion may be extremely difficult and will depend upon specific goals, e.g., the average ambient temperature error is to be minimized, the maximum ambient temperature error is to be minimized, or the character of the temperature profile is to be defined. In view of the fact that no acceptable error criterion has been defined, the current form of the relaxation technique uses a fixed procedure and a number of iterations. This methodology has the limitation that no objective measure is available to determine that additional improvement is or is not possible by increasing the number of iterations. Similarly, no judgement can be made as to whether too many iterations have already been performed.

The following method of implementing the relaxation equation has been developed to eliminate the problems associated with the two methods pre-

viously discussed. After the initially guessed profile $\hat{T}(z)_0$ is used to compute the predicted brightness temperatures $T_B(\theta)_0$, the values of $\epsilon(\theta)_0$ are computed. The relaxation equation is then applied to correct the temperature at grid heights z_{15} and z_{16}. The values of temperature that were used for the heights below z_{15} are again used. The combination of previous temperatures plus new predictions of temperatures at z_{15} and z_{16} comprise the next predicted profile $\hat{T}(z)_1$. Brightness temperatures are calculated using this new set of predicted temperatures and the next set of residuals $\epsilon(\theta)$ is found. Based upon this new set of residuals, the relaxation equation is applied to the grid heights z_{14}, z_{15}, and z_{16}. The values of temperature that were used below z_{14} are again used. The combination of previously-predicted temperatures and new predicted temperatures comprise the next predicted temperature profile $\hat{T}(z)_2$. The process is repeated until on the last iteration temperature corrections are made at all grid heights z_1, z2, ..., z_{16}. As each successive grid height is introduced, it is hoped that the portion of its residual that had been due to temperature errors at higher grid heights will have been eliminated.

A strategy based upon the characteristics of the applicable height (initially guessed) profile is used in connection with the above procedure. When an elevated inversion exists, the applicable height profile averages through the true profile in a manner such that the predicted temperatures are cold above the inversion and warm below the inversion. In view of this characteristic of $\hat{T}(z)_0$, it is desirable that all indicated warm corrections are completed before cold temperature corrections are allowed. This would minimize that portion of the temperature errors at lower heights which are due to predicted temperatures that are too cold at higher heights. A strategy is employed with the procedure outlined above such that no cold temperature correction is accepted unless all the residuals are positive, indicating that cold temperature corrections are required at all grid heights.

3.4.4 Results

Results using the limited range relaxation technique with a model temperature profile having a 5 C elevated inversion from 0.5 - 0.75 km are presented in Fig. 15. The relaxation technique has predicted the elevated inversion to be much weaker and of greater thickness than was actually the case. This may be due to the fact that the lower levels have not been corrected and

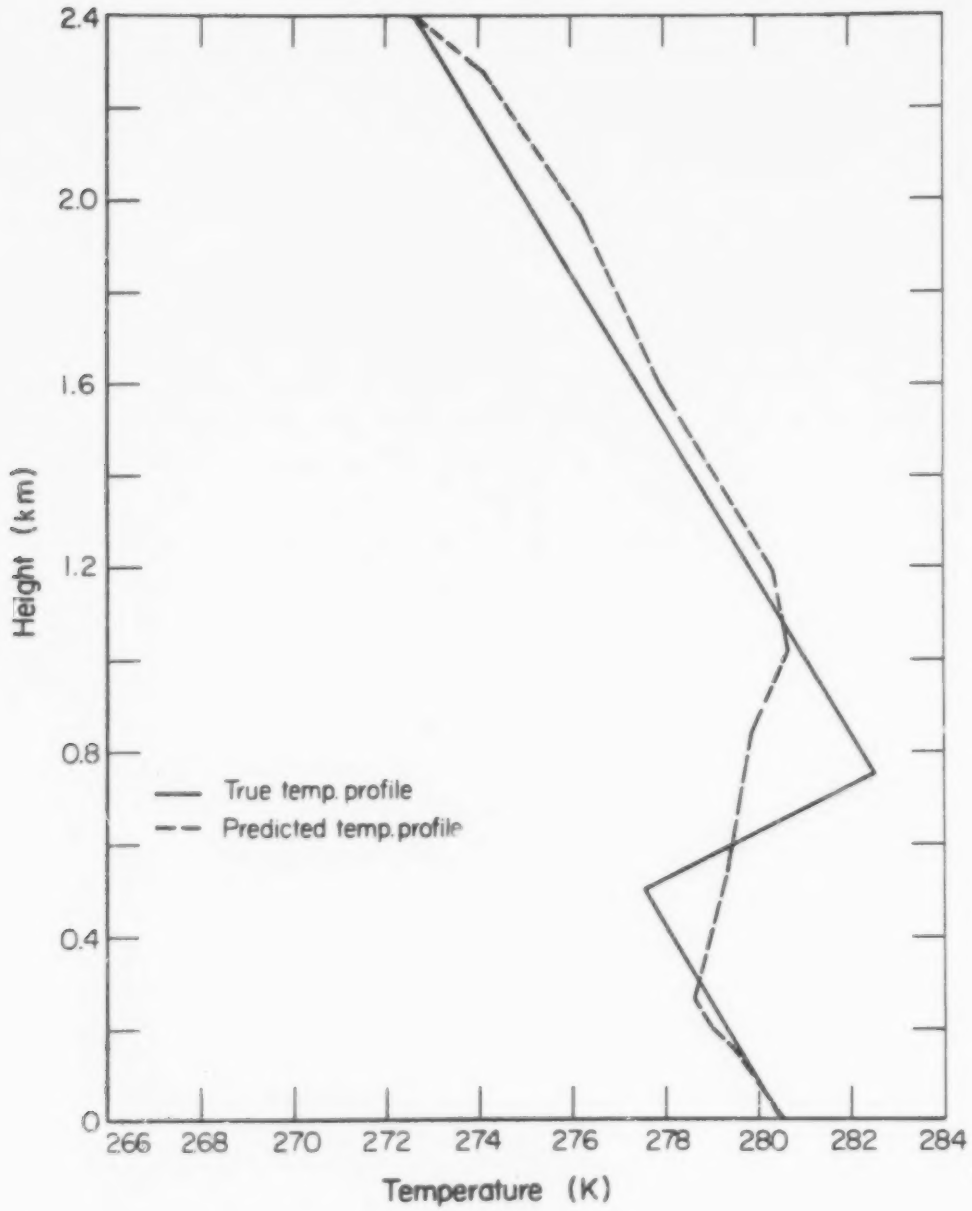

FIG. 15 Relaxation technique applied to the brightness temperatures computed from a model profile having a 5 C elevated inversion from 0.5 to 0.75 km.

are predicted too warm when the first cold temperature corrections are made at the higher levels. Because of this warm influence from the lower levels, the cold temperature corrections are made above the top of the elevated inversion. The relaxation technique compensates for this in the region of an elevated inversion by predicting a weaker elevated inversion having greater thickness. It is believed that this characteristic can be eliminated (since the region of the elevated inversion is bounded) by using additional iterations in combination with an appropriate error criterion. The predicted temperature profile defines the average temperature in the region of the inversion with excellent accuracy. The true average temperature between 0.5 - 0.75 km is 280 K; the predicted average temperature over the same region is 279.5 K. The temperature error, the true minus predicted ambient temperature, was calculated at every 0.1 km from the surface to 2.5 km. The average temperature error between the predicted and true temperature profile for this case was +0.15 C. Note that one's subjective impression of goodness of fit is not consistent with such a small average error. This graphically illustrates why average error is not a good criterion of a good fit.

Figure 16 shows results obtained with the relaxation technique where the brightness temperatures were computed from a model profile having a 5 C elevated inversion between 1.0 - 1.25 km. With previous implementation methods, no successful results were obtained for this case. In this instance, the region of the elevated inversion is clearly identified, although the extremes of the inversion are not well defined. Again, the average accuracy of the predicted temperature profile appears to be excellent. The true average temperature in the region of the inversion is 277.0 K; the predicted average temperature is 277.5 K. The average temperature error from the surface to 2.5 km is only -0.13 C. The same problem exists as in the previous case.

When the elevated inversion extends over a sufficient thickness in the atmosphere, the relaxation technique is able to define its extremes. Figure 17 shows the results using the relaxation technique applied to brightness temperatures computed from a profile observed in St. Louis in 1970 October 6 at 0547 CST. The true profile has a 2.8 C elevated inversion from 0.11 to 0.64 km. The elevated inversion therefore extends over a thickness of 0.53 km, which is better than twice the depth of the previous case. The profile predicted has a 2.2 C elevated inversion between 0.2 and 0.69 km. The predicted profile is an excellent specification of the true temperature profile.

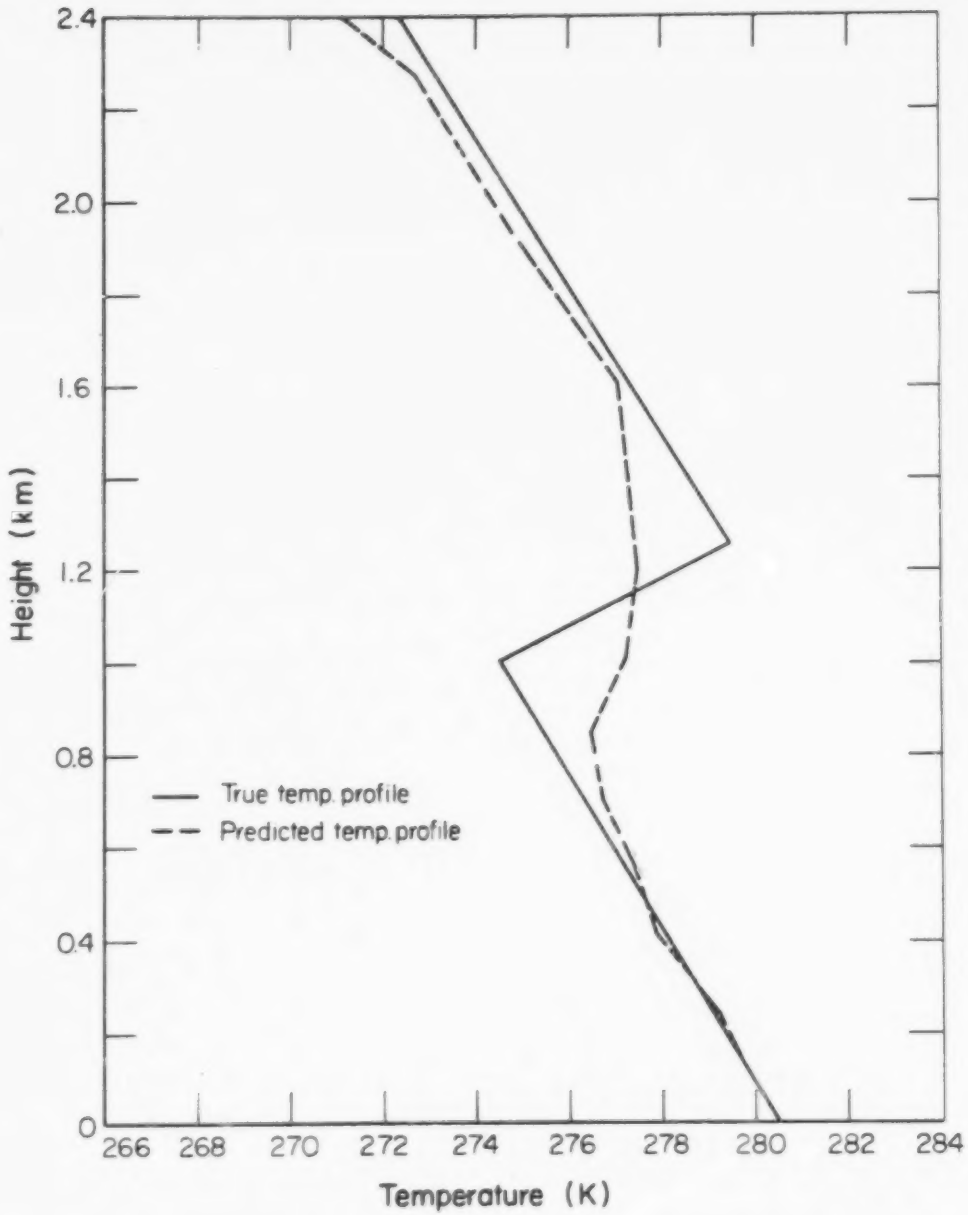

FIG. 16 Relaxation technique applied to the brightness temperatures computed from a model profile having a 5 C elevated inversion from 1.0 to 1.25 km.

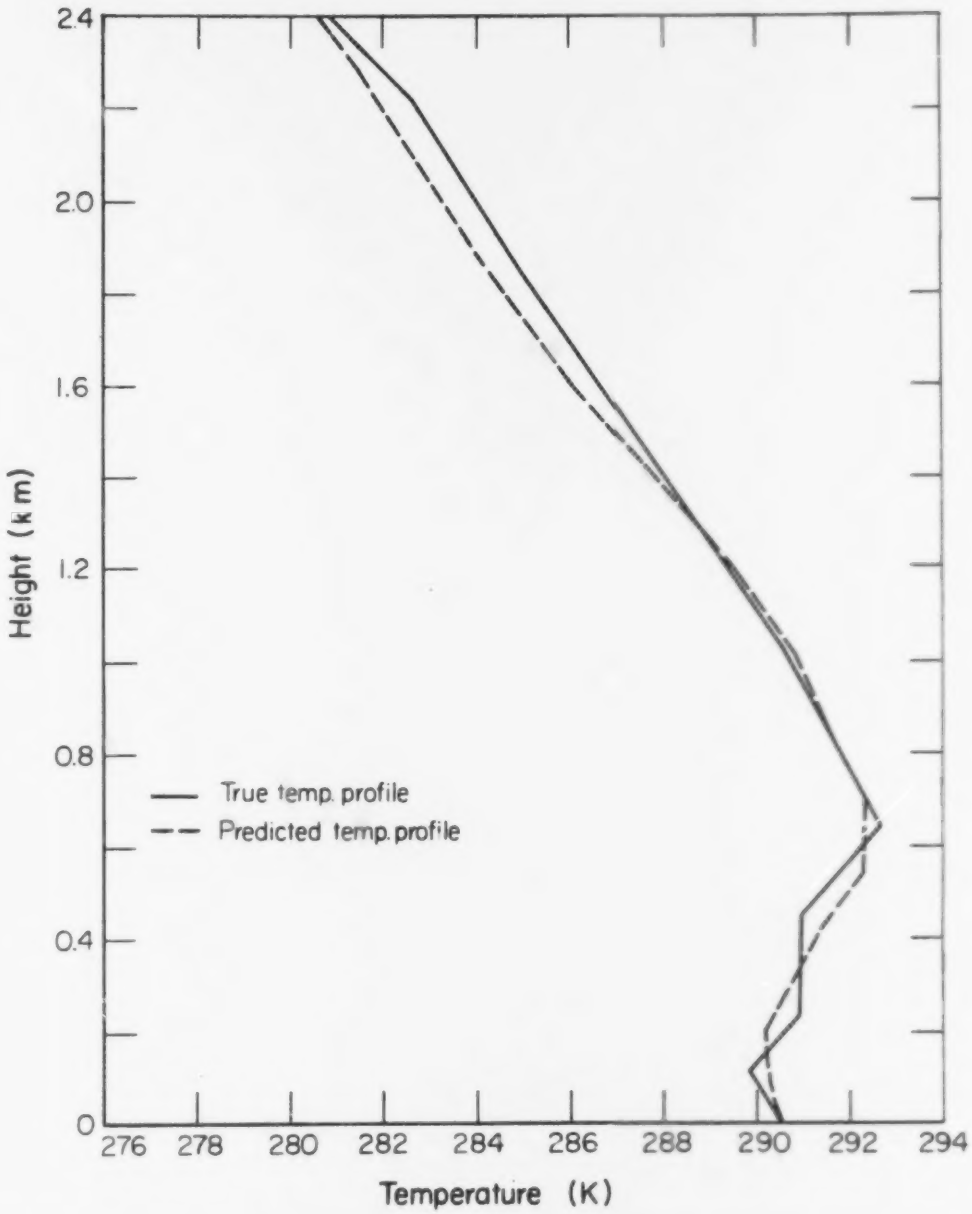

FIG. 17 Relaxation technique applied to the brightness temperatures computed from the observed radiosonde data taken at St. Louis, Mo., 0529 CST, 1970 October 6.

The results indicate that the relaxation technique specifies the existence and location of elevated inversions within the first kilometer of the atmosphere. The accuracy generally depends upon the thickness over which the inversion extends.

Temperature profiles with multiple inversions are another category of considerable importance in air pollution meteorology. The following case indicates the importance of having a meaningful error criterion to judge the number of iterations when using the relaxation technique. Figure 18 shows the results from the relaxation technique when applied to the brightness temperatures computed from a profile observed in St. Louis on 1970 October 15 at 0529 CST. The true temperature profile had a 5 C ground-based inversion from the surface to 0.27 km. In addition, there was 3.2 C elevated inversion from 1.22 to 1.72 km. The relaxation technique (by the current method of a fixed number of iterations) was not allowed to make corrections in the upper levels until the necessary warm corrections had been made at the lower levels. When the ground-based inversion was specified the allowable number of iterations was also completed. The result was that the initially guessed profile was retained at the upper levels. It is believed that the relaxation technique would have at least specified the existence and location of the elevated inversion if the number of iterations had not been constrained.

Work was done during this contract period to make the LRRT compatible with observed radiometric data. The LRRT was developed such that absolute brightness temperatures versus elevation angle are required as input data. However, the observed data is filtered antenna temperatures. Neglecting the antenna effect, i.e., treating the antenna temperatures as brightness temperatures, alters the distribution of the residuals to the extent that a completely erroneous predicted profile results. For this reason, the limited range relaxation technique will not be capable of handling observed data until some antenna beam pattern correction is applied to the observed data or incorporated into the simulation. The antenna effect is discussed in detail in Section 4 of this report. In addition to the antenna effect, there is a "filtering" effect introduced by the output integrator and the elevation angle scan function. This scanning mode produces "filtered" temperatures. Since elevation angle is constantly changing, the antenna temperature at any angle

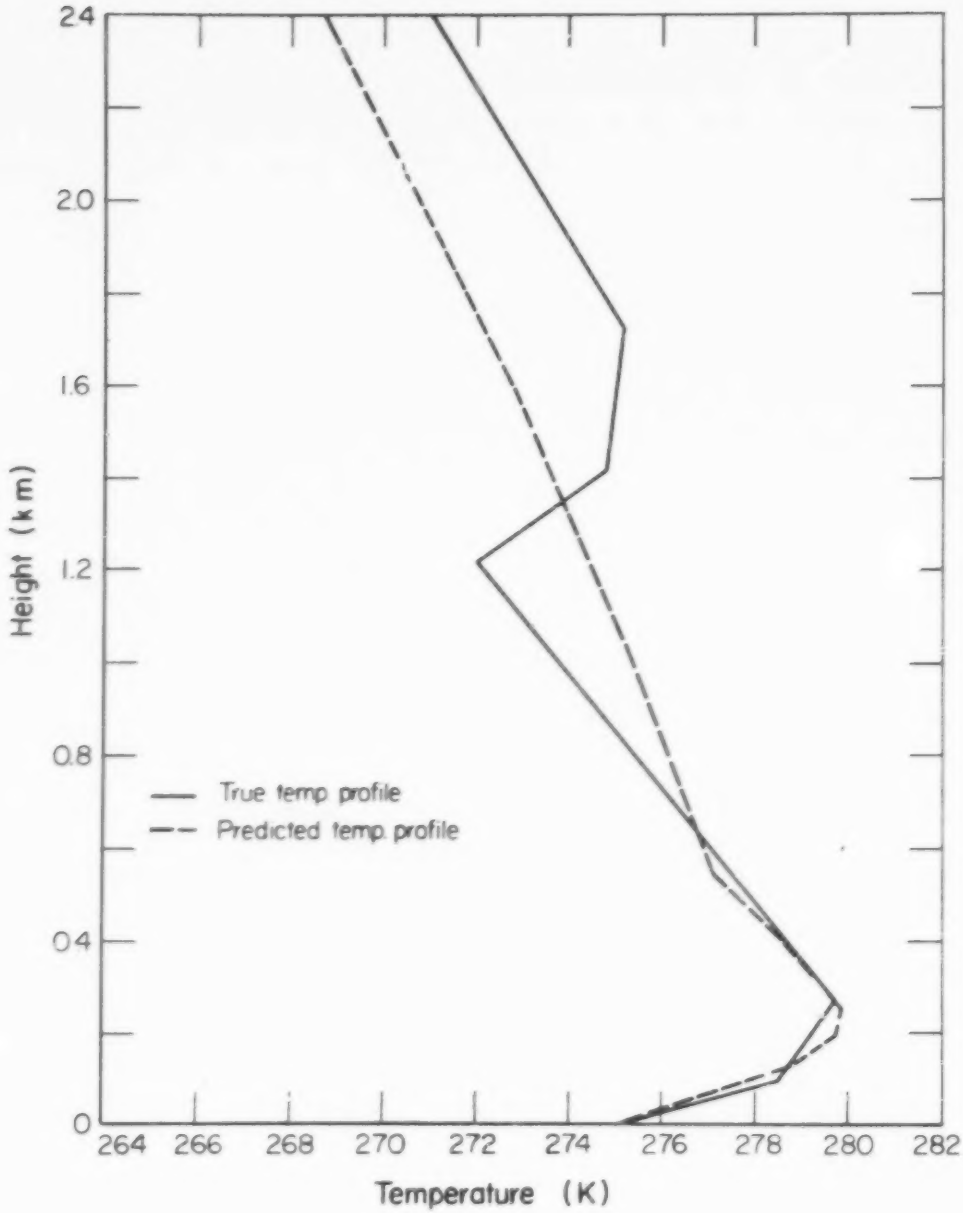

FIG. 18 Relaxation technique applied to the brightness temperatures computed from the observed radiosonde data taken at St. Louis, Mo., 0547 CST, 1970 October 16.

is a weighted average of the absolute antenna temperatures corresponding to that angle and to all previous elevation angles. A computer program was written which inverts the observed filtered antenna temperatures to absolute antenna temperatures. This computer program was incorporated with the relaxation technique to remove scanning effects from the observed data. Therefore, the relaxation technique can use either discrete or scanned angle data.

3.4.5 Suggested Future Work

Inclusion of the antenna beam pattern effect and development of an acceptable error criterion are certainly the two most significant areas of work to be completed before the relaxation technique can be used on an operational basis. Yet, other areas of work must also be completed to fully evaluate the capabilities and limitations of the relaxation technique. These areas include: analyzing the effect of surface pressure; including some measure of the water vapor profile; improving the error estimate $\beta(\theta)$ in the contribution coming from beyond 2.54 km; and investigating the selection of a more optimum angle-height grid. Each of these areas is expected to provide improvement in the results obtained via the limited range relaxation technique.

3.5 COMPARISON OF TECHNIQUES

3.5.1 Introduction

Results of the three inversion techniques (GAM, relaxation, and analog) are compared in this section. Also, computer and manpower requirements for operational usage of each of the techniques are discussed.

The GAM and relaxation methods arrive at a temperature profile by mathematically and statistically minimizing differences between measured antenna temperatures and simulated brightness (or antenna) temperatures. In the analog approach, minimization is accomplished visually by selecting the pre-computed overlay best fitting the measured antenna temperature record. The GAM and relaxation techniques arrive at objective solutions, whereas the analog method reaches a quasi-objective solution.

3.5.2 Data Requirements for Each Technique

The GAM and relaxation techniques require measured antenna temperatures at discrete elevation angles. This information is obtained from the THERMASONDE recorder. The analog method employs a continuous record of antenna

temperature versus angle for each scan. A record of discrete values could be used, but for pattern matching of the overlays and observed scans, a continuous record is desirable. The optimum number of discrete angle observations has not been determined for either the GAM or the relaxation technique. The GAM method used here employed 46 values in 2-degree elevation angle increments between 0 and 90 degrees. The relaxation method used 16 values over the same elevation angle range.

3.5.3 Computer and Manpower Requirements

Computer core storage requirements for present GAM formulation are now more than 40,000 eighteen-bit words. The analog technique does not require real-time or semi-real-time computation, since the analog library is constructed before the technique is used operationally. The relaxation technique presently requires approximately 25,000 eighteen-bit words. These core requirements are quite large, because programs are geared for great computational flexibility and functional applicability. For routine operations, these programs must be optimized to perform only the specific desired function. This would eliminate a large portion of the present core storage and computation time. It is estimated that the present core requirements could be cut by one-half or more. These requirements do not include corrections for antenna beam effects.

These inversion methods require only one man for their execution, and it is expected that temperature profile results will be in hand within 10 to 15 minutes after completion of the THERMASONDE scan. The analog method has been tested extensively in the field and results have, in most instances, been obtained within this time period.

3.5.4 Performance Comparison of the Three Techniques

Simulated brightness and MK I observed antenna temperature scans have been inverted into temperature profiles by the GAM and analog techniques. The relaxation technique performed well on simulated brightness temperature data and has shown greater improvement for these data than the GAM and analog techniques. However, results of tests of the relaxation technique using observed THERMASONDE data were unsatisfactory. This is due, in part, to the simulation-observation discrepancy because this mathematically sophisticated technique relies very heavily upon good agreement between simulation and observation. Relaxation inversion results for observed data are not presented along with the GAM and analog

results, but results for simulated data are shown.

Figures 19 through 22 show inversion results for the three techniques on four typical temperature profiles: lapse, ground-based inversion, and two elevated inversions. These results were obtained for scan data simulated from the radiosonde data obtained at the location, date, and time indicated on each figure. These simulations were performed for a frequency of 54.5 GHz, a 60-second integration time, and for an upward scan from 0 through 90 degrees at a rate of 4 deg/min. No antenna beam pattern correction was used in the simulations. Only the simulated scan data were used with each technique for inversion. Because the relaxation technique is set up to utilize null-balance unscanned brightness temperatures, a self-contained de-scanning algorithm was employed to revert scanned data into unscanned data. The analog overlays used were identical to those that APCO has in its possession. No additional overlays were used.

Since these scan data are simulated from idealized model profiles, there are no observational errors or dynamic variations for the inversion techniques to contend with. Also, there is no simulation discrepancy to hinder the inversion process. Thus, these results may be a somewhat optimistic estimate of the operational capabilities of these techniques in their present state of development.

These figures indicate that on an overall basis, the techniques clearly distinguish between lapse, ground-based inversion, and elevated inversion profiles. None of the techniques shows the small-scale details of the directly observed temperature profiles. For the GAM and the analog techniques, this is partially due to the two or three temperature gradients within which these techniques are presently constrained. The average temperature errors for these inverted profiles are tabulated and discussed later in this section.

In Figs. 23 through 26, the inversion results are shown for MK I-observed data. It is immediately obvious that these results are not as good as those obtained for the simulated THERMASONDE data shown in Figs. 19 through 22. The reasons for this are:

1. Extraneous sky and ground contributions to the antenna temperature (see Sec. 4)
2. Limited number of degrees of freedom available in the data processing techniques

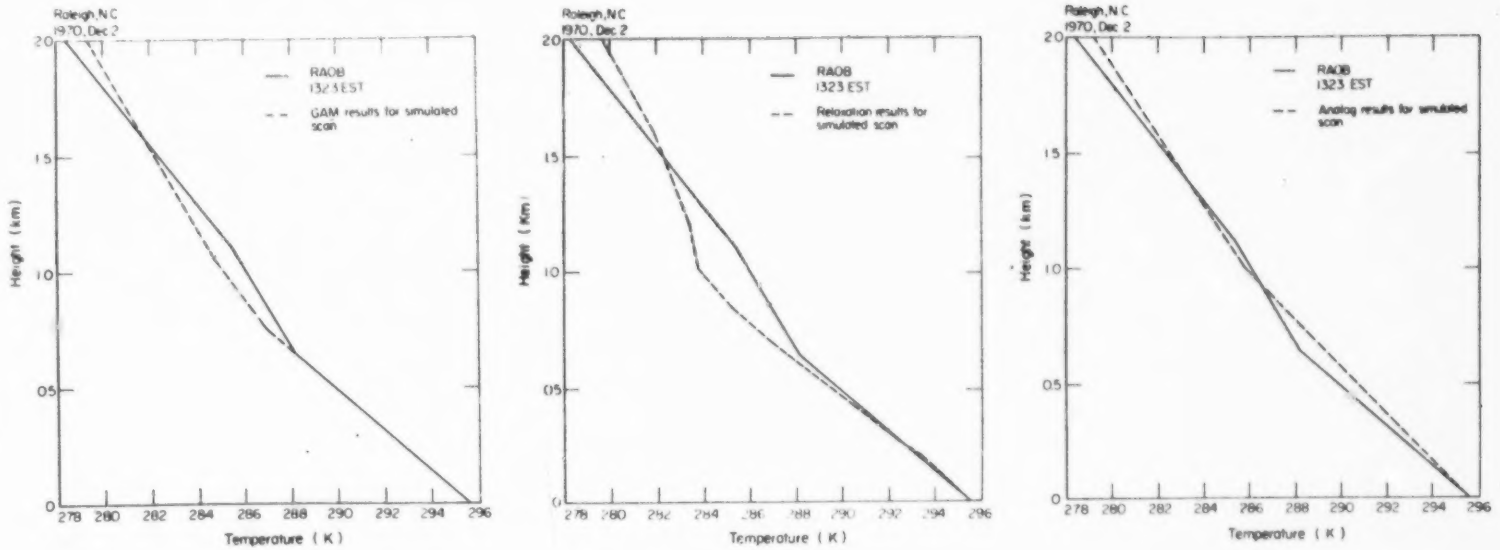

FIG. 19 GAM, relaxation and analog results for simulated data for Raleigh, N.C., 1323 EST, 1970 December 2.

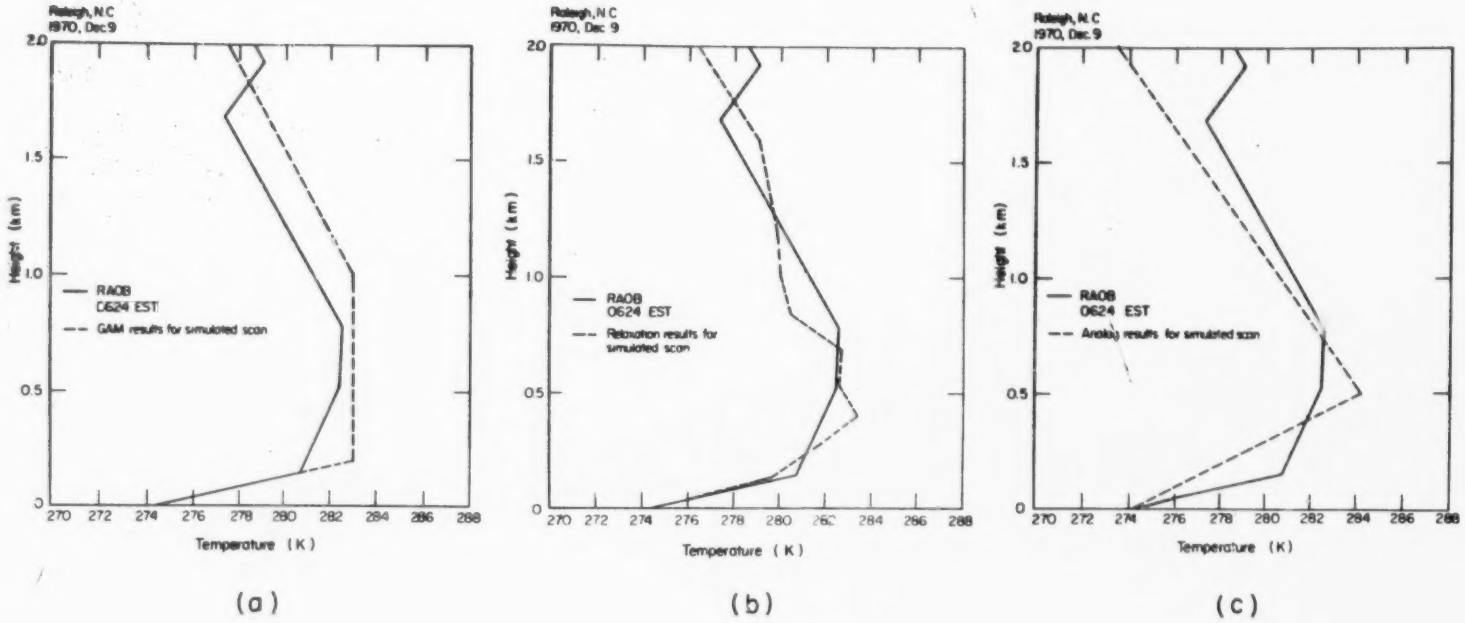

FIG. 20 GAM, relaxation and analog results for simulated data for Raleigh, N.C., 0624 EST, 1970 December 9.

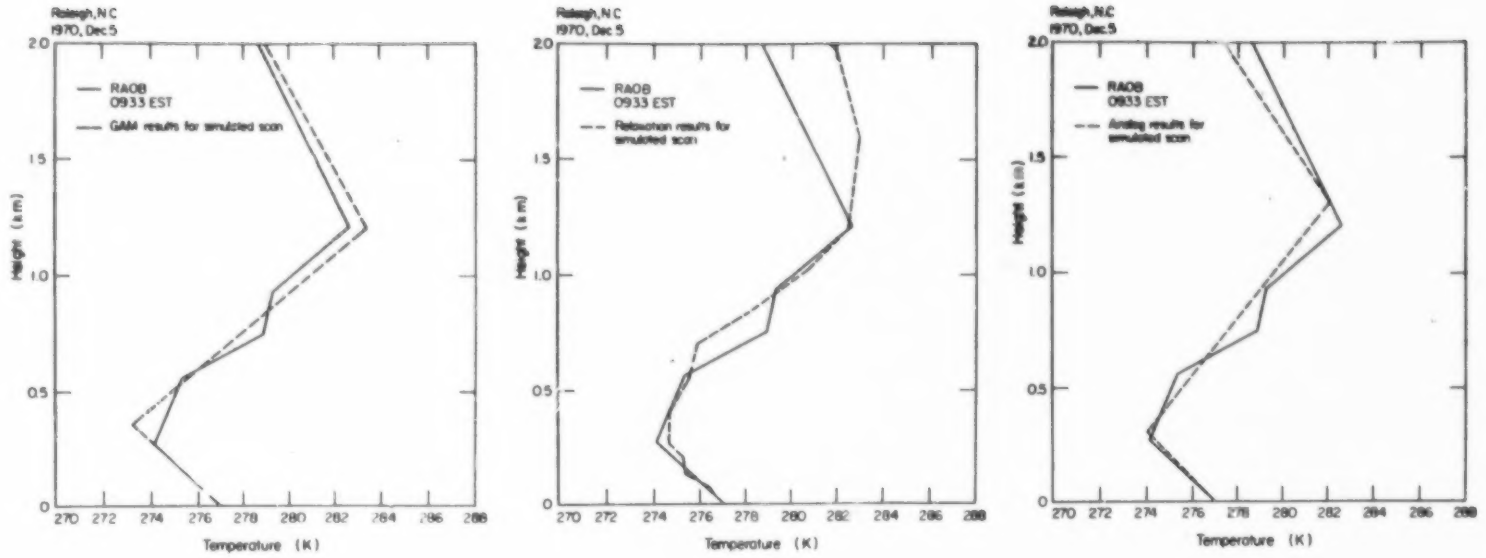

FIG. 21 GAM, relaxation and analog results for simulated data for Raleigh, N.C., 0933 EST, 1970 December 5.

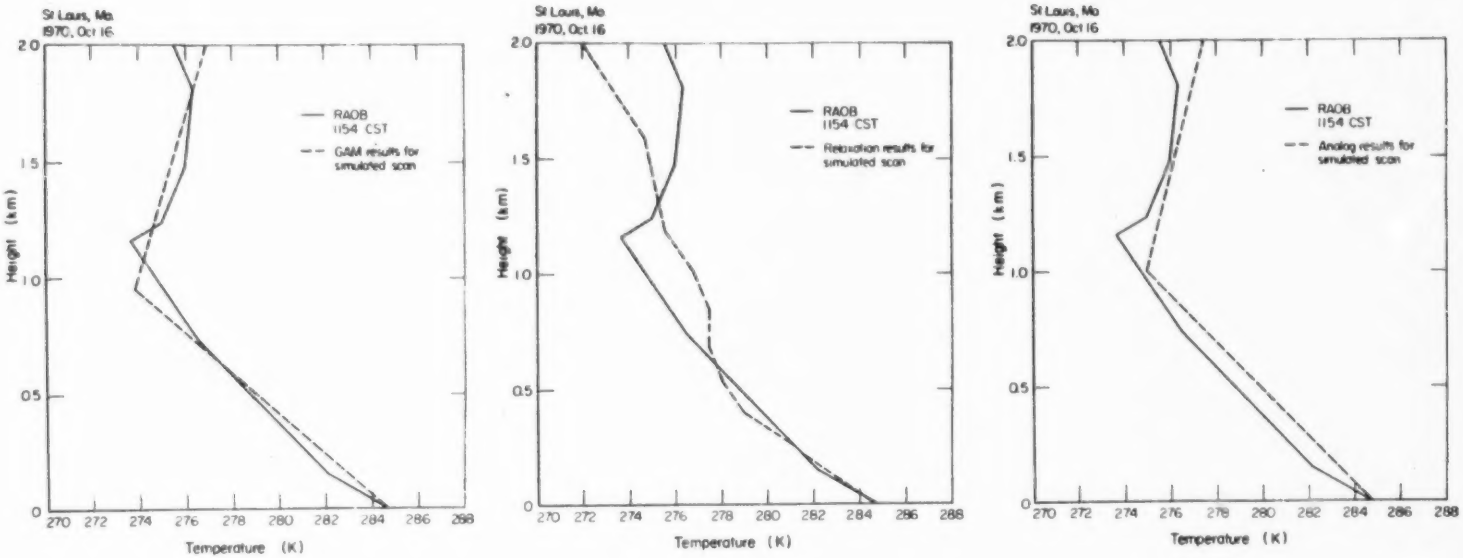

FIG. 22 GAM, relaxation and analog results for simulated data for St. Louis, Mo., 1154 CST, 1970 October 16.

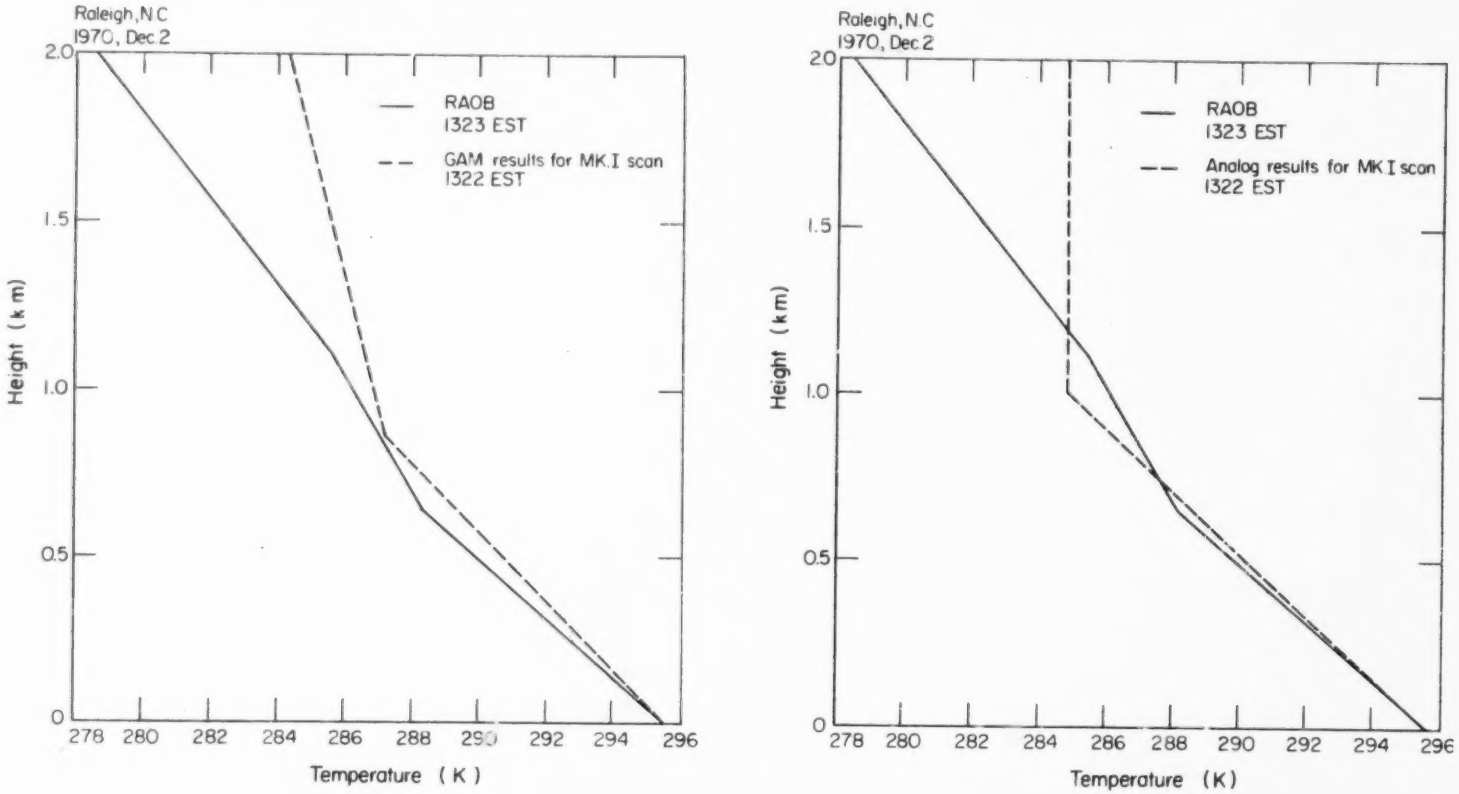

FIG. 23 GAM and analog results for MK I data obtained at Raleigh, N.C., 1322 EST, 1970 December 2.

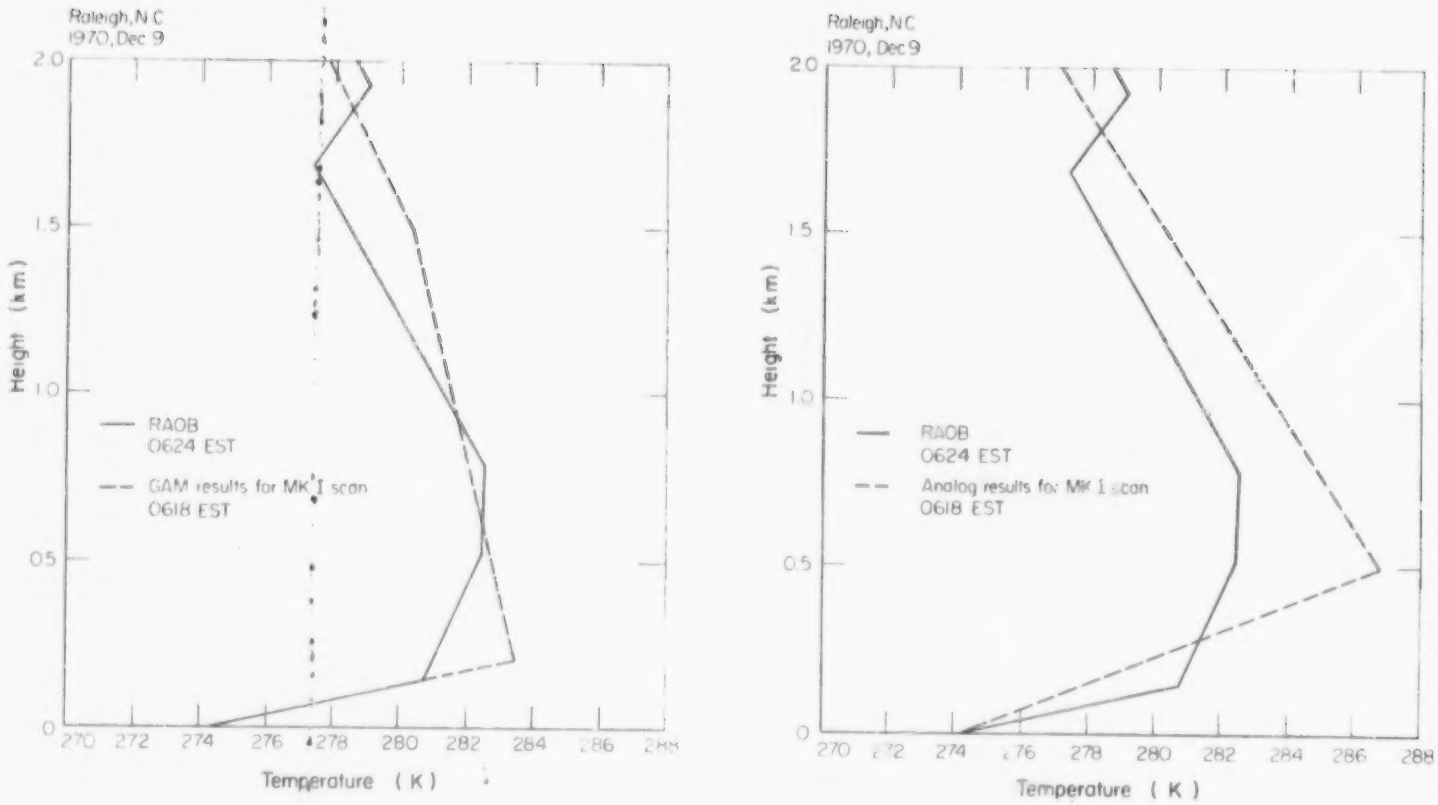

FIG. 24 GAM and analog results for MK I data obtained at Raleigh, N.C., 0618 EST, 1970 December 9.

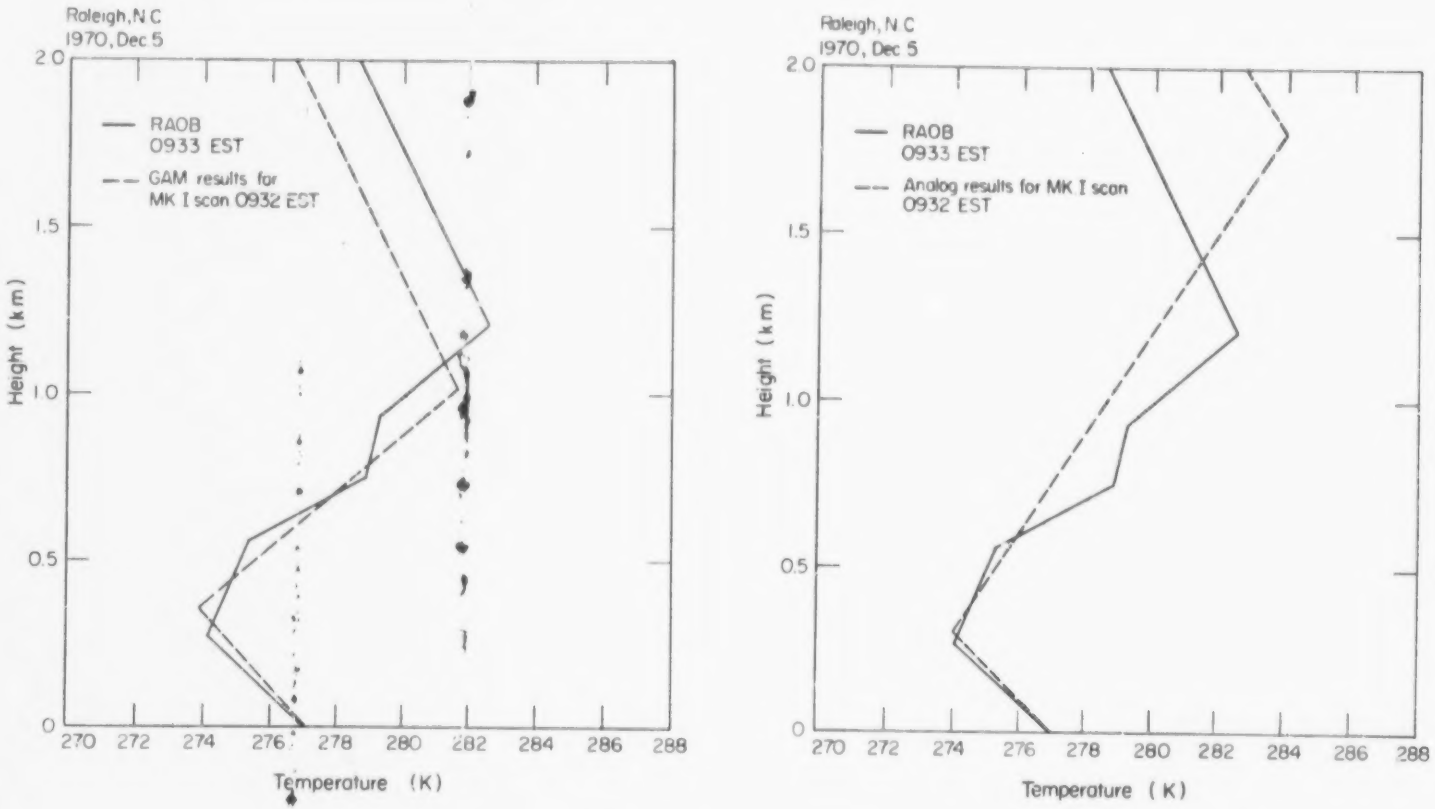

FIG. 25 GAM and analog results for MK I data obtained at Raleigh, N.C., 0932 EST, 1970 December 5.

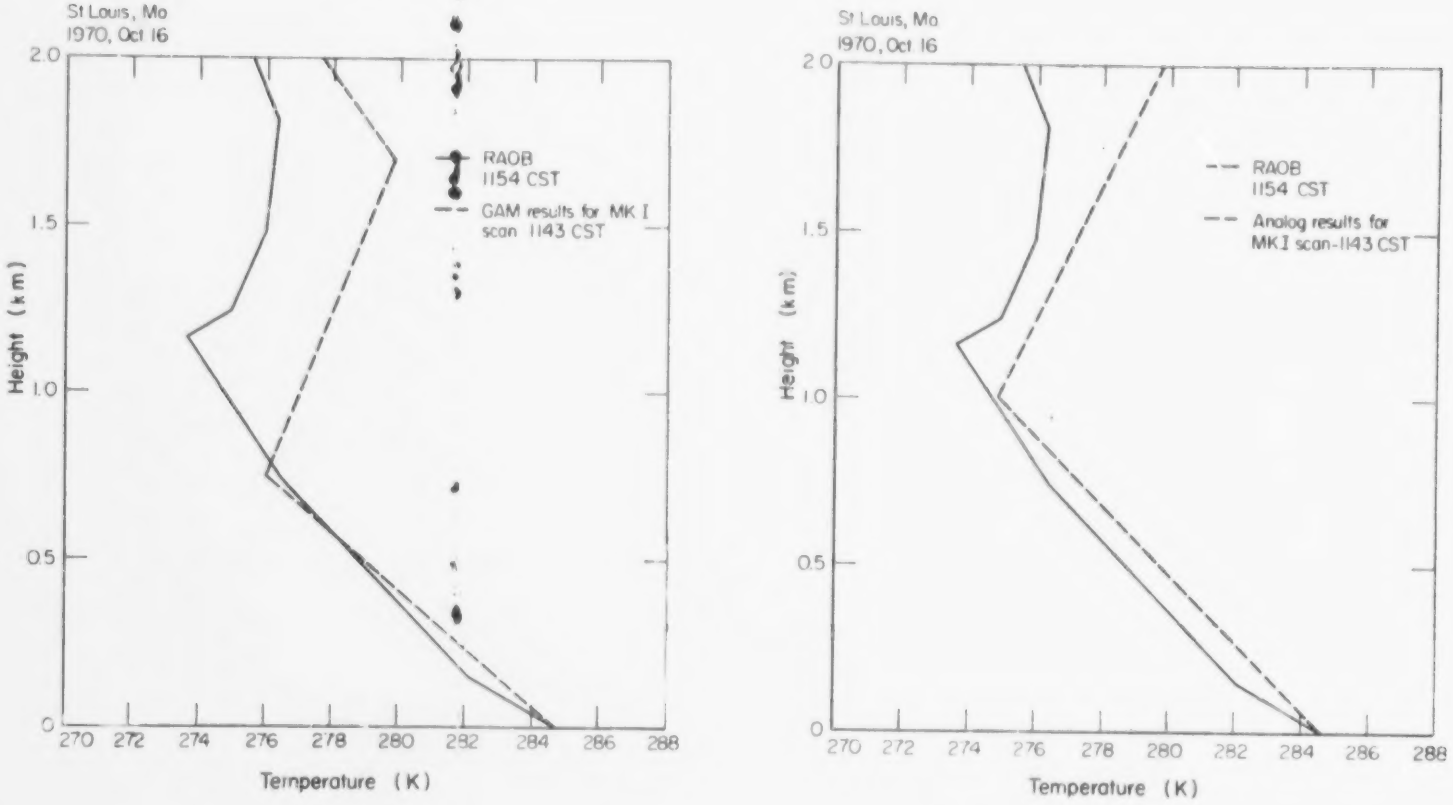

FIG. 26 GAM and analog results for MK I data obtained at St. Louis, Mo., 1143 CST, 1970 October 16.

3. Radiosonde errors
4. Space and time fluctuations in the atmosphere
5. MK I receiver noise

None of these is a factor when inverting simulated scan data. This suggests that, in principle, even better results are obtainable than have been demonstrated for observed data. This can be accomplished most easily by minimizing extraneous sky and ground contributions by improving the direct air and surface temperature measurements and by reducing THERMASONDE noise.

In order to more correctly assess the GAM technique's true performance capability on MK I observed data, the effect of the systematic bias produced by the simulation-observed discrepancy had to be removed. For purposes of this test, effect of the discrepancy was partially offset by performing the brightness computations at 54.6 GHz rather than at the actual operating frequency of 54.5 GHz. This is not considered an illegitimate procedure because, in actual practice, the discrepancy would be eliminated (or at least reduced) by appropriate equipment design and/or data correction. Further, this procedure does not optimistically bias the results because, if carried too far, it introduces more error of its own than it corrects.

The residual temperature profiles (above 5 km) used were the Raleigh, N. C., on-site radiosonde profile for 0825 EST, 1970 December 2 and the Salem, Illinois, National Weather Service radiosonde profile for 1200 GMT, 1970 October 16. The same residual profile was used in all three of the Raleigh cases.

For this test of the analog technique, no new library was constructed (nor warranted) at 54.6 GHz. The existing library was employed and no attempt was made to correct for the simulation-observed discrepancy. Thus, the analog technique results are a pessimistic estimate of its true performance capability. Consequently, we see predicted temperature inversion intensities or thicknesses that are greater than those observed, or occasionally an elevated inversion is predicted for a lapse profile. Correction of the simulation-observation discrepancy will certainly improve this situation.

In Table VIII, the average and average absolute temperature errors (in K degrees) for the different inversion techniques are tabulated. These average errors were obtained by picking off temperature differences between the

TABLE VIII

AVERAGE TEMPERATURE ERRORS FOR THE INVERSION TECHNIQUES

E1 = Average Absolute Error (K); E2 = Average Error (K)

	Simulated Scans						MK I Observed Scans			
	GAM		Relaxation		Analog		GAM		Analog	
Profile	E1	E2	E1	E2	E1	E2	E1	E2	E1	E2
Raleigh 1970 Dec. 2	0.41	-0.27	0.81	-0.55	0.42	0.38	1.55	1.55	1.71	1.56
Raleigh 1970 Dec. 9	1.15	1.04	0.84	-0.55	1.55	-1.40	0.91	0.79	1.82	1.52
Raleigh 1970 Dec. 5	0.43	0.31	1.05	0.84	0.56	-0.54	1.10	-0.89	1.54	0.98
St. Louis 1970 Oct. 16	0.45	0.25	1.28	-0.86	0.76	0.76	1.66	1.65	1.36	1.36
Overall Average	0.61	0.33	1.00	-0.28	0.82	-0.20	1.31	0.78	1.61	1.36

RAOB profile and the profile derived by the inversion method at every even-numbered 0.2 km increment in height from 0 to 2 km, inclusive. Minus signs occur for those cases where the inverted profile is colder on the average than the RAOB profile.

The overall average absolute error is smallest for the GAM technique with simulated scans. The error for observed scans is approximately twice that for simulated scans in both the GAM and analog cases. As already noted, this suggests that there is room for substantial improvement in the results for the observed scans. This will occur when discrepancies between simulation and observation are reduced, and through refinement of the inversion techniques.

3.6 SUMMARY

The original analog library was expanded to include a greater variety of model temperature profiles with particular emphasis on including a greater range of lapse rates. It was shown that analog libraries should be constructed to take into account surface pressure variations for each location. A new library was generated for Boulder, Colorado which incorporated surface pressure as an input parameter. A new format was developed for the library which facilitates rapid selection of the best-fit model. The technique has been used successfully in real-time service by Government personnel at St. Louis, Missouri, and Raleigh, North Carolina. SRRC corroborated these results by post analysis of the data. It has been shown that the analog technique gives a specification of the temperature inversion base height adequate for the air pollution meteorologist's requirements. A new computer program was developed which automatically generates model temperature profiles and the corresponding brightness temperatures. It provides a fast, easy means of creating high-resolution libraries tailored for the user's season, location, and surface pressure. It is anticipated that such libraries will yield significantly better inversion of THERMASONDE data than has been possible heretofore, especially with elimination of the simulation discrepancy.

The GAM technique was refined and tested using four air temperature profiles representative of important air pollution situations. Three different decision criteria were tested and the effects of scanned and discrete angle data were compared.

Since the GAM technique was developed to invert radiometric data into low-level temperature profiles and present the results in a form most meaningful to the air pollution meteorologists, these results are assessed from the viewpoint of how well the radiometrically determined profiles depict the characteristics of the actual profiles which are most important to them. From this point of view, the overall results of these four cases were quite good. Although as presently formulated the program is somewhat slow, it does provide a good indication of the mixing layer conditions.

It has been seen that the maximum correlation coefficient criterion performed better than the minimum sum of squares criterion. More extensive evaluations and field tests are necessary to more firmly establish this conclusion. It was also shown that the GAM technique works equally well with scanned or discrete angle data. Finally, further improvements to the technique were indicated in the areas of an improved shape-matching criterion, less constraint on the third layer gradient, and recoding for shorter running time.

A new method of implementing the relaxation technique was developed during this contract. This method produced a significant improvement in performance and utility for a broader class of temperature profiles than was previously possible. The technique has not been tested on real observed data because of the discrepancy between that and simulated brightness. Model studies covering several important classes of temperature profiles have demonstrated its capability of depicting the existence and location of elevated inversions. Further, these studies have shown that conventional statistical error criteria are unsuited to this application of achieving a shape fit. Principal needs for operational usage are: (1) elimination (reduction) of the antenna beam effects, (2) an improved error criterion, and (3) incorporation of the surface pressure parameter into this technique formulation.

Finally, it was seen that in the present state of development the GAM technique provides better results than the analog or the relaxation technique. The GAM and analog techniques, as presently constituted, provide temperature profiles for field observations with average absolute temperature errors less than 2 K. Eliminating the systematic difference between simulated and observed scans by properly accounting for ground effects, advantageous antenna configuration, and reducing THERMASONDE noise will probably reduce this error to less than 1 K. These factors will significantly improve performance of the relaxation technique for use with observed THERMASONDE data.

SECTION 4

ANALYSIS OF ANTENNA PATTERN EFFECTS

4.1 INTRODUCTION

In section 2.6 it was shown that excellent agreement was obtained between measured and calculated antenna temperatures if the brightness distribution was integrated over the antenna beam pattern. MK 0 measurement data were also corrected for antenna line losses. For MK I this correction is contained in the calibration curve, and since the output indication is already in terms of antenna temperature, no additional correction was necessary. This section gives a brief discussion of the mechanics of calculating antenna temperature from the brightness distribution. Results of such calculations are given for specific brightness distributions and antenna patterns. General implications of these results are examined in terms of minimizing ground and atmospheric contributions which distort the brightness distribution. Finally, consideration is given to the impact of these results upon design of the MK II THERMASONDE and how to achieve an optimum trade off.

4.2 THE PROBLEM

Prior to refurbishment of MK I in 1970 February, it was necessary to calibrate the THERMASONDE by injecting a known calibration temperature into the input terminals just behind the antenna structure. To translate calibration temperature into source brightness temperature, an empirically derived correction, called the antenna factor, was used. This factor provided correction at one elevation angle compatible with other system errors. As increasingly sophisticated data processing techniques require greater measurement accuracy, a more sophisticated model for the antenna-source interaction was needed.

To describe the situation in greater detail requires that the source brightness distribution be specified from 0 to π zenith angle. This means that in addition to emission from the atmosphere, contributions from the ground for zenith angles between $\pi/2$ and π must also be included. Figure 27 illustrates an antenna with its boresight axis oriented at zenith angle α and the total incident brightness $T_B(\xi)$ impinging from the general ray direction ξ. We define the generalized source brightness distribution function $T_B(\xi)$ as

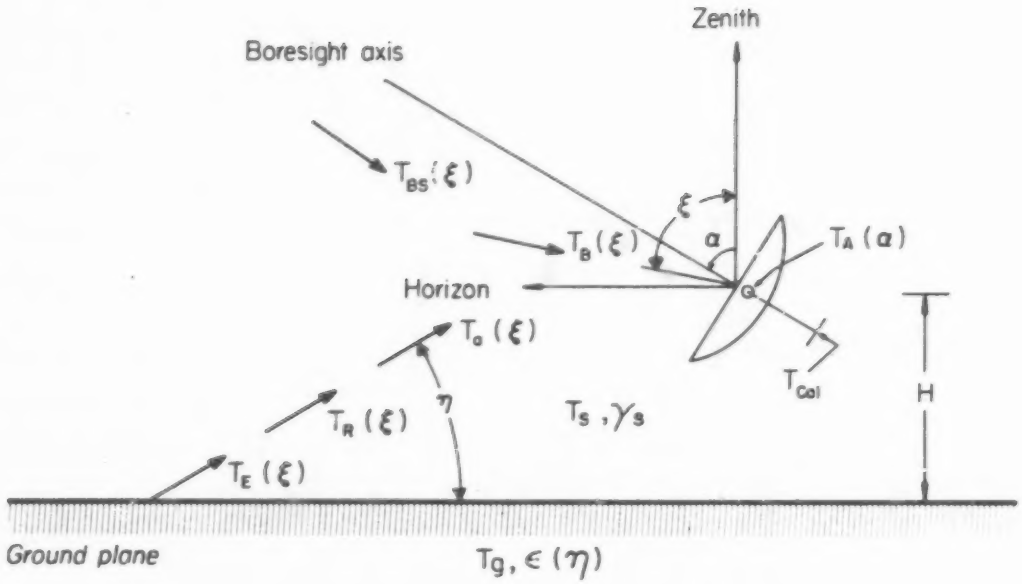

FIG. 27 Contributions to source brightness distribution.

$$T_B(\xi) = \begin{cases} T_{BS}(\xi) & \text{for } 0 \le \xi \le \frac{\pi}{2} \\ \left[T_E(\xi) + T_R(\xi)\right] \exp(-\gamma_S H/\sin\xi) + T_a(\xi) & \text{for } \frac{\pi}{2} < \xi \le \pi \end{cases} \qquad (9)$$

where

the ground-emitted contribution is $T_E(\xi) = T_g\, \epsilon(\eta)$

the ground-reflected contribution is $T_R(\xi) = \left[1-\epsilon(\eta)\right]\left[T_{BS}(\pi - \xi)\right]$

and the contribution of the intervening air is

$$T_a(\xi) = T_S \left[1 - \exp(-\gamma_S H/\sin\xi)\right]$$

given that

α = zenith angle of boresight axis

ξ = zenith angle of a general ray

η = elevation angle of a general ray at ground plane =

$$(\xi - \tfrac{\pi}{2}) \quad \text{for} \quad \pi \ge \xi > \tfrac{\pi}{2}$$

H = height of the antenna above ground plane

T_g = ground temperature

T_S = surface layer air temperature

$T_{BS}(\xi)$ = sky brightness at zenith angle ξ

ϵ = emissivity of ground

γ_S = surface layer absorption coefficient.

For any particular orientation of the boresight axis, the antenna collects energy from all ray directions. The resultant integrated value, called antenna temperature $T_A(\alpha)$, is different from the source brightness temperature in the boresight direction. Furthermore, this difference depends not only upon the source brightness distribution, but also upon the orientation and power response (in each ray direction) of the antenna.

Section 4.3 presents a mathematical description of the antenna temperature calculation.

4.3 CALCULATION OF ANTENNA TEMPERATURE

The antenna temperature $T_A(\alpha)$ is given by the convolution of the antenna normalized power response function $P(\zeta,\phi)$ and the source brightness distribution function $T_B(\xi)$. This is expressed mathematically as

$$T_A(\alpha) = \frac{\int_0^{\pi}\int_0^{\pi} T_B(\xi)\, P(\zeta,\phi)\, \sin\zeta\, d\phi d\zeta}{\int_0^{\pi}\int_0^{\pi} P(\zeta,\phi)\, \sin\zeta\, d\phi d\zeta} \tag{10}$$

where α = zenith angle of the antenna axis

ζ = off-axis angle of an incident brightness ray

ϕ = azimuthal angle in the antenna reference frame of an incident brightness ray

ξ = zenith angle of an incident brightness ray and

a_z = azimuthal angle in the horizon plane of an incident brightness ray.

The angular arcs α, ζ, and ξ (see Fig. 28) form the sides of spherical triangle with an included angle $\pi - \phi$ between the sides α and ζ. Therefore, the angle ξ can be expressed as a function of α, ζ, and ϕ. Similarly, if the incident brightness temperature were a function of a_z, the azimuthal angle in the earth reference frame, this dependancy also could be derived in terms of α, ζ, and ϕ.

The power response function was initially assumed to be a pattern of revolution about the antenna's axis, that is, independent of ϕ. Antennas such as the dual hog horn, however, give rise to power response functions which are decidedly not patterns of revolution.

Usually the power response patterns of an antenna are measured at various off-axis angles ζ from 0 to π radians in two orthogonal planes corresponding,

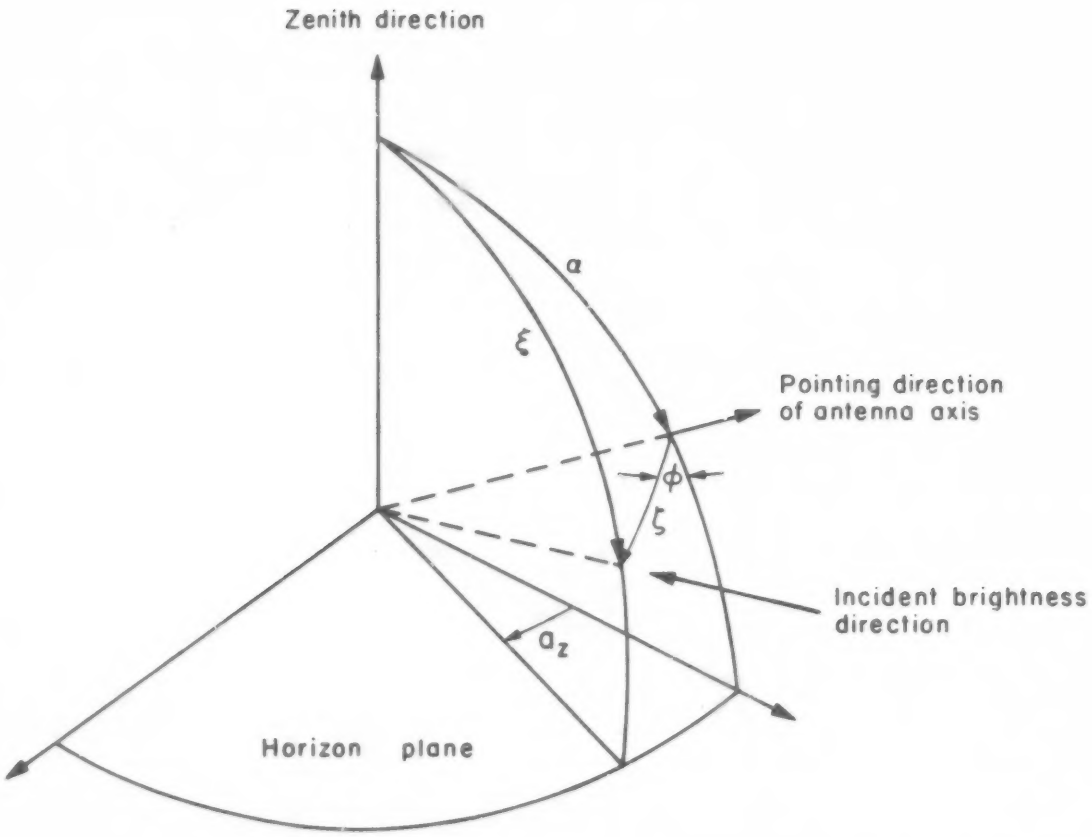

FIG. 28 Angular relationships for antenna temperature calculations.

respectively, to $\phi_1 = 0$ and $\phi_2 = \frac{\pi}{2}$. If the power response pattern is assumed to be one of revolution about the antenna axis, then $P(\zeta_1,\phi_1) = P(\zeta_2,\phi_2)$ when $\zeta_1 = \zeta_2$. If the power response pattern is not one of revolution about the antenna axis, then $P(\zeta_1,\phi_1) \neq P(\zeta_2,\phi_2)$ when $\zeta_1 = \zeta_2$. In this case it is assumed that $P(\zeta,\phi_1)$ and $P(\zeta,\phi_2)$, for ζ constant, define the major and minor axes of an ellipse. Thus, $P(\zeta,\phi)$ for an arbitrary ϕ and a constant ζ is given by the length of the radius vector in the polar coordinate expression for the ellipse. In the case of a pattern of revolution, the ellipse degenerates to a circle of radius $P(\zeta)$.

The finite difference approximation used in the actual calculation of $T_A(\alpha)$ is

$$T_A(\alpha_k) = \frac{\sum_{i=2}^{N(\zeta)} \left\{ \sin\zeta_i \; T_{W_i} + \sin\zeta_{i-1} \; T_{W_{i-1}} \right\} (\zeta_i - \zeta_{i-1})}{\sum_{i=2}^{N(\zeta)} \left\{ \sin\zeta_i \; R_i + \sin\zeta_{i-1} \; R_{i-1} \right\} (\zeta_i - \zeta_{i-1})} \tag{11}$$

where

$N(\zeta)$ = number of increments in ζ from $\zeta = 0$ to $\zeta = \pi$

$$T_{W_i} = \sum_{j=1}^{M_i} \left[T_B\left\{\xi(\alpha_k, \zeta_i, \phi_j)\right\} + T_B\left\{\xi(\alpha_k, \zeta_i, \phi_{j-1})\right\} \right] E_i(\phi_j, \phi_{j-1})$$

$$R_i = \sum_{j=1}^{M_i} E_i(\phi_j, \phi_{j-1})$$

M_i = number of increments in ϕ from $\phi = 0$ to $\phi = \pi$

$E_i(\phi_j, \phi_{j-1})$ = integral of the antenna power response function over the interval ϕ_{j-1} to ϕ_j

k = index of antenna pointing direction angle, and

$\xi(\alpha_k, \zeta_i, \phi_j) = \cos^{-1}\{\cos \alpha_k \cos \zeta_i - \sin \alpha_k \sin\zeta_1 \cos \phi_j\}$.

The value of $N(\zeta)$ is determined by the complexity of the antenna response function, with more increments required for the complex patterns. The ϕ increments, on the other hand, when taken together with preselected values of α and ζ, determine the increments of ξ and should be based on the complexity of the brightness temperature distribution. For the sake of simplicity, the ϕ intervals have been selected such that

$$\xi(\alpha_k, \zeta_i, \phi_j) - \xi(\alpha_k, \zeta_i, \phi_{j-1}) = 1 \text{ degree} .$$

This one-degree change in the zenith angle of the incident brightness results in an adequate tabulation for numerical integration purposes of the most complicated brightness temperature distributions that are normally encountered.

The criterion for the ϕ increments results in very large ϕ intervals for small values of α. When the antenna power response function is not a pattern of revolution, the integrals of the power response functions over the ϕ intervals become elliptic integrals of the first kind. In the case of patterns of revolutions, the elliptic integral reduces to the value of the ϕ increment, i.e., $\phi_j - \phi_{j-1}$. Thus, no matter how large the ϕ intervals may be, $E_i(\phi_j, \phi_{j-1})$ may be accurately determined.

The entire program for calculating antenna temperature (ANTEM) was set up to perform three different functions. First, the source brightness distribution function $T_B(\xi)$ is calculated for ξ between 0 and π [see Eq. (9)] from a prescribed air temperature profile $T(p)$, operating frequency ν, ground temperature T_g, height above ground H, and ground emissivity function $\epsilon(\xi - \frac{\pi}{2})$. Next, the antenna temperature function $T_A(\alpha)$ is obtained by the integration indicated in Eq. (10) for this brightness distribution and a prescribed antenna power response pattern $P(\zeta,\phi)$. Finally, the effect of elevation angle scanning is synthesized from the resulting antenna temperature versus elevation angle function $T_A(\frac{\pi}{2} - \alpha)$ and a prescribed scan rate and integration time. Brightness temperature, antenna temperature, and scanned antenna temperature are listed for each degree of elevation angle from 0 to 90. In addition, for patterns of revolution $P(\zeta)$ certain pattern integrals are calculated from the denominator of Eq. (10) for specified limits on ζ.

An example of results using this program is shown in Fig. 29. The

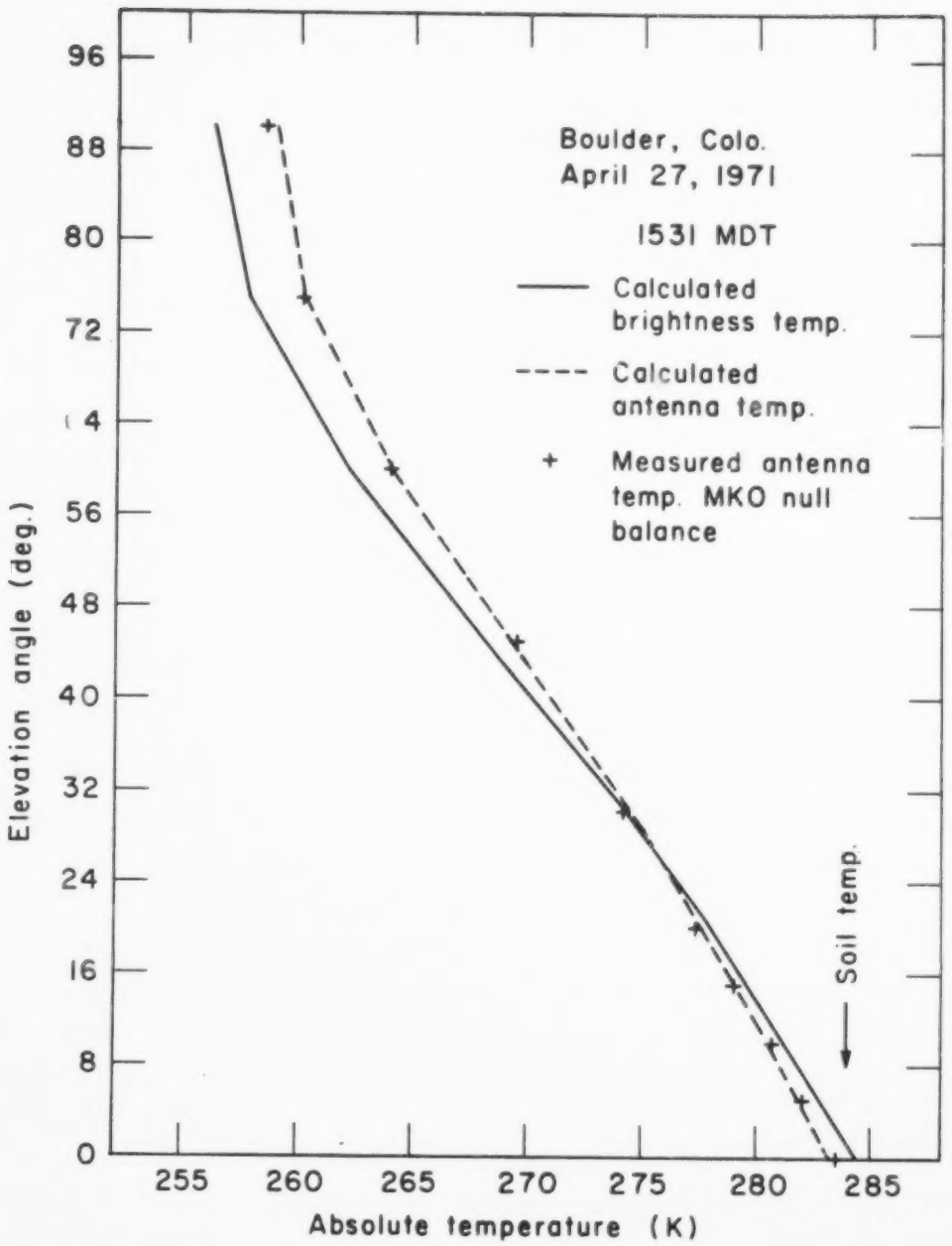

FIG. 29 Results using antenna temperature computation (ANTEMP).

brightness temperature function was calculated using the 1531 MDT RAOB for the air temperature profile, 54.5 GHz for the operating frequency, 284 K for the ground temperature, unity for the ground emissivity, and 3 feet for the antenna height. The E and H plane patterns for the MK 0 antenna were averaged and the resultant pattern was assumed to be the applicable pattern of revolution $P(\zeta)$. The calculated antenna temperatures are shown in the figure. The crosses show corresponding measured antenna temperatures using MK 0. This figure clearly shows that the computer program does indeed give results which are well substantiated by measurement.

The difference between the solid and dashed curves in Fig. 29 is the discrepancy discussed at length in Section 2.0. The necessity to minimize effects of this discrepancy has already been mentioned. Clearly, it would be desirable that the antenna temperature distribution be a faithful reproduction of the brightness distribution. Thus, for our purpose, antenna performance can be measured by the similarity of these distributions. The next two subsections (4.4 and 4.5) are a discussion of the interaction between the brightness distribution and the antenna pattern leading toward specification of optimum antenna design parameters.

4.4 OPERATIONAL SIGNIFICANCE OF THE ANTENNA PATTERN RESPONSE

Figure 30 shows a comparison of calculated responses to a step change in an isothermal brightness distribution for an ideal antenna and for the MK I antenna. Such a brightness distribution is not physically realistic, but the response tells a good deal about the system performance. The effect of the main beam is clearly seen in the region of rapid change between ± 4 degrees. The effect of the side and back lobes is given by the remainder of the response pattern. This result shows that the principal deviation from ideal response is due to the side and back lobes. If this response were reduced even by as little as one-half without changing the beamwidth, a respectable improvement could be obtained. This suggests that the MK II antenna design ought to be optimized for maximum main-beam efficiency, rather than minimum beamwidth.

To obtain an indication of the ground contribution to total antenna temperature, the antenna temperature distribution was calculated for a typical high, weak elevated inversion profile with a ground plane whose emission temperature was 10 C different from the surface air temperature. The horizontal

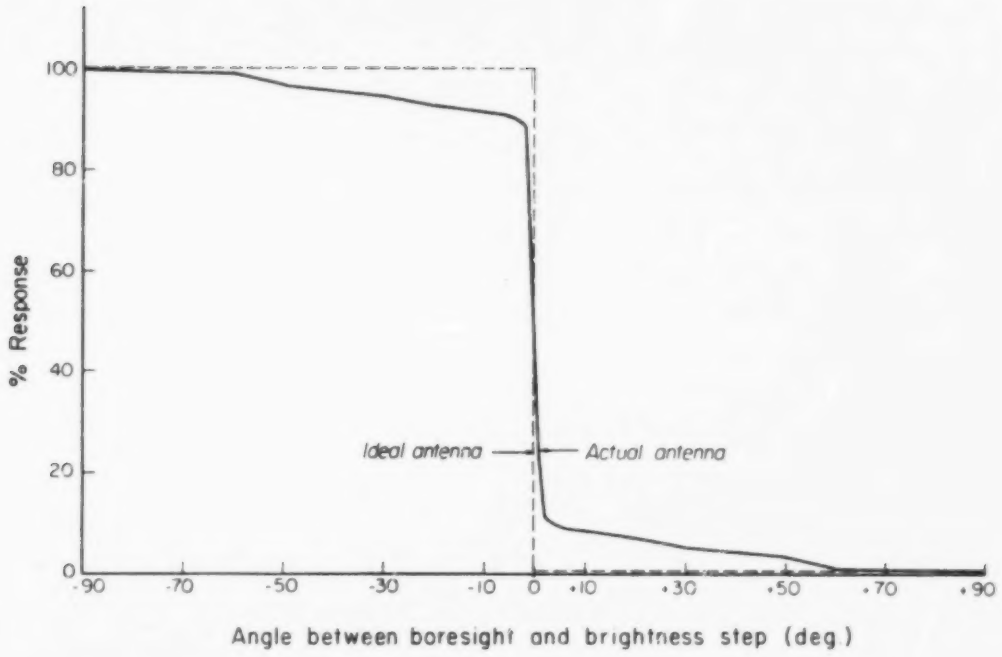

FIG. 30 Antenna response to a step brightness change.

ground plane was assumed 3 feet below the antenna, and the ground emissivity was assumed equal to 0.89 sin(elevation angle). From this distribution we subtracted antenna temperatures calculated for the same situation, except that the ground plane temperature was assumed equal to the surface air temperature. The difference provides an indication of the variation of magnitude of the ground contribution. The result is shown in Fig. 31, where the difference (expressed as a percentage of the maximum possible contribution (10 C)) is plotted as a function of elevation angle. The contribution of ground radiation entering the lower half of the main beam decreases smoothly from 4.5 per cent as boresight elevation angle increases over the first 70 degrees. There is a relatively constant variation, from radiation entering the side and back lobes, throughout the remaining 20 degrees of elevation angle.

If the ground is hotter than the surface air, as is usually the case for a lapse off-the-surface condition, then the observed antenna temperature is higher than the surface air temperature and the indicated decrease with increasing elevation angle is accentuated. Conversely, if the ground is colder than the surface air, as is usually the case for ground-based inversions, then the observed antenna temperature is less than the surface air temperature and the indicated increase with elevation angle is also accentuated. Although the magnitude of this accentuation diminishes rather rapidly as elevation angle increases, it is seen to persist up to about 60 degrees for the MK I antenna. Reducing the side lobe response is clearly necessary to minimize propagation of ground contribution effects to such high elevation angles.

A second major consequence of a non-ideal antenna pattern is the apparent distortion of the source brightness distribution. An indication of the magnitude of this effect was calculated for the 9 December RDU temperature profile with ground temperature assumed equal to the surface air temperature. The result is shown in Fig. 32. Here, the differences between the source brightness temperature and the integrated antenna temperature for each elevation angle are plotted as a function of elevation angle. The distortion shown by the abscissa values can be thought of as an "atmospheric contribution" which must be added to the observed antenna temperature to give the source brightness temperature. For angles below about 28 degrees, the brightness temperature is underestimated, i.e., antenna temperature is less than brightness temperature.

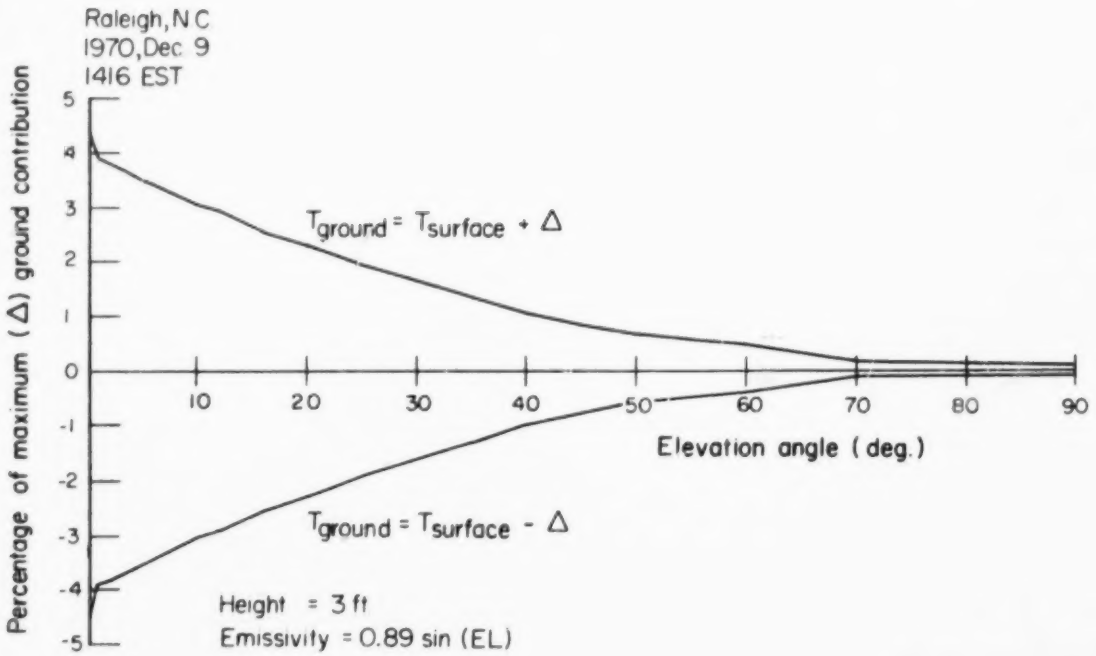

FIG. 31 Ground contribution variation.

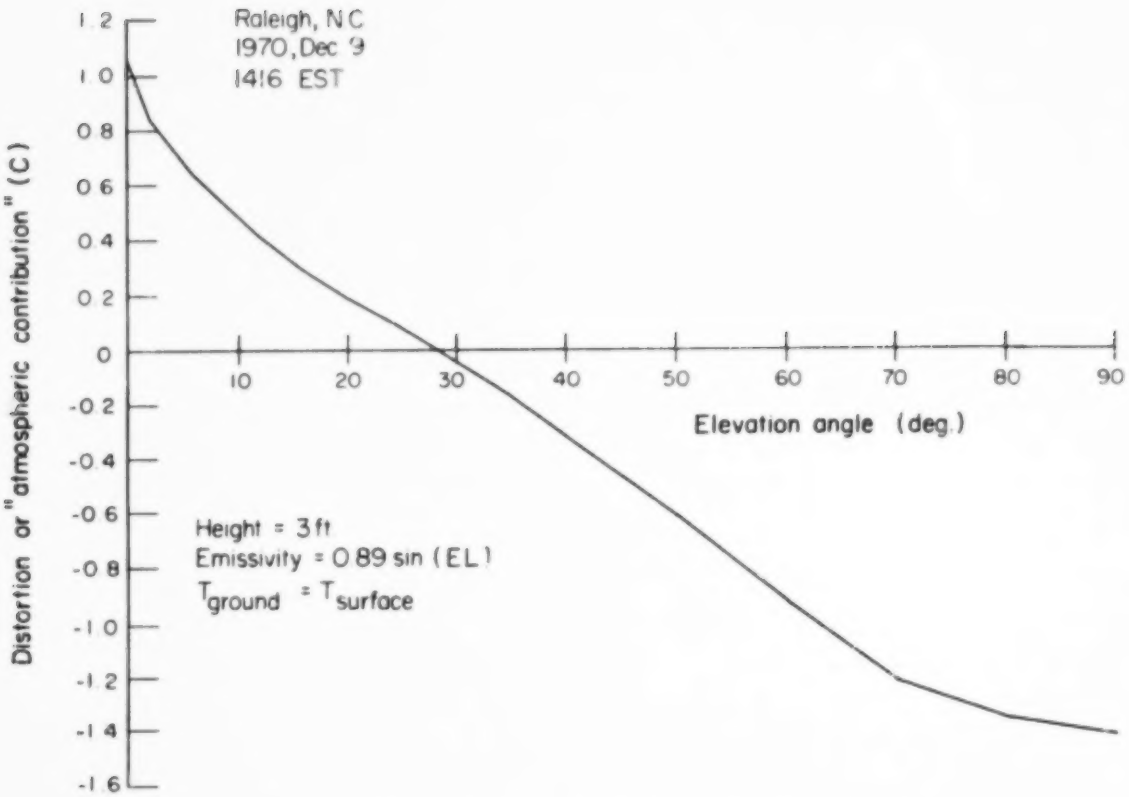

FIG. 32 Distortion of sky brightness distribution.

Above 28 degrees, the situation is reversed. Although the detailed structure of this distortion curve depends greatly upon the brightness distribution, this one serves to illustrate the general nature for a large class of profiles where the brightness gradient is always negative.

It is significant to note that the distortion component in the horizontal (0 degrees) is less than that in the vertical direction (90 degrees). This arises because in the vertical orientation every ray entering the antenna is hotter than that for the boresight direction (90 degrees). Consequently, the antenna temperature must be maximum with respect to the brightness temperature at 90 degrees. For the horizontal orientation, half of the entering rays are at the same brightness temperature and only the other half are colder than the brightness at zero degrees. Thus one expects less reduction of brightness temperature at zero degrees elevation than the corresponding increase produced at 90 degrees. Extending this qualitative argument to a fan-beam of the same vertical angle beam width, one might predict less distortion in the horizontal direction but greater distortion for vertical orientation. Just what the net result of decreasing the vertical beam width and increasing the horizontal beam width (as for a fan beam antenna) would be is difficult to predict from such qualitative arguments. It is, however, amenable to quantitative study by prescribing a fan beam antenna pattern and calculating the resultant antenna temperatures. Judging from the magnitude of the distortion component for the MK I antenna, such a calculation was definitely warranted.

There are three alternative ways to reduce the influence of antenna effects upon performance of the data processing techniques: The antenna beam pattern can be made to approach the ideal; the observed data can be corrected for the atmospheric and ground contributions; and the data processing techniques can be modified to perform the comparison between measured antenna temperature distribution and that predicted from an assumed model air temperature profile. In addition, it may be possible in some cases to elevate the antenna above ground level to reduce ground contributions. Each possibility has economic and operational advantages and disadvantages. Consequently, there are trade offs which can be made to achieve the best balance for any particular application.

4.5 ANTENNA OPTIMIZATION STUDY

4.5.1 Objective and Approach

The objective of this study was to determine an effective means of

eliminating, as much as possible, the unwanted effects of extraneous ground and sky radiation. It was desired to determine the amount of reduction possible through improved antenna design and, consequently, how much additional reduction might be necessary through data processing. Furthermore, any hardware changes had to be compatible with existing MK II THERMASONDE design concepts and be cost effective from a manufacturing point of view. It was desirable that any hardware change have minimum reaction upon the data processing techniques as presently constituted. That is, no significant increase in complexity, running time, or storage requirement was acceptable.

The approach was to calculate objective performance criteria for several measured antenna patterns representative of types of antenna systems suitable for this application. The different patterns available for analysis were determined in cooperation with Sperry Microwave Electronics Division to insure that results obtained would be a physically realizable measure of achievable performance for producible antenna configurations.

4.5.2 Procedure Used

Consequences of including the antenna temperature calculation routine in the three data processing technique formulations were evaluated. It was determined that to merge the present antenna temperature routine with the two iterative techniques (GAM and LRRT) would likely result in excessively costly data processing. Merging with the analog technique would be feasible, but at the expense of considerably increased library production time and cost.

An exploratory calculation of the performance of a hypothetical antenna whose power response pattern represented a modest improvement to that of MK I indicated that significant performance improvement was possible. It was clear that improved antenna design was a worthwhile procedure to achieve the desired error reduction.

Discussions were held with SMED engineers to consider candidate antenna types from the standpoint of electrical performance, development cost, production cost, and availability of suitable pattern data. The preliminary list of types deemed suitable for this application included:

1. Dielectric lens corrected horn
2. Offset paraboloid
3. Full paraboloid with J-feed

4. Horn-reflector (echo type)

5. Cassegrain

6. Fan beam (dual hog horn).

Patterns representative of each of the above types were measured on models and scaled, as necessary, to the desired operating wavelength and aperture dimension. In some cases theoretical patterns were computed from idealized aperture distributions to provide an indication of the theoretical limit obtainable. From these patterns, antenna temperature distributions were calculated for the step function brightness distribution and for several representative air temperature profiles.

4.5.3 Results Obtained

From these computations, three figures of merit were derived and indications of the ground and sky contribution were obtained using a representative RAOB profile. The first figure of merit is called main beam efficiency and is given by the ratio of the pattern integral [see denominator of Eq. (10)] over the main beam (to first null) to that over the entire π radians. It is the fraction of all energy collected by the antenna that is received only through the main beam. This number should be as near unity as possible to minimize collection of extraneous energy from the ground and sky. The second figure of merit comes from the step function response as shown in Fig. 30. One can think of the "actual antenna" curve as being the error in reproducing the step brightness change. The angle for which this error reduces to 2% indicates how rapidly the error diminishes. Obviously, this figure should be as small as possible. Finally, the last figure of merit is given by the area under the curve in Fig. 30. It is an integrated error over the entire 90 degrees. Only the positive angles are considered, since the negative half is simply an inverted reflected image. The measures of ground and sky contribution were discussed in Sec. 4.4 and shown in Figs. 31 and 32, respectively.

Table IX shows a summary of the significant performance characteristics calculated for the various types of antennas considered in this study. It is evident from examination of these results that the narrow vertical beam width of the fan beam type has achieved some improvement over MK I, particularly in integrated error and reduction of sky contribution. The wide horizontal beam width contributes to poor efficiency and slow reduction of error. Further,

TABLE IX

SUMMARY OF ANTENNA PERFORMANCE CHARACTERISTICS

Antenna Type	Aperature Diameter - Inches	Vertical Half-Power Beamwidth - Degrees	Horizontal Half-Power Beamwidth - Degrees	Main Beam Efficiency - %	Angle for 2% Error - Degrees*	Integrated Error K-Degrees*	Contribution from Ground - % of Max.□	Max. Contribution from Sky at 0° and 90° Elevation K
MK I	6	2.4	2.4	79.0	56	30.60	4.39	+1.07 -1.50
Fan Beam	12x2½	1.4	4.4	74.4	64	23.30	2.77	+0.35 -0.72
Cassegrain	24	0.64	0.64	87.0	11	9.88	1.24	+0.33 -0.31
Horn Lens	2	7.1	7.1	99.0	5.2	11.70	0.50	+0.40 -0.10
Horn Lens	4	3.5	3.5	98.5	3.4	7.45	0.32	+0.36 -0.08
Horn Lens	6	2.4	2.4	98.5	2.5	6.31	0.41	+0.25 -0.05
Tapered-J	8	2.5	2.5	94.5	4.5	6.95	1.35	+0.40 -0.25
Tapered-J△	8	2.2	2.2	99.7	1.5	2.88	0.45	+0.15 -0.01
Tapered-J△	10	1.8	1.8	99.8	1.0	2.15	0.33	+0.11 -0.0
Tapered-J	10	1.9	1.9	93.4	13.0	8.90	1.23	+0.35 -0.22
Tapered-J	6	3.2	3.2	93.7	19.0	14.40	1.81	+0.50 -0.40

* Calculated from two-valued (10K step) brightness distribution.

□ Calculated from RDU, 9 Dec. 1970, 1416 EST, RAOB profile. Ground temperature assumed 10 K colder than surface air.

△ Calculated from theoretical pattern.

Note: Antenna assumed 3 feet above surface, and ground emissivity = 0.89 sin (elevation angle).

it is clear that the fan beam antenna does not achieve as good ground contribution reduction as some of the other types. Thus, the fam beam concept is not indicated for the MK II THERMASONDE.

Results shown for the horn lens (dielectric lens) type are also representative of the horn-reflector (echo) type because both are completely unblocked circular apertures. The tapered J-fed paraboloid results are for a cosine-squared feed pattern adjusted so that the first null occurs at the angle subtended by the reflector rim. Some difficulty was experienced with adjusting the offset paraboloid model, so no pattern data were obtained and no results are available. This is unfortunate, because this type of antenna should yield excellent performance because of its unblocked aperture. Also, it is economically and mechanically attractive.

The table shows that extremely good performance can be obtained with beam widths on the order of 2 degrees, if very high main beam efficiency is maintained. On the other hand, extremely narrow beam widths, i.e., less than one degree, are not beneficial unless accompanied by high main beam efficiency.

Additional experiments at SMED indicated that power losses in the dielectric lens would be higher than desirable unless extremely costly materials were used. The effects of lens losses were considered serious enough to abandon the horn lens antenna in favor of the tapered J or the offset parabola types.

Although the horn-reflector antenna is capable of high efficiency, its poor space utilization and manufacturing cost make it a less desirable choice. The cassegrain design is characteristically less efficient, except for very large aperture diameter.

The theoretical (unblocked) response of a tapered J-feed configuration shows excellent performance in all respects. Actual performance of a 10-inch prototype was somewhat poorer than theoretical (because of blockage by the J feed line) but three-to-four times better than MK I. Its compact design, ease of fabrication and adjustment, and good performance make this the most attractive possibility of those examined.

To extend our estimate of antenna performance, the 10-inch tapered J-fed paraboloid pattern was tested with five additional model air temperature profile types, each representative of important air pollution situations.

The profiles were:

1. Lapse
2. Lapse with superadiabatic layer at surface
3. Moderately intense, middle-height, elevated inversion
4. Intense, low elevated inversion
5. Intense, ground-based inversion

These profile models were generated for fall conditions at White Sands, New Mexico (surface pressure approx. 878 mb). Antenna temperature distributions were calculated assuming the antenna was 3 feet above the surface, the ground temperature equalled the surface air temperature, and that ground emissivity varied as 0.89 sin (elevation angle). Differences between antenna temperature and brightness temperature were listed, and the maximum range (i.e., plus and minus error) and maximum magnitude (i.e., plus or minus error) were selected for each profile. Results are shown in Table X. For comparison, data for the MK I antenna are shown also.

TABLE X

MAXIMUM ANTENNA ERRORS FOR DIFFERENT PROFILES
(10-inch Tapered J-Fed Paraboloid)

	Max. Error -C	
Profile	Max. Range	Magnitude Max. Abs.
Lapse	0.64	0.35
Lapse with Super	0.84	0.49
Mod., Mid., E.I.	0.53	0.33
Int., Low, E.I.	0.44	0.32
Int., G.B.I.	0.51	0.36
*Weak, High, E.I.	0.57	0.35
MK I		
*Weak, High, E.I.	2.90	1.45

*RDU 9 Dec. 1970

When scanned antenna temperatures were compared with the brightness distribution, the resultant differences were somewhat larger than those shown in Table X. Further examination showed that the small residual error due to

the elevation angle scanning function could be up to twice as large as the antenna error for normal operating conditions. Additional antenna temperature distributions were made for different combinations of scan rate and integration time, all using the intense ground-based inversion profile model. This time, the maximum antenna error (maximum difference between brightness and antenna temperature), scan error (maximum difference between antenna and scanned antenna temperature), and combination error (maximum difference between scanned antenna and brightness temperature) were determined. Results are shown in Table XI.

TABLE XI

ERRORS FOR DIFFERENT SCAN PARAMETERS

(Intense Ground-Based Inversion Conditions
and 10-inch Tapered J-Fed Paraboloid Antenna)

Scan Parameters	Maximum Error -C					
	Max. Range			Max. Abs. Magnitude		
	Ant.	Scan	Both	Ant.	Scan	Both
4 deg./min.; 64 sec.; (2 BW/IT)*	0.51	1.43	1.62	0.36	0.76	0.82
4 deg./min.; 32 sec.; (1 BW/IT)	0.52	0.77	0.97	0.36	0.44	0.51
2 deg./min.; 64 sec.; (1 BW/IT)	0.52	0.77	0.97	0.36	0.44	0.51
2 deg./min.; 32 sec.; (½ BW/IT)	0.52	0.40	0.63	0.36	0.23	0.39

*Beam widths per integration time

As expected, the antenna error does not change, since it is independent of the scan function. But scan error decreases as beam width per integration time decreases. The most significant feature of these data is that the improved antenna has reduced antenna error to a level well below the scan error. By decreasing both the scan rate and integration time by a factor of 2, scan error was reduced by about 3.5 to a level compatible with the antenna error.

4.6 SUMMARY

The requirement for an accurate estimate of the source brightness distribution necessitated replacement of the antenna factor concept with the more exact method of integrating the brightness distribution, including ground radiation, to obtain the antenna temperature distribution. A computer program was developed and described to perform the required integration. Model studies

have shown that ground and extraneous sky radiation can enter the antenna through the side lobes in sufficient amounts to significantly distort the observed brightness distribution. Three figures of merit and two operational criteria were developed and appropriate determinations were made for a variety of antenna patterns and types. Each type of antenna was evaluated with respect to its electrical performance, mechanical compatibility, manufacturing suitability, and economic competitiveness. The optimum choice from those examined was a 10-inch full paraboloid fed with a cosine-squared distribution tapered to the first null. This optimum design showed reduction of the antenna error to about 25 to 30 percent of the MK I antenna. This degree of performance improvement was sufficient to warrant further reduction in scan error by reducing the beam width per integration time parameter to one half. Of course, the de-scan algorithm in LRRT could be used in lieu of physically altering the scan rate.

It is likely that the offset paraboloid would achieve superior performance, but we were unable to verify this for lack of a measured pattern on a suitable model.

Finally, we were unable to complete analysis of the effects of the residual antenna errors (and scan errors) upon the data processing techniques in time for inclusion in this report.

SECTION 5

CONCLUSIONS AND RECOMMENDATIONS

5.1 CONCLUSIONS

Improved performance of the MK I THERMASONDE and availability of a relatively large sample of field observations from diverse locations revealed a systematic discrepancy between computer simulated and actually observed data. This difference was typically 3 K, which significantly degrades performance of existing data-inverting techniques. Therefore, it was mandatory to isolate and minimize the effects of this discrepancy if full capability of the data-reduction techniques was to be realized. To this end, efforts were redirected, as needed, and this work has established that the discrepancy results from excessive side lobe response of the general utility antenna used in the MK 0 and MK I instruments. This side lobe response allows radiation from the ground and from off-axis directions in the atmosphere to distort, or alter, the indicated shape of the observed brightness distribution. A computer program was developed which properly accounts for this distortion and permits measured antenna temperature distributions to be simulated, from corresponding measured air temperature profiles, to within 3/4 C rms. This includes radiosonde error of approximately $\mp$ ½ C. Including measured ground temperature data in the simulation model will improve the simulation capability.

The potential impact of extraneous ground and sky brightness contributions upon performance of the proposed MK II system was evaluated. An analysis of alternative approaches to reducing these effects has shown that error reduction by proper antenna design is practical, adequate, and cost-effective. A comprehensive quantitative evaluation of several physically realizable antennas revealed that very high main beam efficiency is required (about 95%), with only modest (1 to 2 degrees) beam width requirements. Very narrow beams (hence large apertures) are not indicated. A suitable antenna design for the MK II THERMASONDE was specified. Performance of a prototype model of this antenna was computed for six representative air temperature profiles and was shown to be compatible with other system errors and with ground truth errors. Examination of the residual errors showed that further attempts to reduce them through data correction were unwarranted at this time.

Errors due to the scan function can be important unless they are corrected in the data processing technique (as in the analog and LRRF technique). If not, the scan function parameters should be changed to give a beam width per integration time equal to or less than 1 (e.g., 4 deg./min. scan rate and 30 sec. integration time for a 2-degree beam width).

The analog technique was refined and tested on simulated and field data. Government development personnel (APCO) and operating personnel (EMSU) have successfully applied the technique on relatively large samples of data observed with the MK I THERMASONDE at Raleigh, North Carolina; St. Louis, Missouri; and Boulder, Colorado. This experience has shown that the technique is capable of indicating the mixing layer depth to within an average of about ± 15 % of the true height over the surface to 1500 meters. This performance level was obtained using an analog library with only 7 discrete mixing heights and despite existence of the systematic simulation discrepancy resulting from extraneous ground and atmospheric contributions to antenna temperature. The technique is the least sophisticated and simplest to apply of the three developed. It is quasi-objective, trading the computer's mathematical objectivity (which is often very limited) for the meteorologist's subjective experience, skill and judgement. It requires no computing hardware for its implementation, save the one-time process of generating an appropriate library. It is presently the most limited of the techniques with respect to the degree of temperature profile resolution obtainable, but it is also probably the fastest with respect to time elapsed between observation and availability of the predicted profile. Operational performance of the analog technique will be significantly improved because: (a) improved antenna design will significantly reduce error from extraneous ground and sky radiation, (b) automatic production of the analog library will increase available profile resolution, and (c) introduction of the surface pressure parameter will aid profile selection.

The gradient-altitude model technique was refined and tested on a small sample (approximately 5) of simulated and field data. Although the number of different profiles which were tested was small, the results which are available confirm the greater resolution of the GAM technique. GAM is a completely objective decision-making technique, but it can also take advantage of the meteorologist's "input" to help limit the ensemble of possible test profiles. This feature reduces computing time. In its present formulation, GAM

is not an optimum technique, but in comparison with other existing radiometric data analysis techniques, we believe that it a usable technique. For best results, it presently requires specification of a residual profile (usually from a previous nearby RAOB sounding) and more than one pass through the data. A typical pass takes less than 30 minutes on a Univac 418-III or about 3 minutes on a Univac 1108. No attempt has been made to streamline the program and computer running time.

A new method of implementing the limited range relaxation technique was formulated and tested on a small sample of simulated brightness temperature distributions. This technique produced excellent specification of the existence and height range of elevated inversions. Poorer specification of intensity may have been the result of performing only a limited number of iterations. This procedure was used because no good error criterion has yet been established and built into the technique. The LRRT is relatively easy to use, requiring only the input of 16 brightness temperature measurements. A typical run requires about three minutes on a Univac 418-III or about 18 seconds on a Univac 1108. LRRT has no provision for human input, but objectively defines a temperature-height profile with 16 pairs of numbers covering a height range to 2.54 km.

Surface pressure has been shown to be an important parameter in accurate inversion of radiometric data into temperature profiles. A computer program was developed to automatically generate model profiles and simulated brightness scans for rapid production of user-oriented analog libraries. This program includes the surface pressure refinement.

From the above results, we conclude that three different techniques for translating THERMASONDE data into temperature-height profiles have been developed and refined. Two of them are essentially at a serviceable status. In their present forms, both the GAM and analog techniques have demonstrated capability of depicting the air temperature profile to within less than 2 C on the average, with ultimate capability less than 1 C. The gradient altitude model using the maximum correlation coefficient criterion provided the best performance to date. Each technique has shown sufficient success in indicating mixing layer depth to warrant incorporating the additional computer programming sophistication needed to reduce running time and core storage requirements.

The Sperry Rand Research Center provided assistance and participation in Government-sponsored field experiment activities. These experiments provided a good data base from which to develop and test the three data-processing techniques, and to experimentally verify the simulation model. In addition, the frequency meter in MK I was calibrated. Experience has shown that this type meter has marginally adequate resolution; consequently, a better means should be sought to establish the correct operating frequency in the MK II system. Further, a high degree of operating frequency stability will be required.

5.2 RECOMMENDATIONS

Based upon the achievements and experience obtained in performing the work reported herein, the Sperry Rand Research Center recommends the following future actions.

1. The MK II THERMASONDE should incorporate an improved antenna designed especially for maximum main beam efficiency (about 95%) and beam width between 1 and 2 degrees. A 10-inch tapered J-fed paraboloid and an offset parabola type antenna meet these requirements and are suitable for both construction and field use.

2. The MK I THERMASONDE should be retrofitted with an improved high-beam efficiency antenna.

3. A well designed, statistically sound field evaluation experiment should be performed, either with the improved MK I or MK II THERMASONDE, to compare operational performance of the available data processing techniques.

REFERENCES

(1) Carter, C. J., R. L. Mitchell and E. E. Reber, "Oxygen Absorption Measurements in the Lower Atmosphere," J. Geophys. Res. 73 (10), 3113 (1968).

(2) Meeks, M. L. and A. E. Lilley, "The Microwave Spectrum of Oxygen in the Earth's Atmosphere," J. Geophys. Res. 68 (6) 1683 (1963).

(3) Mount, W. D., B. R. Fow, C. V. Wick, and C. M. Maloy, "Three Radiometric Data Analysis Techniques for Measuring Air Temperature Profiles," Final Report, APCO Contract No. CPA 22-69-116, October 1970.